学位論文

Bone dynamics changes in modeling mice replaced by *Xenopus Brn-1/Pou3f3*

（神経系 POU 転写因子 *Brn-1/Pou3f3* の
ゼノパス型置換モデルマウスにおける骨動態変化）

平成２５年１２月　博士（理学）申請

東京大学大学院　理学系研究科
生物科学専攻

五十嵐　惇

DOCTORAL THESIS

Bone dynamics changes in modeling mice replaced by *Xenopus Brn-1/Pou3f3*

Atsushi Igarashi

Department of Biological Sciences

Graduate School of Science

The University of Tokyo

2013.12

ABSTRACT

One of major differences between genomes of mammals and other vertebrates is the presence or absence of homopolymeric amino acid repeats, sequences without interruptions in the run of a single amino acid residue. Some types of homopolymeric amino acid repeats modulate protein–protein interactions and/or transcriptional regulation. I investigated the functional meanings of homopolymeric amino acid repeats present in mammalian *Brn-1/Pou3f3* transcription factor that is prominently expressed in brain. Mammalian BRN-1/POU3F3 has eight homopolymeric amino acid repeats, each of which consists of alanine, glycine, histidine, and proline amino acid residues. In contrast, only two of these repeats are present in *Brn-1/Pou3f3* orthologues of amphibians and fishes. This remarkable feature is well conserved in both positions and numbers of the repeats among mammals, showing these repeats were acquired specifically in the mammalian lineage.

To analyze what kinds of phenotypic diversification were produced by acquisition of these repeats during mammalian evolution, I newly generated non-mammalized mice (*xPou3f3* knock-in mice) in which the entire coding region of the murine *Pou3f3* gene was replaced with that of the amphibian (*Xenopus tropicalis*) orthologue. Both mouse and *Xenopus Brn-1/Pou3f3* genes are intron-less, and their amino acid

sequences of the DNA-binding domain called POU domain are completely identical. Both homozygous and heterozygous *xPou3f3* knock-in mice grew to adulthood and appeared normal. There were no changes in appearance, body weight, growth, or fertility. Both the expression pattern and the expression level of the *xPou3f3* (*tro*) allele were similar to those of the wild-type allele. Brain weight per body weight did not differ between wild-type and *tro*/*tro* mice. Further, no histologically abnormal changes were detected within the brain. In *xPou3f3* knock-in mice, there was no deterioration of maternal behavior observed in *xPou3f2* knock-in mice, in which transcription factor *Brn-2/Pou3f2*, a paralogue of *Brn-1/Pou3f3*, was replaced with the *Xenopus tropicalis* orthologue. However, pre-pulse inhibition of the *xPou3f3* knock-in mice was significantly stronger than that of wild-type mice, showing schizophrenia-like abnormalities. In addition, the *xPou3f3* knock-in mice showed significantly longer immobility time in both tail suspension test and forced swimming test than wild-type mice. This means that the *xPou3f3* knock-in mice tend to be depressive. Then, I exposed the mice to various kinds of chronic stress including immobilization stress, and performed measurement of various molecular indexes about the stress and comprehensive transcriptome analysis. The chronic stress raises expression of precursor polypeptide of an adrenocorticotropic hormone released by pituitary gland. In the *xPou3f3* knock-in mice, the degree of the rise

was significantly lower than wild-type mice. In contrast, the chronic stress causes decrease of gene expression in various types of glutamate and GABA receptors. However, only few receptors showed decrease of gene expression in the *xPou3f3* knock-in mice. The immobilization stress is known to cause induction of various anti-oxidant enzymes. Among 111 anti-oxidant genes, 22 genes were up-regulated by the chronic stress in the wild-type mice, whereas only 4 genes were in the *xPou3f3* knock-in mice. 8-OHdG concentration of urine, an oxidative stress marker, increased by stress in the *xPou3f3* knock-in mice. This suggests that quick response against oxidative stress was not occurred. In addition, blood alkaline phosphatase and bone density decreased by chronic stress in the wild-type mice, but there were no changes in the *xPou3f3* mice. I clarified that the following influences were induced by replacing transcription factor *Brn-1/Pou3f3* of the mouse with the amphibian type (orthologue): (1) schizophrenia-like response and the depressed tendency, and (2) low response against stress.

Table of Contents

1. INTRODUCTION

Brn-1/Pou3f3, also known as *Brain-1/Otf-8/Oct-8*, has been identified as one of the members of class III POU transcriptional factor [1,2]. *Brn-1/Pou3f3* contains both POU-homeo and POU-specific DNA binding domains, which recognize octamer motif, ATGGTA. *Brn-1/Pou3f3* is prominently expressed in the central nervous system including the cortex, amygdala, thalamus, hypothalamus, brainstem and cerebellum [1]. *Brn-1/Pou3f3* knockout mice display hypoplasia of Henle's loop, macula densa and distal convoluted tubule in the kidney, also showing histological abnormalities in the hippocampus, and die within 48 hours of birth [3]. Together with ASCL1, *Brn-1/Pou3f3* up-regulates *DLL1* gene, a human homologue of the Notch Delta ligand, that plays a key role in neurogenesis [4]. The spatiotemporal expression pattern of *Brn-1/Pou3f3* resembles that of *Sox11* in the face, brain and kidney from the embryonic to postnatal development, and it is shown that *Brn-1/Pou3f3* and *Sox11* synergize and trans-activate each other [5, 6].

Compared with the amphibians and fish BRN-1/POU3F3, mammalian BRN-1/POU3F3 has a remarkable feature that there are eight homopolymeric amino acid repeats (sequences without interruptions in the run of a single amino acid residue). In contrast, only two of these repeats are present in *Brn-1/Pou3f3* orthologues of amphibians and fishes. This remarkable feature is well conserved in both positions and numbers of the repeats among mammals, showing these repeats were acquired specifically in the mammalian lineage [7]. And each of

these repeats consists of alanine, glycine, histidine, and proline amino acid residues. In human genome, approximately 650 genes contain one or more homopolymeric amino acid repeats. Some types of homopolymeric amino acid repeats modulate protein–protein interactions and/or transcriptional regulation. For example, HAP-1 [8], HIP-1 [9], GAPDH [10], LANP [11] and PQBP-1 [12] interact with poly-glutamine repeats. EVH-1 can interact with poly-proline repeats [13]. Homopolymeric amino acid repeats are known to contribute to up-/down-regulation of transcription. Yeast transcriptional factor GAL4 artificially fused with glutamine repeats of 10 to 30 residues or proline repeats of 10 residues increase transcriptional activation [14], while alanine repeats suppress its transcriptional activity [15]. Homopolymeric amino acid repeats are considered to form intrinsically disordered protein regions. Disordered regions can be highly conserved between species and often function as a target in numerous biological processes, protein-protein interaction and molecular recognition by kinases, transcription factors and translation inhibitors [16, 17]. Furthermore, intrinsic disordered regions can contribute to serve as a structural basis for hub protein promiscuity, to bind to a structured hub protein, and to provide flexible linkers between functional domains [18].

In addition to these observations, both mouse and *Xenopus Brn-1/Pou3f3* genes are intron-less, and their amino acid sequences of the DNA-binding domain called POU domain are completely identical. Then, to address the biological implications of homopolymeric amino acid repeats in mammalian evolution, I generated non-mammalized mice (*xPou3f3* knock-in

mice) in which the entire coding region of the murine *Pou3f3* gene was replaced with that of the amphibian (*Xenopus tropicalis*) orthologue, and compared their physiological, behavioral and morphological phenotypes with those of wild-type mice.

2. MATERIALS AND METHODS

2-1. Multiple alignments

POU3F3 amino acid sequences were obtained from Ensembl (http://asia.ensembl.org/index.html) and NCBI (http://www.ncbi.nlm.nih.gov) (Table. 1). Full-length amino acid sequences were chosen and all partial sequences were manually removed. To determine the amphibian *Pou3f3* sequence, *X. tropicalis* genomic DNA was extracted from a piece of liver tissue of male individual. The *Pou3f3* orthologous region in *X. tropicalis* was amplified by polymerase chain reaction (PCR) using KOD-Plus- DNA polymerase (TOYOBO Co., Ltd., Japan) and specially designed primers. The primer sequences were

Forward: 5'-GAAGTGATGGCCACGGCTGCC-3',

Reverse: 5'-CACTCCAGTCATTGCACACTAGTCTGC-3'.

In amplification process, the thermal cycler settings were: 94°C for 2 min; 30 cycles of 94°C for 15 sec, 59°C for 30 sec and 68°C for 90 sec; 72°C for 10 min. TA cloning was performed on the amplified PCR products with the addition of dA using Target Clone™-Plus- (TOYOBO Co., Ltd.). The *X. tropicalis* orthologous sequence was determined by fluorescent labeling of BigDye terminator ver.3.1 using ABI PRISM® 3100 Genetic Analyzer (Applied Biosystems, USA).

28 vertebrate POU3F3 amino acid sequences were automatically aligned by MUSCLE algorithm [19] and manually arranged according to repetitive sequences on MEGA 6.06 [20]. Alignment results were displayed with conserved

score and base information using ClustalX 2.1 [21]. The POU3F3 phylogenic trees were reconstructed by the NJ/BioNJ method using 1000 bootstrap replicates. Other settings were as follows:

Model; Jones-Taylor Thornton (JTT) model,

Rates among sites; Uniform rates,

Gaps/Missing Data Treatment; Complete deletion,

Blanch Swap Filter; very strong,

Number of Threads=1.

2-2. Gene targeting

To generate *Pou3f3* specific non-mammlaized knock-in mice, *Pou3f3* in *X. tropicalis (xPou3f3)* was chosen with less of homopolymeric amino acid repeats and 100% homology in entire region of POU domains. The isolated *xPou3f3* in section 3-1 was cloned using TOPO TA Cloning Kit (Invitrogen, USA). The targeting strategy is shown in Fig. 2. According to this, a targeting vector (TV) was constructed including a *xPou3f3* open reading frame (ORF) wedged between 8681bp upstream and 3814bp downstream coincident with *M. Musculus*. As a positive selection marker, the *Lox*P franked neomycin resistance gene (Neo^r) was inserted downstream the *Pou3f3* ORF. Diphtheria toxin A (*DT-A*) was arranged into the upstream of mouse consensus *Pou3f3* as a negative selection marker.

32 μg of TV was linearized by a restriction enzyme, *Cla*I (New England

BioLabs Inc., USA), and well mixed into E14.1 embryonic stem (ES) cells at a cell density of 1.0×10^7 cells. This mixture set into the 0.4 cm cuvette and electroporated with 500 μF and 230 V using Gene Pulser II (Bio-Rad Laboratories, Inc., USA). In the 1st screening, electroporated cells were isolated by pipetting and exposed to antibacterial agent G418, a neomycin, on dish. Some of the electroporated cells had incorporated the TV into cell body and *M. musculus Pou3f3* locus was replaced with targeted allele including *xPou3f3* and *Neo*^{r}. From these the cell masses capable of surviving under the medium condition containing G418 were retrieved. The TV replacement was identified accurately by Southern blot hybridization using two different probes designing to 3' and 5' region (using NEO probe in *Neo*^{r} as supplements, data not shown). Genomic DNA were digested by *Eco*81I (Takara Bio Inc., Japan) with 5' probe and *Bam*HI (New England BioLabs Inc.) with 3' probe and the buffer compositions were as follows;

*Eco*81I	50 mM NaCl
	10 μg/ml Tris-HCl (pH7.5)
	10 mM $MgCl_2$
	1 mM Dithiothreitol
*Bam*HI	100 mM NaCl
	50 mM Tris-HCl
	10 mM $MgCl_2$
	100 μg/ml BSA

Two distinct lineages of ES cells including targeted allele and *Neo*^{r} were cultured at a cell density of 1.0×10^7 cells. To remove *Neo*^{r}, purified 26μg of pIC-Cre vector were well mixed into each ES cells. These mixtures were electroporated independently and cultured with and without G418 separately. The neomycin-sensitive clones were retrieved and checked removal of a *Lox*P-flanked *Neo*^{r} cassette by Southern blot hybridization under *Eco*81I and *Bam*HI restriction (2^{nd} screening).

Two independent clones lost *Neo*^{r} by pIC-Cre recombinase and were injected into blastocysts of a C57BL/6J background to generate two lines of chimeric male mice. The chimeric male mice mated with C57BL/6J female (CLEA Japan, Inc.) and produced F1, which have *xPou3f3* expression throughout their entire body. Their genotypes were checked by PCR amplification as described in section 2-3.

Next, the sequencing amplification primers were constructed with an expected size of amplification of 1,657 bp. PCR was performed in a 20μl volume containing 0.5 μM of each primers, 1mM $MgSO_4$, 0.2mM dNTPs, 5% dimethyl sulfoxide (DMSO), 1 unit of KOD-plus- DNA polymerase and 20ng of genomic DNA as a template. The cycling PCR conditions were at 94°C for 4 min; 31 cycles of 94°C for 15 sec, 66°C for 30 sec and 68°C for 90 sec; 68°C for 10 min. Amplification primer sequences were as follows:

Forward primer: 5'-GGCTGCTGCTGACCGAGGCTAG-3',

Reverse primer: 5'-GAGGAGGAGGCGGCGGAGAAGG-3'.

After PCR amplification, the position of 1,657 bp band was excised from agarose

gel and the PCR products were purified using Nucleospin® Extract (MACHEREY-NAGEL GmbH & Co. KG, Germany). Fragment containing gel slice was dissolved in buffer NT and loaded on a Nucleospin® Extract II Column. After DNA binding step, silica membranes were washed two times and dried by the centrifuge for 2 min at 11,000*g*. Purified PCR products were dissolved out with elution buffer NE and acquired by the centrifuge for 1 min at 11,000*g*. Cycle sequencing was performed using BigDye® Terminator v3.1 under the following conditions: 96°C for 3 min; 25 cycles of 96°C for 30 sec, 50°C for 15 sec and 60°C for 4 min; 60°C for 5 min. The PCR products were dried and dissolved with formamide. The replaced sequences in *xPou3f3* knock-in mice were determined by ABI prism 3100 genetic Analyzer and sequencing primers used were as follows:

Forward primers: 5'-GGCTGCTGCTGACCGAGGCTAG-3',

5'-GAGGAGGAGGCGGCGGAGAAGG-3'

5'-CATGGCCACGGCTGCCTCTAACC-3'

5'-ATGGCCACGGCTGCCTCTAACCCC-3'

5'-ACGGCGGCTTCTAACCCCTACCT-3'

5'-CAGAGCGACTTCATGCAGGGGGC-3'

5'-CAGAGCGACTTCATGCAGGGGGC-3'

5'-ATCAAGGGCATCCAGGAGGCTGGG-3'

5'-GGACTCAACAGCCACGACC-3'

5'-CGCCGGGCCCGGTGGCGCGCTCA-3'

5'-TTCAAGAACATGTGCAAGCTC-3'

5'-CGGCGCCAAAAGGAGAAG-3'

Reverse primers: 5’- GGCTGCTGCTGACCGAGGCTAG-3’

5’-CACTCCAGTCATTGCACACTAGTCTGC-3’

5’-GCGTGGTGCGGGTGCGGCGGGTGAG-3’

5’-GAACTGCTCCAGGTCGTCAGA-3’

5’-GTCCGAGTGAGGGTCGTGGCTGT-3’

5’-GCTGCTGCTGCTGCTGGTGA-3’

5’-GCGCCGCTGCTTGAACTG-3’

5’-GCCCCCTGCATGAAGTCGCTCTG-3’

5’-GACAGAGGACGGGTCCCCCCGGTAG-3’

5’-CGGCGGCGCTGCCCGGCTGCA-3’

2-3. Genotyping

Genotyping was performed when the pups were 4 weeks old. Mice ears were punched for the individual discrimination and pieces of tissue were collected. Ear tips were dissolved in lysis buffer (5M NaCl, 1M Tris-HCl pH8.0 and 0.5M EDTA pH8.0) with 1% sodium dodecyl sulfate (SDS), 1 μg/μL pronase E and 0.1 μg/μL proteinase K at 55°C overnight. The next day, the tissue lysates were treated and purified with phenol, phenol-chloroform isoamyl alcohol (PCIAA) and chloroform. Then the mouse genomic DNA for genotyping was acquired after isopropanol precipitation.

Two positions of repeats were chosen as PCR polymorphism marker:

poly-G product contained consecutive 20 glycine and poly-PAG contained consecutive each repeat of proline, alanine and glycine in mice *Pou3f3*. Expected sizes of amplification were; poly-G: 233 bp (mice) / 176 bp (*X. tropicalis*), poly-PAG: 714 bp (mice) / 624 bp (*X. tropicalis*). The poly-G genotyping was performed in 20μl volume containing 0.5μM of each primer, 0.2mM dNTPs, 1 unit of KOD FX DNA polymerase (TOYOBO Co., Ltd.) and 20ng of genomic DNA as a template. The poly-PAG genotyping was performed in 20μl volume containing 0.5μM of each primer, 1mM $MgSO_4$, 0.2mM dNTPs, 5% dimethyl sulfoxide (DMSO), 1 unit of KOD-plus- DNA polymerase and 20ng of genomic DNA as a template. The both cycling PCR conditions were at 94°C for 4 min; 31 cycles of 94°C for 15 sec, 65°C for 30 sec and 68°C for 60 sec; 68°C for 10 min. Primer sequences were as follows:

G-forward primer: 5'-ACGGCGGCTTCTAACCCCTACCT-3',

G-reverse primer: 5'-GCCCCCTGCATGAAGTCGCTCTG-3',

PAG-forward primer: 5'-CAGAGCGACTTCATGCAGGGGGC-3',

PAG-reverse primer: 5'-GTCCGAGTGAGGGTCGTGGCTGT-3'.

2-4. Mice

All living modified organisms (LMO) and experimental animals were approved by The University of Tokyo, and conducted in accordance with the guidelines on animal experimentation and laboratory animals.

All mice were bred in constant temperature (22-24°C) and constant humidity (30-70%) under the 12-12 hours light-dark cycle (light on at 08:00 hour and off at 20:00 hour). Food and water were provided *ad libitum*. Weaned mice, which reached 4 weeks of age, were transferred with 2-4 littermates in small cage (210W × 165D × 120H mm) or with 5-6 littermates in medium cages (280W × 200D × 130H mm) (CLEA Japan, Inc.). Tested mice were used at 10-13 weeks of age, the so-called young-adult period. All mice had C57BL/6J strain background and experienced more than 7 times backcross with C57BL/6J female or male (CLEA Japan, Inc.).

2-5. Tissue preparation for immunohistochemistry

Mice at 10 weeks of age were anesthetized deeply with 100 mg/kg pentobarbital, and perfused through the heart with 15-20 ml of ice-cold phosphate-buffered saline (PBS, pH 7.4), and immediately followed by 50 ml of fixative containing 4% paraformaldehyde and 0.2% glutaraldehyde in PBS. The animals were kept on crushed ice throughout the procedure. After perfusion, whole brain was removed from the skull and postfixed with the same fixative solution at 4°C for 2 hours, then placed in 10% buffered sucrose at 4°C for overnight. Each brain block was embedded in Tissue-Tek® O.C.T.™ Compound (Sakura Finetek Europe B.V., Netherlands) and frozen in liquid nitrogen. Frozen tissue blocks were sectioned serially at 20 μm in thickness in Microm HM 505 E

Cryostat (Thermo Fisher Scientific Inc., USA) and sliced sections were mounted on 0.5% gelatin-coated slide glasses. Coronal brain slices located in approximately 4.30 mm and 1.98 mm rostral from the interaural line were chosen for *Pou3f3* immunohistochemistry. Sagittal brain slices located in approximately 1.20 mm lateral from longitudinal fissure of cerebrum were chosen for hematoxylin and eosin (HE) stain.

The immunohistochemical staining procedure was performed in accordance with the methods and conditions in previous report [22]. Since a polyclonal antibody to POU3F3 (GTX88112, GeneTex, Inc. USA) can recognize the shared amino acid sequence, C-HMLSHAHQWVTAL-N, between POU3F3 and xPOU3F3, GTX88112 was used as the primary antibody. Slices were rinsed with PBS four times for a total of 60 min. The primary antibody was diluted to 1:200 with PBS and reacted for 12 hours at 4°C. After the reaction stage, these slices were rinsed four times with PBS for a total of 60 min. Next, DyLight®488 rabbit anti-goat IgG H&L preadsorbed (ab96915; abcam, UK) was selected as the secondary antibody. To label POU3F3 locations, the secondary antibody was diluted to 1:100 with PBS and reacted at 24°C for 3 hours. After this second reaction stage, these slices were rinsed four times with PBS for a total of 150 min and finally embedded in 10% glycerin PBS. Throughout all the staining processes, we humidified slices in a dark box and calibrated them to their horizontal surface. For fluorescent observation, Pou3f3-positive cells were identified using confocal laser scanning biological microscope, FLUOVIEW and FV1000 (OLYMPUS, Japan).

In the immunohistochemistry for TH and TPH2, a polyclonal antibody to TH (AB152, EMD Millipore Co., USA) and TPH2 (ABN60, EMD Millipore Co.) were used as primary antibody. Fluorescein isothiocyanate-labeled goat anti-rabbit IgG (65-6111, Invitrogen) was used as secondary antibody. The TH and TPH2 on brain section were recognized by the same operating procedure in the staining of POU3F3. The quantitative analysis of TH or TPH2 examined using a microphotometry system, MapAnalyzer (Yamato Scientific Co., Ltd, Japan) [23, 24]. Approximately 130,000 -200,000 data points were obtained in whole brain section and measured at 20 μm intervals. The operating conditions were as follows: excitation range, 465 -495 nm; photomultiplier voltage, 800 V; objective, 20×/0.50 (magnification/numerical aperture); field diaphragm, 10 μm diameter; and photometry diaphragm, 40 μm diameter. The standard value of fluorescence intensity was calibrated using 1 mM quinine sulfate in 0.05 M sulfuric acid (100 mm in depth), which is proportional to a fluorescence intensity of 100 [23]. As quantitative analysis, 10 regions for TH (located in approximately 0.74 mm rostral from bregma) and 10 regions for TPH2 (located in approximately 4.60 mm caudal from bregma) were chosen. The individual numbers were seven to ten mice per genotype and averaged their fluorescent intensities on both sides of two to four slices. Fluorescence intensity of TH was calculated as a ratio to the mean intensity of four control regions (primary motor cortex (P1), primary sensory cortex (S1), dysgranular insular cortex (DI), and piriform cortex (Pir)) and that of TPH2 was calculated as a ratio to the mean intensity of five control regions (external cortex of the inferior colliculus (ECIC), mesencephalic reticular

formation (mRt), lateral lemniscus (LL), decussation of the superior cerebellar peduncle (xscp), and reticulotegmental nucleus of the pons (RtTg)).

2-6. Locomotor activity

Animal locomotion reflects the self-propulsion endogenously originated in each individual. Increasing and decreasing of locomotor activity deeply reflects mood disorders [25], and the amount of brain monoamines [26].

All of measurements were started at 14:00 and were carried out following the analysis schedule for 120 hours, including light periods of total 60 hours and dark periods of total 60 hours. Mice at 10 weeks of age were put into 290W × 180D × 130H mm specialized cage with a CCD camera placed directly above and '24 hour home cage and social behavior monitoring' test (Time-HC, O'HARA & CO., LTD, Japan) was performed. Each CCD camera captured a mouse movement images at 2 frame/sec. Each image frame was converted into a binary image and total migration distance was calculated by tracking the elliptical subject particle. Other parameters are set as; bin duration: 1800 sec, frame size: 250W × 150H mm, subject size: 300 to 3000 pixels, moving criterion: 3 cm/sec, number of erode: 1, number of dilate: 2, and luminance: 0 (Min) to 55 (Max). Lighting was turned off at 20:00 and turned on at 8:00 automatically. The test schedule was divided into six light periods (L1 ~ L6) and five dark periods (D1 ~ D5) in consideration of nocturnality. The room temperature, humidity and

light-dark cycle follow the condition of the animal breeding room.

In the analysis, 23 of wild type (*+/+*) male mice and 22 of homozygous (*tro/tro*) male mice were used. The transitions of activities in 120 hours were calculated in every period. The activities in light or dark periods were averaged each migration distance in 6 light periods or 5 dark periods, respectively. The 0-90 min activity from start of measurement was regarded as novel-seeking activity, which is considered one of the temperament dimensions of personality including heritable factor (excitability, anxiety, impulsiveness and mood disorders). Because the high performance of novel-seeking activity decreased with time, the activities in three different time-windows (-30 min, -60 min and -90 min) were calculated.

2-7. Prepulse inhibition

Mice at 10-12 weeks of age were tested for their sensorimotor gating function using 'Startle response & prepulse inhibition' test (O'HARA & CO., LTD, Japan). Prepulse inhibition (PPI) is a common biological response in which a weak stimulus (prepulse) inhibits the response to a subsequent strong startling stimulus (pulse) [27]. PPI is utilized as a neurobehavioral test for many test species, from rodents to human [28]. Test subjects were put into a cylindrical chamber and secured to acceleration sensor. Measurement setup was as follows; trial numbers: 10, repeat numbers: 8, intertrial interval (ITI): 10-30 sec, sampling

time: 400 msec, pulse duration: 40 msec. Six different pulse intensities were set to 70 dB, 80 dB, 90 dB, 100 dB, 110 dB and 120 dB. From 70 dB to 90 dB pulse test, mice were measured simply for their startle response without prepulse. From 100 dB to 120 dB pulse test, mice were exposed to 3 different prepulse intensity conditions, 0 dB (no prepulse), 75 dB, and 80 dB, respectively, before 100 msec of pulse. 10 trials and ITIs were presented in pseudorandom order corresponding to each trial type. White noise (70 dB) was constantly presented as background. Startle intensity was measured as peak-to-peak values of waveform quantified by the acceleration sensor. PPI rate was calculated as how much the startle response intensity was suppressed by the prepulse.

2-8. Depressive-tendency tests

Before the assay, the mice aged 10-12 weeks were moved to the test room and kept there for at least 1 week under certain conditions. These tests require the time spent holding immobility posture as an index of depressive mental condition. The mice would retain posture without moving in the context of 'behavioral despair' based on the supposition that animals have 'give up hope of escaping' by Porsolt *et al.* (1978) [29]. Immobility time was measured, arising from their disappointment in both behavioral tests, manually by two different observers.

In tail suspension test (TST) mice were suspended by their tails with

clipping above the board. Their tails penetrated the board through a small hole preventing from tail-climbing problem. Mice were suspended at the height of approximately 20 cm above the ground and recorded by video camera for 10 min. Immobility was defined as a posture lacking their limb motion and body swinging.

In forced swimming test (FST), a cylindrical container (13 cm in diameter, 20 cm deep) was filled with 30°C water to a depth of half the bulk. Mice were placed into this cylinder and their activity was recorded for 10 min. In this trial, the sidewall of the cylinder was too high to overcome and the tip of the tail also was kept away from bottom. Test mice showed either as struggling to escape or in a no motion state including a feeling of powerlessness. Immobility was regarded as absence of any movement other than that necessary to float and keep the head and nose above the surface of water.

2-9. Modified unpredictable chronic stress test

Mice after the measurement of locomotor activity were returned their home cage and stimulated with various continued chronic stresses unpredictably and pseudo-randomly. This stress-loading procedure were based on previous studies [30-33], and revised to be able to observe the reaction to stronger stress and immobilization stress. This modified unpredictable chronic stress (modified UCS) procedure consists of combination of multiple stressors for six consecutive

days. Mice were exposed to 3 long-period mild stressors (decline stress, wet bedding and shake stress) and 4 short-period strong stressors (auditory startle/restraint stress, forced swimming stress, tail suspension stress and heat stress). Stress-loading schedule are shown in Fig. 10A. In decline stress, cages put at a 30-degree angle for 3 hours. In wet bedding stress, clean wood chips were wetted by approximately 100 ml clean water for 3 hours. In shaking stress, cages were reciprocated at 100 round per minute for 3 hours. In auditory startle/restraint stress, mice were immobilized in cylindrical chambers, and exposed to startle pulses presented semi-randomly for an hour. The forced swimming and tail suspension stresses were carried out following the same protocol as described in section 2-8. In heat stress, mice were placed on hot-plate temperature to 55°C and covered by a glass beaker for 10 min.

After all stress-loading processes, behavioral quantification was performed to evaluate the internal stressful state through the light-dark transition test. This behavioral test is a one of most widely used tests for anxiety-like behavior based on a conflict between the natural aversion of an illuminated area and the novelty-seeking attribute. Generally, stress-loads make mice stay for a longer duration in dark box (in contrast, shorter in light box). So, stress-loaded mice were checked their anxiety condition through the measurement of 10 min Light-dark transition test. Test apparatus was 220W × 150D × 160H mm of light and dark boxes with an opening door (80W × 25H mm).

2-10. Preparation of serum, brain and bone

To examine the effects of chronic stress against each genotype, various biological specimens were extracted and prepared. Non-stress-loaded mice had these procedures undertaken after the measuring their locomotor activities, and those of the stress-loaded groups were undertaken shortly after the last of the restraint stress step.

Mice at 10-12 weeks of age were anesthetized deeply with 100 mg/kg pentobarbital. 0.6~1.0 ml blood sample was obtained from heart and separated by 30 min centrifuge at 1,500 rpm. For RNA extraction, the left hemisphere of their brains was immediately frozen by liquid nitrogen. The frozen brains were homogenized with two types of beads (5 mm in diameter and 10 mm in diameter) using a Mixer Mill MM 300 (Retsch GmbH & Co. KG, Germany) for 2 min at 25Hz. For preparation of bone, the muscular structure surrounding the eviscerated right femur was removed using wipers. Both ends of the femur were cut and their bone marrow was flushed with PBS. Bone tissues were wrapped in aluminum foil and frozen by liquid nitrogen. Frozen bones were put into the cell part of a cool mill (TOYOBO Co., Ltd.) and cooled in liquid nitrogen once again. Next, the well-cooled cell parts were banged on a rubber plate 200-300 times. Shattered bone samples were scraped using well-cooled medicine spoon and retrieved by the addition of ISOGEN (NIPPON GENE CO., LTD., Japan). Then, these crashed tissues were dissolved in ISOGEN before proceeding to the step of RNA extraction. Bone tissues for morphological analysis were eviscerated from

the mouse's right leg and dissected into their separate femur and tibia/fibula components. The femur and tibia/fibula were soaked in 70% ethanol overnight. After removing muscular structure, femur samples were dried out overnight and used for μCT imaging and bone morphological analysis in section 2-14.

2-11. Gene expression analysis

2-11-1. RNA extraction

ISOGEN solutions in which sample tissues were well-dissolved were stored for 5 min at room temperature. After this incubation, 200 μl of chloroform was added and the solutions were shaken for 15 sec vigorously, and placed in a centrifuge set to 12,000*g* for 15 min at 4°C. The aqueous phase was retrieved and mixed 0.8 volume of isopropanol well. After 5-10 min incubation, RNA was precipitated by 12,000*g* centrifuge for 15 min at 4 °C and rinsed by 70% ethanol. Briefly air-dried RNA precipitation was dissolved into RNase-free water. RNA quality was measured using two devices, a spectrophotometer (NanoDrop 1000, Thermo Fisher Scientific Inc.) and a microchip type electrophoresis device (2100 BioAnalyser, Agilent Technologies, Inc., USA). The extracted samples were divided into 4 groups, no-stress (*+/+* and *tro/tro*) and stress (*+/+* and *tro/tro*). To reduce the effect of biological variations and experimental error, each RNA sample was pooled two - four individuals.

2-11-2. cDNA synthesis

The Illumina® TruSeq® Stranded mRNA Sample Preparation kit (Illumina, Inc. USA) was used for cDNA synthesis. Detailed handling operations were carried out according to the 'TruSeq Stranded mRNA Sample Preparation Guide'. A brief sample preparation workflow is as follows: 1) purification and fragmentation of mRNA, 2) first strand cDNA synthesis, 3) second strand cDNA synthesis, 4) 3' ends adenylation, 5) adaptors ligation, 6) PCR amplification, 7) library validation and 8) normalization and pooled library.

In the step of 1) Purification and fragmentation of mRNA, total RNA solutions in section 2-11-1 were diluted 50 μl final volume with 4 μg total RNA. In the step of 5) adaptor ligation, eight RNA adaptor indices were added to distinguish each group and those sequences were as follows:

AR002: CGATGT(A)

AR004: TGACCA(A)

AR013: AGTCAA(C)

AR014: AGTTCC(G)

AR015: ATGTCA(G)

AR016: CCGTCC(C)

AR018: GTCCGC(A)

AR019: GTGAAA(C)

2-11-3. Quantification of cDNA library

cDNA quantities were determined by real-time (RT) PCR using KAPA Library Quantification Kit – Illumina / ABI Prism® (KK4835; KAPA BIOSYSTEMS, USA). This kit is ideally suited for the quantification of libraries for Illumina next-generation sequencing platform. It is constructed with Illumina adaptors containing the following qPCR primer sequences:

Primer P1: 5'-AAT GAT ACG GCG ACC ACC GA-3',

Primer P2: 5'-CAA GCA GAA GAC GGC ATA CGA-3',

In preliminary adjustment, all libraries were diluted to 5 ng/μl. These libraries were diluted to 1:1000, 1:2000, 1:4000 and 1:8000. According to the protocol, KAPA SYBR FAST qPCR Master Mix and each diluted template were mixed together well. The qPCR program was run using StepOnePlus™ (Real-Time PCR System, Applied Biosystems) with the settings: 95°C for 5 min; 35 cycles of 95°C for 30 sec and 60°C for 45 sec. Each reaction was duplicated.

Second cDNA quantification was performed using a 2100 BioAnalyzer according to the appropriate protocols. The measurement was performed using an Agilent DNA 1000 assay kit (Agilent Technologies, Inc.). 1 μl of resuspended constructs were loaded on the DNA-specific chip and confirmed their peaks in 266-281 bp (The final product should be a band at approximately 260 bp).

2-11-4. RNA-seq

RNA-seq was performed using a next-generation sequencer Miseq and Miseq v2 reagent kit (Illumina, Inc.). All samples were diluted to 4 nM each and denatured with freshly prepared 0.2N NaOH. Denatured cDNA libraries were mixed into these diluted samples and diluted once more to a final concentration of 10 pM. The libraries were sequenced on Miseq and sequence data was collected automatically with respect to sequence tags.

To analyze and map the sequenced reads on Fastq files, we used the CLC Genomics Workbench ver.7.5.1 (CLCbio, Denmark) along with mouse sequence reference MGI_4.2. With this software, GeneOntology (GO) functional annotations were added based on MGI 5.21 annotation reference file.

2-12. ELISA

The urinary samples excreted when retained mice were retrieved at 10~13 weeks age. The concentration of urinary 8-OHdG was measured using New 8-OHdG Check ELISA (Japan Institute for the Control of Aging, NIKKEN SEIL Co., Ltd, Japan). The experiment procedures were followed accompanying protocol. All urinary samples and standards were assayed in duplicate and dispensed to each well. The primary antibody solution was dispensed and reacted for 1 hour at 37°C. After this incubation, each well was rinsed with wash buffer for three times. The secondary antibody solution was reacted in each well for 1 hour at 37°C. room temperature. After same wash session, each well was

developed for 15 min at room temperature. Stop solution was added after exactly 15min and the plate was assayed absorbance at a wavelength of 450nm using the SpectraMax® Paradigm® Multi-Mode reader (MOLECULAR DEVICES, USA).

2-13. Measuremenr of blood components

The concentrations of calcium (Ca), inorganic phosphorus (IP), alkaline phosphatase (ALP), uric acid (UA) and blood urea nitrogen (BUN) in blood were determined using a FUJIFILM DRI-CHEM 3500 system (FUJIFILM, Japan). Before each measurement, a QC card was swiped through the card reader to perform a calibration. The measurement slide was then set into a slide cartridge and a 10 μl drop of sample serum was placed on the reaction surface. A DRI-CHEM 3500 system incubated slides for several minutes at 37°C and automatically measured the concentration of target blood component.

2-14. Bone μCT analysis

Bone structural estimation was done using μCT for detailed 3D tomographic images, and X-ray absorption rate for density data. This density data allows accurate identification of various bone parameters, detailed 3D structure and biological internal morphology in vivo.

The images of the mice bone 3D-structure in each genotype were acquired with an in vivo micro X-ray CT system R_mCT2 (Rigaku Co., Japan). Scanning conditions were as follows: Voltage, 90 kV; Current, 80 μA (CT mode) and 60 μA (X-ray live mode); and field of view (FOV), 5 (φ5 mm × H5 mm). Acquisition time was set to FINE mode (3 min). The imaging data were exported as multi-TIFF files including 500 slices.

Tomographic TIFF images were reconstructed using 3DBone (RATOC SYSTEM ENGINEERING Co. Ltd., Japan). The R_mCT2 Viewer Package software analyzed using the 3-dimensional ordered subsets-expectation maximum algorithm with 3 iterations.

2-15. Statistical analysis

In all behavioral tests and physiological assay, each data were shown using calculation of means and SEMs. I denoted the number of mice in each method. To compare two paired values in behavioral test and physiological analysis, the differences were detected using the 2-tailed Student's *t*-test. *P* values less than 0.05 were considered as statistically significant and 3 stepwise significance were indicated as $*P<0.05$, $**P<0.01$ and $***P<0.001$ in the figure.

In RNA-seq analysis, 'CLC Genomics Workbench ver.7.5.1' was employed for the analysis of massive data in RNA-seq. In stress related phenotypic analysis, the gene expression changes were identified in comparison

of between stress-loaded groups (*+/+* (stress+) vs. *tro/tro* (stress+)). First, statistical significance were detected using Kal's Z-test and indicated as †P<0.05, ††P<0.01 and †††P<0.001 in '*WS vs. HS*' column. Next, the distribution analysis of GeneOntology (GO) and Hypergenometric (HyperG) test on annotations was conducted to search bias among the significantly changed gene clusters. The candidate genes were compared using Baggerley's test between stress-loaded groups (*+/+* (stress-) vs. *+/+* (stress+) or *tro/tro* (stress-) vs. *tro/tro* (stress+)) and statistical significances were indicated as *P<0.05, **P<0.01 and ***P<0.001 (shown in 'P' column in *+/+* or *tro/tro*, respectively) (Fig.11).

3. RESULTS

3-1. Multiple alignments

To examine species variations of POU3F3 amino acid sequences through the process of evolution, sequence comparisons were performed using multiple POU3F3 sequences obtained from database. 28 POU3F3 full-length sequences were acquired from the database along with their species names, accession numbers and amino acid length (summarized in Table 1).

Xenopus tropicalis Pou3f3 (*xPou3f3*) sequence was not decided at the onset. So the first, *xPou3f3* gene and protein sequences were determined using PCR and TA cloning. After this sequencing, this POU3F3 sequence was confirmed on Xenbase (http://www.xenbase.org/entry/) (XP_002941201). While some primate *Pou3f3* sequences were found to exist in database, all were found to be partial sequences and therefore too short for further analysis. Teleost *Pou3f3* generally had two different forms, *pou12* (also known as *brn1*) and *pou23*. As a result, the multiple alignments were performed using 28 POU3F3 transcripts (including six mammals, an bird, two reptiles, two amphibians, and seventeen fishes) (Fig. 1A). The neighbor-joining phylogenic tree was created based on these sequences (Fig. 1B). The POU-specific domain and POU-homeo domain were highly conserved between vertebrates with the obvious exception that both type of *Xiphophorus maculatus* POU3F3 had largely deletions of 32 amino acids in POU-specific domain. Furthermore, in database, teleost *Pou3f3* accompanied

information on some splicing variants because of the short intron insertions.

Since the teleost *Pou3f3* were diverged, multiple alignments and phylogenic tree analysis were re-examined based on 10 tetrapods POU3F3 amino acid sequences (Fig. 1C, D). Through the detailed comparison, it became clear that the conservation scores were comparatively high over the whole area, especially in C-terminal regions containing POU domain. On the other hand, the N-terminal regions were diverged and several species-specific insertions of homopolymeric amino acid repeats were revealed. Mammalian POU3F3 possessed seven or eight homopolymeric amino acid repeats; poly-G, poly-A, poly-P, poly-P, poly-A, poly-G, poly-H and poly-G in order from N-terminus. Since the eighth poly-G specifically-existed in *Homo sapiens*. In other vertebrates, bird and reptile shared three and amphibian shared two homopolymeric amino acid repeats with mammalian POU3F3.

Whereas, to examine whether this tendency of ease to insert of homopolymeric amino acid repeats is specific in *Pou3f3*, *M. musculus* POU3F1, POU3F2, POU3F3 and POU3F4 were aligned and compared those sequences (Fig.1E). The POU3F2 had three distinct insertions of quite long two homopolymeric amino acid repeats (poly-G and poly-Q) and comparatively short poly-P repeats. The POU3F1 had four insertions in N-terminal (poly-A and three poly-G) and two short insertions of homopolymeric amino acid repeats in C-terminal (poly-P and poly-H). The POU3F4 did not show any insertions of homopolymeric amino acid repeats.

3-2. Generation of *xPou3f3* knock-in mice

To examine a functional role of the mammalian specific sequences containing homopolymeric amino acid repeats in *Pou3f3*, I generated knock-in mice carrying a non-mammalized *Pou3f3*. As a non-mammalized and ancestral sequence, I chose *xPou3f3*, which contains only two homopolymeric amino acid repeats as opposed to eight repeats in mouse, yetand 100% homology in the entire region of POU domains (Fig. 2A). Fish *Pou3f3* sequences were not adopted in consideration of their specific diversification by an event of the third round of whole genome duplication.

Targeting vector (TV) with *xPou3f3* was constructed as described in the section 2-2 (Fig. 2B). I knocked-in a *xPou3f3* allele into E14-1 stain of mouse ES cells and selected two rounds of screening (G418 treatment and Southern blot hybridization). In the 1st screening, 205 clones were retrieved and checked for the recombination with TV by Southern blot hybridization. Two clones (#14 and #25) showed double bands with expected size of the targeted allele (15,513 bp in *Eco*81I or 5.844 bp in *Bam*HI restriction, Fig. 2C). Next, to eliminate the *Neo*^{r} in the targeted allele, these clones were electroporated with pIC-Cre recombinase. In the 2nd screening, 244 clones were retrieved and cultured with or without G418. Finally in two distinct clones (#100 and #84 derived from #14 and #25, respectively), the pIC-Cre induced deletions of *Neo*^{r} were confirmed by Southern blot hybridization (13,533 bp in *Eco*81I or 3.915 bp in *Bam*HI restriction, Fig. 2D). These clones were injected into C57BL/6J blastocysts to generate chimeric mice.

Surrogate mother mice delivered chimeric pups with germ-line cells derived from injected knock-in blastocysts. Chimeric mice were backcrossed more than 7 times, and I tried to uncover the phenotypes in this non-mammalized (*xPou3f3*) knock-in mouse.

3-3. Morphological characteristics

xPou3f3 heterozygous (*+/tro*) and homozygous (*tro/tro*) knock-in mice were born normally at first glance. Physical abnormalities, irrational behavior and visible diseases were not observed in these mice (Fig. 3A) and their body weights had no difference between wild type (*+/+*) and *tro/tro* (Fig. 3B). Their face conditions were checked as the indices of sociality, emotion and intracranial changes [34, 35], but visible facial barbering, alopecia, enlarging circumference of head characteristic of hydrocephalus and eye abnormalities were not observed in *+/tro* and *tro/tro* at 10 weeks age (Fig. 3C). Jeong *et al.* reported that *Pou3f3* knock-out mice were largely missing the squamosal bone (SQ) and jugal bone (JG) [36]. To examine this morphological phenotype, I performed alcian blue / alizarin red staining in E16.5. However, *+/tro* and *tro/tro* mice did not have the abnormal cranial bone or costral bone (Fig. 3D).

Furthermore, since *Pou3f3* knock-out mice showed brain structural abnormalities [37, 38], I analyzed brain slices by HE staining. In brain, whole or regional atrophy and formation of ectopic layer were not observed (Fig. 4A-C).

Next, I examined whether the *xPou3f3* was expressed in appropriate locations. The immunohistochemical fluorescent staining identified the signals of POU3F3 of both *+/+* and *tro/tro* mice with indistinguishable patterns in the neocortex (Fig. 4D), neostriatum (Fig. 4E), nucleus accumbens (Fig. 4F) and hypothalamus (Fig. 4G). This suggests that the distributions of the xPOU3F3 signals were roughly matched to POU3F3.

3-4. The comparative analysis between non-mammalized *Pou3f2* and *Pou3f3* knock-in mice

3-4-1. Weaning ratio and reproductive performance

Ahead of this research, our projects generated 2 distinct types of non-mammalized *Pou3f2* knock-in mice. Although *Mus musculus* POU3F2 had three quite extended homopolymeric amino acid repeats (also shown in section 3-1 and Fig. 1E), definitely loss of these insertions in other vertebrates were revealed. To examine the role of homopolymeric amino acid repeats in *Pou3f2*, generation of *Pou3f2 ΔGQP* knock-in mice with complete deletion of the three homopolymeric amino acid repeats and *xPou3f2* knock-in mice in which the entire coding region of the *Pou3f2* was replaced with that of *X. tropicalis Pou3f2* orthologue, were conducted. It was suggested that female maternal behaviors in previous reports [39], I analyzed the differences in

sexual behaviors and pups weaning ratio between non-mammalized *Pou3f2* and *Pou3f3* knock-in mice.

First, basic reproductive alterations were checked. But their fertility and litter sizes didn't differ from the wild type. The genotypic ratio of the pups obeyed Mendel's law in both *Pou3f2 ΔGQP* knock-in mice (Fig. 5A) and *xPou3f3* knock-in mice (Fig. 5B).

Second, as one of the index of sexual behaviors and fetal development, the latency from mating to delivery was measured. Although the latency until delivery in *Pou3f2 ΔGQP* homozygous mating pairs (*Δ/Δ* vs. *Δ/Δ*) showed more extensive tendency than wild type (*+/+* vs. *+/+*) (Fig. 5C), that in *xPou3f3* homozygous mating pairs (*tro/tro* vs. *tro/tro*) showed no differences (Fig. 5D).

Third, to investigate the differences in weaning ratio and pups surviving by the replacement with non-mammalized form, the numbers of weaned pups were counted through the various combinations of parent genotypes. In *Pou3f2 ΔGQP* knock-in mice, the genotypes of dams affected pups weaning ratio and this nurturing performance of *Δ/Δ* dams was reduced two-thirds that of *+/+* (Fig. 5E). Because this tendency was independent of sires and pups genotypes, it indicated that the genotypes of dams were crucial factor. Whereas, weaning ratio was not differed in both combinations of mating in *xPou3f3* knock-in mice (*+/+* vs. *+/+* and *tro/tro* vs. *tro/tro*) (Fig. 5F).

3-4-2. Quantification of brain monoamine expression

To make sure of the cause of reduced weaning ratio, brain monoamines were measured because various studies pointed to the relationship between maternal behaviors and dopamine (DA) [40-42] / serotonin (5-HT) [43-46]. Since *Pou3f2 ΔGQP* and *xPou3f3* knock-in mice showed reduction of the pups viability in common, the quantitative analysis was performed using fluorescence microphotometry system, MapAnalyzer (Yamato Scientific Co., Ltd) [22]. Both TH and TPH2, rate-limiting enzymes of DA and 5-HT synthesis respectively, were quantified at the levels of the nucleus.

The immunohistochemical distributions of TH and TP are shown in Fig. 6A-D and Fig. 6E-H, respectively. The extremely high expression of TH was observed in neostriatum (STlat and STmed), nucleus accumbens (AcbS and AcbC) and olfactory tubercle (Tu). The extremely high expression of TPH2 was observed in dorsal and median raphe nucleus (DRD, DRV, DRL, MnR and PMnR). As a result, both of brain monoamines were significantly decreased in most regions (Fig. 6C and 6G).

A reduction rates in 3 different types of knock-in mice were summarized (Fig. 6I-L). *Xenopus* form of *Pou3f2* homozygous mice (*tro/tro*) displayed more prominent decreasing manner in TH (69.7%, Fig. 6I) and TPH2 (67.9 %, Fig. 6K). However, *Pou3f2 ΔGQP* homozygous mice (*Δ/Δ*) also showed significantly decreased TH (78.6%) and TPH2 (83.9%). Although measurement procedure was not the same, *xPou3f3* knock-in mice showed the same directional

monoamine expression changes in the results of RNA-seq (Fig. 6J, L). In *xPou3f3* (*tro/tro*), TH expression was slightly decreased (83.1%, not significant) (Fig. 6J) and TPH2 expression significantly decreased (43.3%, $P<0.01$) (Fig. 6L). Interestingly, *xPou3f3* (*tro/tro*) displayed more remarkable changes in TPH2 in contrast to non-mammalized *Pou3f2* knock-in mice (*Δ/Δ* and *tro/tro*). It is therefore intriguingly to examine behavioral analysis related to brain serotonin (5-HT), for example locomotor [47, 48], depression [49-51] and anxiety [52, 53].

3-5. Locomotor activity

The measurement of mice locomotor activity is useful as a screening test for inherent background, physical abnormality or changes of neurological condition. The animal locomotion reflects the physical vitality and daily neurological activity in spite of no phenotypes at first glance. Especially *Pou3f3* is highly expressed in the brain, it is important to investigate innate biological behavioral manner.

In *tro/tro* mice, the average amount of activities were significantly increased in some light periods; L4 ($P<0.05$) and L6 ($P<0.05$), and in some dark periods; D4 ($P<0.05$), D5 ($P<0.05$) and D6 ($P<0.05$) (Fig. 7A). Especially, the activity in all dark periods showed consistently increasing tendency (D1, 1.14-fold; D2, 1.10-fold; D3, 1.19-fold; D4, 1.18-fold; D5, 1.25-fold). These

differences became more remarkable as time advanced through the experiment time. Despite increasing activity were observed in some light periods, L2 activity was significantly reduced at 0.86-fold (P<0.05). Although the average activity in light period showed not significant (Fig. 7B), that in dark period showed significantly increased (1.16-fold, P<0.05) (Fig. 7C). Whereas, all of novel seeking activity (30-, 60- and 90-min) represented high performance value in comparison with the activity in any other periods. But no significant differences were observed between any time scale windows (Fig. 7D). Additionary, female tro/tro mice acted with more significant increasing tendency and their recorded data were shown in Supplementary Fig. 2.

3-6. Psychiatric behavioral assessments

Prepulse inhibition (PPI) is known as a kind of neurological phenomenon, sensorimotor gating, and the abnormalities in this response are considered as a biological marker for some mental disorders, especially in schizophrenia [28]. At first, the 6 levels of pulse intensities (from 70 dB to 120 dB) were presented to check the capacity of hearing using stepwise sounds. Despite a startle response to 110 dB pulse was significantly increased (P<0.05), no significant differences were observed between genotypes in most of pulse intensities (Fig. 8A). Next, with respect to PPI, I measured startle responses by the presentation of 2 pulse intensities (110 dB and 120 dB) against 2 prepulse (75 dB and 80 dB). In this

result, higher prepulse caused higher inhibition rate. The *tro/tro* male mice showed significant reduction of prepulse inhibition rate in an experimental set of 75 dB prepulse and 120 dB pulse ($P<0.05$) (Fig. 8B). Likewise, the combination of 80 dB prepulse and 120 dB pulse also showed reduction tendency of prepulse inhibition rate. No significant reductions were observed in both of 110 dB pulse trials.

The tail suspension test (TST) and forced swimming test (FST) have been recognized as useful behavioral paradigms to assess the antidepressant effect and measure depressive-like behavior [28, 55, 56]. In these tests, mice are subjected to inescapable affliction with no end in sight and their feelings of giving up, hopelessness and impotence shorten the escaping movement. In TST, most 1-min time windows demonstrated significantly increased inactive time in *tro/tro* (Fig. 9A). Accordingly, total inactive time was significantly increased by 123% on average ($P<0.001$), *tro/tro* displayed shorter periods of struggle (Fig. 9B). In FST, same directional tendency was also caused. A half of 1-min time windows also demonstrated significantly increased inactive time in *tro/tro* (Fig. 9C). Total inactive floating time was also significantly increased by 149% in *tro/tro* mice ($P<0.001$) (Fig. 9D).

However, anxiety behavior was not changed. Light-dark transition test is based on natural aversion of mice to visit illuminated area (light-box), widely used to assay the effect of anti-anxiety agents and mental conditions. Generally, mice tend to visit in the light-box dominantly when they are searching novel environment, but conversely visiting time in the dark-box increase dependent on

anxiety and fearfulness. Though there was no significant difference in visiting time in dark-box between *+/+* and *tro/tro* (Fig. 10B).

3-7. Biological response to chronic stress-loading

What kind of advantage came from evolving from *Xenopus* type to mammalian type *Pou3f3* in organisms? The forced swimming and tail suspension are considered as strong stressors, therefore, their resistant reactions might be inhibited significantly in *tro/tro* (Fig. 9). These behavioral results evoked a hypothesis that *tro/tro* possess vulnerable properties against stressful condition and it caused changes in behavioral aspects.

To examine whether *xPou3f3* knock-in mice are able to express normally stress responses, stress response activities were validated through the modified UCS loading schedule (Fig.10A). Prolonged chronic stress cause the various characteristic internal reactions; alteration in neural activity, anti-oxidative response, immune response and psychopathological syndromes [57]. Since rapid stress response strongly contribute to the survival rate and the continued existence of the species, internal and external adequate reactions are highly conserved.

3-7-1. Stress-induced anxious behaviors

With regard to behavioral aspects, mice in stressful situation display inborn fight/flight reactions to impending danger, pain and threat and elevate fear and anxious psychiatric state [58]. After 1-week exposure to the sustained modified stress schedule, light-dark transition test was performed to confirm whether mice sense fearfulness and anxiety normally. Stress-loaded individuals showed longer visiting time in dark box in both *+/+* and *tro/tro* (*+/+* (stress-) vs. *+/+* (stress+), $P<0.001$; *tro/tro* (stress-) vs. *tro/tro* (stress+), $P<0.001$) (Fig. 10B). No significant changes were shown in comparison between genotypes.

3-7-2. Stress-induced gene expression changes

Next, I performed gene expression analysis to detect any differences of stress response between genotypes. RNA-seq, which is a powerful tool for whole-transcriptomic analysis through whole-genome shotgun sequences, was conducted on 4 groups, no-stress (*+/+* and *tro/tro*) and stress (*+/+* and *tro/tro*). Obtained read data were automatically mapped to MGI reference (ver.4.2). In the mapping results, the average number of mapped all sequences in pair was 2,692,192 reads and the number of those mapped to gene was 1,346,096 reads. Outstanding abnormal biases were not found in these samples because the coefficients of variation (CV) indicated 16.0% and

16.4%, respectively.

I explored characteristic changes accompanying with stress loading and genotypes through the comparison between stress-loaded groups (*+/+* (stress+) and *tro/tro* (stress+)). First, up-regulated and down-regulated genes (P<0.01) were picked up and analyzed their significance in the bias of significance in GO terms by HyperG test. 15 of 98 GO terms related to synaptic transmission and cognitive function, and 12 of 98 GO terms related to ion transport were listed in up-regulated genes in *tro/tro* (Fig. 11A and all GO terms were listed in Supplementary Table 1A). On another front, 3 of 98 GO terms related to oxidative response and 10 of 98 GO terms related to ATP biosynthesis process were listed in down-regulated genes in *tro/tro* (Fig. 11B and all GO terms were listed in Supplementary Table 1B).

From the screening of GO functional analysis, further analysis about the genes displayed discrepancy in stress-related expression changes was performed. First, the expression level of *pro-opiomelanocortin* (*Pomc*) was increased by stress condition in both genotypes. POMC is a precursor polypeptide for synthesis of ACTH, which is major protein released from anterior pituitary gland and constitute capital factor of HPA-axis. The expression value of *Pomc* was significantly increased in *+/+* (7.53-fold, P<0.001) and *tro/tro* (4.04-fold, P<0.05) under modified UCS condition (Fig. 11C). Since lower stress sensitiveness was observed in *tro/tro,* the magnitude of stress response might be affected in various brain components.

Second, because the 15 of 73 GO terms responsible to neural activity and cognitive function were listed, some neural receptors were analyzed in depth. As shown in Fig. 11D-G, the large number of neurotransmitter-associated genes was inhibited during modified UCS in *+/+*, but not promoted in *tro/tro*. Indeed, remarkable suppression of pattern was indicated in glutamate receptors. The stress-induced expression changes were shown widely in 3 types of glutamate receptors, AMPA, kainate and NMDA. Although all AMPA (*Gria1, P*<0.001; *Gria2, P*<0.001; *Gria3, P*<0.001; *Gria4, P*<0.001), 2 of the 5 kainate (*Grik2, P*<0.01; *Grik3, P*<0.001) and 3 of the 9 NMDA (*Grin2a, P*<0.001; *Grin2b, P*<0.001; *Grin3a, P*<0.05) receptors were significantly decreased, only 2 genes were decreased in *tro/tro* (Fig. 11D and Supplementary Table 2A). In addition, gaseous neurotransmitter, nitric oxide (NO), is synthesized by nitric oxide synthase (NOS) in downstream of the AMPA and NMDA signaling pathway. The NO signal works as a spatial signaling module and has been implicated in the contribution to spatial lerning and memory [59]. Neural NO synthetic enzyme, NOS1 and NOS1 adaptor proteins, were also decreased significantly in *+/+* (*Nos1, P*<0.01 and *Nos1ap, P*<0.05, respectively), but not in *tro/tro* (Fig. 11E).

Third, as far as GABA, inhibitory interneuron have a crucial role in controlling the neural excitation in hippocampus [60], and a benzodiazepine and adinazolam, which enhance the effect of $GABA_A$ receptor signaling, act on blockade of dendritic atrophy in stress [57, 61]. $GABA_A$ receptors were consistently suppressed in 5 of the 16 genes (*Gabra4, P*<0.01; *Gabra6, P*<0.01;

Gabrb2, $P<0.001$; *Gabrb3,* $P<0.01$; *Gabrg2,* $P<0.05$), and this declining tendency was widely present throughout the $GABA_A$ receptor family in *+/+* (Fig. 11F and Supplementary Table 2B). In *tro/tro*, however, $GABA_A$ receptors displayed the same level of expression except *Gabra3* ($P<0.05$) and *Gabrd* ($P<0.001$) in spite of similarity strong stress loaded conditions to *+/+* (Fig. 11F). In some opioid signaling are related to the antidepressant effect, analgesic action and euphoric mood. Opiate signaling mediate stress-induced impairment of LTP because an opiate antagonist is able to block this [62]. As a result, 4 opioid receptors were consistently suppressed by stress in *+/+* only, in particular *Oprk1* and *Oprm1* were significantly down-regulated ($P<0.05$ each) (Fig. 11G). A weak similar pattern was observed in brain serotonin (5-HT) receptors and acetylcholine (ACh) receptors with less number of genes than those mentioned above (data not shown). On the other hand, these trends were not shown in following receptors, such as dopaminergic, adrenergic and histamine receptors.

Finally, neurotrophic factors were also changed. Eph family receptors are subunits of receptor tyrosine kinase (RTK) regulating axon guidance, synapse formation and cell migration [63]. The expressions of Eph receptors were most influenced by stress and displayed two directional changes. Although Eph receptor A family showed negative and Eph receptor B family showed positive alterations in *+/+* mice by stress-loading, *tro/tro* mice showed insensitive pattern in neurotrophic factors (Fig. 11H). Especially, Epha4 ($P<0.001$), Epha5 ($P<0.001$), Epha6 ($P<0.01$) and Ephb1 ($P<0.05$) were

significantly changed only in *+/+* mice. These facts indicated opposite regulation in Eph receptors by stress-loading. Whereas, expression changes in most of ligands (e.g. ephrins and BDNFs) and other neurotrophic receptors were not altered.

3-7-3. Oxidative stress response

It has been shown that neurodegeneration caused by stress may be involved in an elevation of reactive oxygen species (ROS) [64-66]. Internal ROS (e.g. superoxide anion ($O_2^{-\bullet}$), hydrogen peroxide (H_2O_2) hydroperoxide, hydroxyl (OH) and peroxyl (ROO)), can directly injure cellular proteins, DNA and lipids from peroxidation reactions [67]. Therefore, to neutralize ROS, organism widely employ anti-oxidant enzymes: copper, zinc-superoxide dismutase (Cu,Zn-SOD, *Sod1*); catalase (*Cat*); and selenium-dependent glutathione peroxidase (Se-GSH-Px, *Gpx*). Cu,Zn-SOD converts $O_2^{-\bullet}$ to O_2 and H_2O_2, while CAT and Se-GSH-Px remove H_2O_2 [68].

From the screening of GO functional analysis between stress-loaded group (*+/+* (stress+) vs. *tro/tro* (stress+)) (Fig.11B), the genes, which displayed the less expression in stress-loaded *tro/tro,* were analyzed in detail. Three GO terms, response to oxidative stress (GO:0006979), regulation of stress-activated MAPK cascade (GO:0032872), and hydrogen peroxide catabolic process (GO:0042744), were listed (P<0.001). Actually, in

GO:0006979 response to oxidative stress, 22 of the 111 genes were significantly increased in *+/+*, but only 4 of 111 genes showed an increasing manner in *tro/tro* (threshold of the significance was $P<0.05$) (Fig. 11I and all of 111 anti-oxidant genes data were in Supplementary Table 2C and Supplementary Fig. 4A). Interestingly, *+/+* mice brain up-regulated the transcription of major anti-oxidant genes, containing *Sod1, Gpx1, Gpx4, Prdx1, Prdx2* and *Prdx4,* by stress-loading to protect the brain from ROS injury. But many genes related to oxidative stress response are insensitive in spite of stressful conditions in *tro/tro* mice.

To validate the internal oxidative stress conditions, I measured the concentration of urinary 8-hydroxy-2'-deoxyguanosine (8-OHdG) using the enzyme-linked immunosorbent assay (ELISA). The 8-OHdG is eliminated from the body through the metabolism of ROS-induced oxidative lesions, and has therefore been widely assayed as a biological marker of oxidative stress [69]. It is also reported the correlation between higher serum SOD activity and lower circulating levels of 8-OHdG [70]. Despite small sampling number (N=5~6), more increasing tendency by modified UCS-loading was demonstrated in *tro/tro* (190%) than *+/+* (87%) (Fig. 11J).

3-8. The changes in blood components

The replacement of *xPou3f3* gave rise to insensitive brain neural signaling regulation and delayed response to oxidative stress. Since such rapid response deeply linked to maintenance of internal environment, I assessed the amplitude of the effect from the aspect of blood components.

I used a FUJI DRI-CHEM 3500 system to measure multiple concentrations of Ca, IP, ALP, UA and BUN in blood. These were examined in the 4 groups; *+/+* (stress-), *+/+* (stress+), *tro/tro* (stress-) and *tro/tro* (stress+). The stress-induced alterations were classified into 3 distinct patterns. First, some blood components decreased independently to genotypes. Significant reductions by modified UCS loading were observed in BUN (*+/+*, 79.7%, $P<0.001$; *tro/tro*, 85.8%, $P<0.01$) and Ca (*+/+*, 95.6%, $P<0.01$; *tro/tro*, 95.7%, $P<0.01$) (Fig. 12A). Second, there was a remarkable elevation in the *tro/tro* genotype-specific. Although the IP concentration was significantly elevated by modified UCS loading in *tro/tro* mice (122.8%, $P<0.001$), it was not significantly changed in *+/+* (105.8%) (Fig.12B). Finally, the contents significantly decreased in *+/+* only, but not in *tro/tro*. This tendency suggests a low sensitiveness to stressful conditions in *tro/tro* and it evoked the result of gene expression analysis in RNA-seq. ALP was remarkably reduced in stress-loaded *+/+* (81.3%, $P<0.001$), whereas this reduction was suppressed in *tro/tro* (92.0%, not significant) (Fig. 12C). As for UA, the concentrations of UA were not changed significantly in each combination of genotypes.

3-9. Measurement of the bone parameters

Blood concentration of ALP is deeply related to bone metabolisms. Normal bones are constantly undergoing bone remodeling in order to maintain a well-balanced relationship between bone formation and resorption. Bone ALP is designed when reflect the biosynthetic activity of these bone-forming cells, called osteoblast [71]. Some previous studies had reported the reduction of bone metabolism in stressful environment [72]. micro-CT (μCT) imaging were performed to investigate the alterations in multiple bone parameters using femurs. In *+/+* mice, the bone mass was remarkably reduced by stress-loading in the section of femur (Fig. 12D). The bone volume/total volume (BV/TV), which is a commonly used indicator as amount of bone mass, was significantly decreased in stress-loaded *+/+* (84.3%, $P<0.05$) (Fig. 12D). Furthermore, other bone parameters, bone surface (BS) and bone mineral contents (BMC), were also decreased (85.8%, $P<0.05$; and 78.9%, $P=0.07$ respectively) (Fig. 12D). However, *tro/tro* mice didn't show this decreasing tendency by stress-loading. These trends were concordant with blood ALP pattern, and this characteristic patterns might be reflect the internal insensitiveness against environmental stress.

4. DISCUSSION

The *xPou3f3* knock-in mice grew to adulthood, and no distinguishable abnormalities were observed. There were no changes in appearance, body weight, growth, or fertility. Brain weight per body weight did not differ between the wild-type (*+/+*) and the homozygous *xPou3f3* (*tro*/*tro*) mice. Further, no histologically abnormal changes were detected within the brain, and blood components did not show any symptoms of renal failure. The knock-in mice of *Brn-2/Pou3f2* gene, a paralogue of *Brn-1/Pou3f3*, showed a reduction of pup weaning ratio caused by abnormal retrieving behavior, in which the transcription factor *Brn-2/Pou3f2* was replaced with the *Xenopus tropicalis* orthologue lacking all of the homopolymeric amino acid repeats of mammalian POU3F2 or all of the homopolymeric amino acid repeats of mammalian POU3F2 were removed. Most of the pups born to these non-mammalized mice died within days after birth, depending on the dam genotype alone. Quantitative immunohistochemical analysis revealed significant decreases of tyrosine hydroxylase (TH) and tryptophan hydroxylase 2 (TPH2) in various brain structures (Fig. 6). TH and TPH2 are the rate-limiting enzymes of dopamine and serotonin synthesis, respectively. On the contrary, there was no deterioration of maternal behavior observed in *xPou3f3* knock-in mice, and the pups delivered from homozygous parents showed normal weaning ratios. But RNA-Seq data using whole brain showed decrease of TH and TPH2 also in the *xPou3f3* knock-in mice: 0.86-fold ($p>0.05$) and 0.43-fold ($p<0.01$) for TH and THP2, respectively (Fig. 6). Serotonin

are important for the regulation of various psychological and physiological functions, such as pleasant feelings, anxiety, fear, mood control, motivation, cognition, reward, and movement. Pre-pulse inhibition was significantly stronger in the *xPou3f3* knock-in mice than in wild-type mice, suggesting schizophrenia-like abnormalities.

Significantly longer immobility time in the *xPou3f3* knock-in mice was observed in both tail suspension test and forced swimming test than those in wild-type mice. Tail suspension test and forced swimming test are used for examining the effects of anti-depressant agents [54-56]. This means that the *xPou3f3* knock-in mice tend to be depressive. The hypothalamic-pituitary-adrenal axis (HPA axis) is a major part of the neuroendocrine system that controls reactions to stress, and is involved in mood disorders including depressive disorder [73, 74]. In addition, dopamine and serotonin are important in regulating the HPA axis [62]. The chronic stress including immobilization stress raises expression of precursor polypeptide of an adreno-corticotropic hormone released by pituitary gland, but the degree of the rise was significantly lower in the *xPou3f3* knock-in mice than in wild-type mice. In contrast, the chronic stress causes decrease of gene expression in various types of glutamate and GABA receptors in wild-type mice, whereas only few receptors showed decrease of gene expression in the *xPou3f3* knock-in mice. Furthermore, the immobilization stress is known to cause induction of various anti-oxidant enzymes [66, 75]. Among 111 anti-oxidant genes, 22 genes were up-regulated by the chronic stress in the wild-type mice, but only 4 genes were in the *xPou3f3* knock-in mice.

The present findings clearly indicate that the *xPou3f3* knock-in mice reduce their response against stress, showing the schizophrenia-like response and the depressed tendency. According to Hans Selye [76], "stress" is defined as the non-specific response of the body to any demand for change. The sympathetic nervous system becomes primarily active during a stress response, regulating many of the body's physiological functions in ways that ought to make an organism more adaptive to its environment. Compared with the wild-type mice, response level against stress was low in the *xPou3f3* knock-in mice. Two causes can be considered. One possibility is that disturbance of the biological balance/homeostasis caused by stressors is less in the non-mammalized mice. Another possibility is that the biological balance/homeostasis can be maintained with low responsiveness in the non-mammalized mice. In the former case, it can be considered that mammals have received higher influence from stressors of the same strength. The latter case means that mammals have acquired higher responsiveness against stressor of the same strength. Even in any case, there would be no doubt that response system to stressor has been drastically changed during mammalian evolution.

5. CONCLUSION

I generated non-mammalized mice (*xPou3f3* knock-in mice) in which the entire coding region of the murine *Pou3f3* gene was replaced with that of the amphibian (*Xenopus tropicalis*) orthologue. Both mouse and *Xenopus Brn-1/Pou3f3* genes are intron-less, and their amino acid sequences of the DNA-binding domain called POU domain are completely identical. Mammalian BRN-1/POU3F3 has eight homopolymeric amino acid repeats, each of which consists of alanine, glycine, histidine, and proline amino acid residues. In contrast, only two of these repeats are present in *Brn-1/Pou3f3* orthologues of amphibians and fishes. This remarkable feature is well conserved in both positions and numbers of the repeats among mammals, showing these repeats were acquired specifically in the mammalian lineage. Some types of homopolymeric amino acid repeats are known to modulate protein–protein interactions and/or transcriptional regulation.

Both homozygous and heterozygous *xPou3f3* knock-in mice grew to adulthood and appeared normal. There were no changes in appearance, body weight, growth, or fertility. Both the expression pattern and the expression level of the *xPou3f3* (*tro*) allele were similar to those of the wild-type (*+*) allele. Brain weight per body weight did not differ between *+/+* and *tro*/*tro* mice. Further, no histologically abnormal changes were detected within the brain. In *xPou3f3* knock-in mice, there was no deterioration of maternal behavior observed in *xPou3f2* knock-in mice, in which transcription factor *Brn-2/Pou3f2*, a paralogue of

Brn-1/Pou3f3, was replaced with the *Xenopus tropicalis* orthologue. However, pre-pulse inhibition of the *xPou3f3* knock-in mice was significantly stronger than that of wild-type mice, showing schizophrenia-like abnormalities. In addition, the *xPou3f3* knock-in mice showed significantly longer immobility time in both tail suspension test and forced swimming test than wild-type mice. This means that the *xPou3f3* knock-in mice tend to be depressive. Then, I exposed the mice to various kinds of chronic stress including immobilization stress, and performed measurement of various molecular indexes about the stress and comprehensive transcriptome analysis. The chronic stress raises expression of precursor polypeptide of an adrenocorticotropic hormone released by pituitary gland. In the *xPou3f3* knock-in mice, the degree of the rise was significantly lower than wild-type mice. In contrast, the chronic stress causes decrease of gene expression in various types of glutamate and GABA receptors. However, only few receptors showed decrease of gene expression in the *xPou3f3* knock-in mice. The immobilization stress is known to cause induction of various anti-oxidant enzymes. Among 111 anti-oxidant genes, 22 genes were up-regulated by the chronic stress in the wild-type mice, whereas only 4 genes were in the *xPou3f3* knock-in mice. 8-OHdG concentration of urine, an oxidative stress marker, increased by stress in the *xPou3f3* knock-in mice. This suggests that quick response against oxidative stress was not occurred. In addition, blood alkaline phosphatase and bone density decreased by chronic stress in the wild-type mice, but there were no changes in the *xPou3f3* mice. I clarified that the following influences were induced by replacing transcription factor *Brn-1/Pou3f3* of the

mouse with its orthologue of *Xenopus tropicalis*: (1) schizophrenia-like response and the depressed tendency, and (2) decreased response against stress.

6. ACKNOWLEDGEMENTS

I would like to acknowledgement my supervisor. Professor Shintaroh Ueda for a lot of instruction, assistance and encouragement to me throughout research. I would like to greatly appreciate Professor Nobuaki Yoshida, and technical staff Reiko Sakamoto of Laboratory of Developmental Genetics in Center for Experimental Medicine in the University of Tokyo for their collaboration to generate my knock-in mice. I also would like to appreciate Professor Koichi Matsuo and laboratory members of Laboratory of Cell and Tissue Biology in Keio University, Professor Gen Suwa of Laboratory of Paleoanthropology and Evolutionary Morphology, Associate Professor Kazuya Iwamoto of Department of Molecular Psychiatry in the University of Tokyo for collaboration to use biological measurement apparatus. I would like to appreciate Meguru Ito for construction of the targeting vector and Eri Sasayama and Haruka Seki for measurement of behavioral tests.

I would like to thank to Ueda Lab. members and all mice.

7. REFERENCES CITED

1. He X, Treacy MN, Simmons DM, Ingraham HA, Swanson LW, Rosenfeld MG. Expression of a large family of POU-domain regulatory genes in mammalian brain development. Nature. 1989 Jul 6;340(6228):35-41.
2. Alvarez-Bolado G, Rosenfeld MG, Swanson LW. Model of forebrain regionalization based on spatiotemporal patterns of POU-III homeobox gene expression, birthdates, and morphological features. J Comp Neurol. 1995 May 1;355(2):237-95.
3. Nakai S, Sugitani Y, Sato H, Ito S, Miura Y, Ogawa M, Nishi M, Jishage K, Minowa O, Noda T.Crucial roles of Brn1 in distal tubule formation and function in mouse kidney. Development. 2003 Oct;130(19):4751-9.
4. Castro DS, Skowronska-Krawczyk D, Armant O, Donaldson IJ, Parras C, Hunt C, Critchley JA, Nguyen L, Gossler A, Göttgens B, Matter JM, Guillemot F. Proneural bHLH and Brn proteins coregulate a neurogenic program through cooperative binding to a conserved DNA motif. Dev Cell. 2006 Dec;11(6):831-44.
5. Kuhlbrodt K, Herbarth B, Sock E, Enderich J, Hermans-Borgmeyer I, Wegner M. Cooperative Function of POU Proteins and SOX Proteins in Glial Cells. J Biol Chem. 1998 Jun 26;273(26):16050-7.
6. Kim DK, Han SB, Hong ST, Choi YJ, Sun W, Geum D, Kim H. Expression of Sox11 and Brn transcription factors during development and following transient forebrain ischemia in the rat. Neurosci Lett. 2008 Mar

15;433(3):259-64.

7. Sumiyama K, Washio-Watanabe K, Saitou N, Hayakawa T, Ueda S.Class III POU genes: generation of homopolymeric amino acid repeats under GC pressure in mammals. J Mol Evol. 1996 Sep;43(3):170-8.
8. Li XJ, Li SH, Sharp AH, Nucifora FC Jr, Schilling G, Lanahan A, Worley P, Snyder SH, Ross CA.A huntingtin-associated protein enriched in brain with implications for pathology. Nature. 1995 Nov 23;378(6555):398-402.
9. Himmelbauer H, Wedemeyer N, Haaf T, Wanker EE, Schalkwyk LC, Lehrach H. IRS-PCR-based genetic mapping of the huntingtin interacting protein gene (HIP1) on mouse chromosome 5. Mamm Genome. 1998 Jan;9(1):26-31.
10. Burke JR, Enghild JJ, Martin ME, Jou YS, Myers RM, Roses AD, Vance JM, Strittmatter WJ. Huntingtin and DRPLA proteins selectively interact with the enzyme GAPDH. Nat Med. 1996 Mar;2(3):347-50.
11. Matilla A1, Koshy BT, Cummings CJ, Isobe T, Orr HT, Zoghbi HY.The cerebellar leucine-rich acidic nuclear protein interacts with ataxin-1. Nature. 1997 Oct 30;389(6654):974-8.
12. Waragai M, Lammers CH, Takeuchi S, Imafuku I, Udagawa Y, Kanazawa I, Kawabata M, Mouradian MM, Okazawa H. PQBP-1, a novel polyglutamine tract-binding protein, inhibits transcription activation by Brn-2 and affects cell survival. Hum Mol Genet. 1999 Jun;8(6):977-987.
13. Carl UD, Pollmann M, Orr E, Gertlere FB, Chakraborty T, Wehland J. Aromatic and basic residues within the EVH1 domain of VASP specify its

interaction with proline-rich ligands. Curr Biol. 1999 Jul 1;9(13):715-718.

14. Gerber HP, Seipel K, Georgiev O, Höfferer M, Hug M, Rusconi S, Schaffner W. Transcriptional activation modulated by homopolymeric glutamine and proline stretches. Science. 1994 Feb 11;263(5148):808-11.
15. Galant R, Carroll SB.Evolution of a transcriptional repression domain in an insect Hox protein. Nature. 2002 Feb 21;415(6874):910-3.
16. Dunker A, Brown C, Lawson J, Iakoucheva L, Obradovi Z. 2002. Intrinsic disorder and protein function. Biochemistry 41:6573–6582.
17. Dyson HJ, Wright PE. Intrinsically unstructured proteins and their functions. Nat Rev Mol Cell Biol 2005; 6: 197-208.
18. Dunker AK, Cortese MS, Romero P, Iakoucheva LM, Uversky VN. Flexible nets: The roles of intrinsic disorder in protein interaction networks. FEBS Journal 2005; 272: 5129-48.
19. Edgar R.C. MUSCLE: multiple sequence alignment with high accuracy and high throughput. Nucleic Acids Res. 2004 Mar 19;32(5):1792-1797.
20. Tamura K, Stecher G, Peterson D, Filipski A, Kumar S. MEGA6: Molecular Evolutionary Genetics Analysis version 6.0. Mol. Biol. Evol. 2013 Dec;30(12):2725-9.
21. Larkin MA, Blackshields G, Brown NP, Chenna R, McGettigan PA, McWilliam H, Valentin F, Wallace IM, Wilm A, Lopez R, Thompson JD, Gibson TJ, Higgins DG. Clustal W and Clustal X version 2.0. Bioinformatics. 2007 Nov 1;23(21):2947-8.
22. Sutoo D, Akiyama K, Yabe K. A novel technique for quantitative

immunohistochemical imaging of various neurochemicals in a multiple-stained brain slice. J Neurosci Methods. 2002 Jul 30;118(1):41-50.

23. Sutoo D, Akiyama K, Yabe K. Quantitative mapping analyzer for determining the distribution of neurochemicals in the human brain. J Neurosci Methods. 1998 Dec 1;85(2):161-73.
24. Sutoo D, Akiyama K, Yabe K. Comparison analysis of distributions of tyrosine hydroxylase, calmodulin and calcium/calmodulin-dependent protein kinase II in a triple stained slice of rat brain. Brain Res. 2002 Apr 12;933(1):1-11.
25. Bahi A, Mineur YS, Picciotto MR. Blockade of protein phosphatase 2B activity in the amygdala increases anxiety- and depression-like behaviors in mice. Biol Psychiatry. 2009 Dec 15;66(12):1139-46.
26. Holmes A, Hollon TR, Gleason TC, Liu Z, Dreiling J, Sibley DR, Crawley JN. Behavioral characterization of dopamine D5 receptor null mutant mice. Behav Neurosci. 2001 Oct;115(5):1129-44.
27. Braff DL, Geyer MA. Sensorimotor gating and schizophrenia. Human and animal model studies. Arch Gen Psychiatry. 1990 Feb;47(2):181-8.
28. Seong E, Seasholtz AF, Burmeister M. Mouse models for psychiatric disorders. Trends Genet. 2002 Dec;18(12):643-50.
29. Porsolt RD, Anton G, Blavet N, Jalfre M. Behavioural despair in rats: a new model sensitive to antidepressant treatments. Eur J Pharmacol. 1978 Feb 15;47(4):379-91.
30. Mineur Y.S, Prasol D.J, Belzung C and C rusio W.E. Agonistic behavior and

unpredictable chronic mild stress in mice. Behav. Genet. (2003);33: 513–9.

31. Vyas A, Mitra R, Shankaranarayana Rao BS, Chattarji S. Chronic stress induces contrasting patterns of dendritic remodeling in hippocampal and amygdaloid neurons. J Neurosci. 2002 Aug 1;22(15):6810-8.
32. Miller LL, Ward SJ, Dykstra LA. Chronic unpredictable stress enhances cocaine-conditioned place preference in type 1 cannabinoid receptor knockout mice. Behav Pharmacol. 2008 Sep;19(5-6):575-81.
33. Pandey DK, Pati D, Joshi A, Mahesh R. Chronic unpredictable stress: possible animal model of comorbid depression. Int J Preclin Pham Res. 2010: 54-63
34. Feusner JD, Hembacher E, Phillips KA. The mouse who couldn't stop washing: pathologic grooming in animals and humans. CNS Spectr. 2009 Sep;14(9):503-13.
35. Greer JM, Capecchi MR. Hoxb8 is required for normal grooming behavior in mice. Neuron. 2002 Jan 3;33(1):23-34.
36. Jeong J, Li X, McEvilly RJ, Rosenfeld MG, Lufkin T, Rubenstein JL. Dlx genes pattern mammalian jaw primordium by regulating both lower jaw-specific and upper jaw-specific genetic programs. Development. 2008 Sep;135(17):2905-16.
37. Sugitani Y, Nakai S, Minowa O, Nishi M, Jishage K, Kawano H, Mori K, Ogawa M, Noda T. Brn-1 and Brn-2 share crucial roles in the production and positioning of mouse neocortical neurons. Genes Dev. 2002 Jul 15;16(14):1760-5.

38. McEvilly RJ, de Diaz MO, Schonemann MD, Hooshmand F, Rosenfeld MG: Transcriptional regulation of cortical neuron migration by POU domain factors. Science (2002) 295:1528-1532.

39. Nasu M, Yada S, Igarashi A, Sutoo D, Akiyama K, Ito M, Yoshida N, Ueda S. Mammalian-specific sequences in *pou3f2* contribute to maternal behavior. Genome Biol Evol. 2014 Apr 7;6(5):1145-56.

40. Hansen S, Harthon C, Wallin E, Löfberg L, Svensson K. The effects of 6-OHDA-induced dopamine depletions in the ventral or dorsal striatum on maternal and sexual behavior in the female rat. Pharmacol Biochem Behav. 1991 May;39(1):71-7.

41. Keer SE, Stern JM. Dopamine receptor blockade in the nucleus accumbens inhibits maternal retrieval and licking, but enhances nursing behavior in lactating rats. Physiol Behav. 1999 Nov;67(5):659-69.

42. Numan M, Numan MJ, Pliakou N, Stolzenberg DS, Mullins OJ, Murphy JM, Smith CD. The effects of D1 or D2 dopamine receptor antagonism in the medial preoptic area, ventral pallidum, or nucleus accumbens on the maternal retrieval response and other aspects of maternal behavior in rats. Behav Neurosci. 2005 Dec;119(6):1588-604.

43. Lerch-Haner JK, Frierson D, Crawford LK, Beck SG, Deneris ES. Serotonergic transcriptional programming determines maternal behavior and offspring survival. Nat Neurosci. 2008 Sep;11(9):1001-3.

44. Alenina N, Kikic D, Todiras M, Mosienko V, Qadri F, Plehm R, Boyé P, Vilianovitch L, Sohr R, Tenner K, Hörtnagl H, Bader M. Growth retardation

and altered autonomic control in mice lacking brain serotonin. Proc Natl Acad Sci U S A. 2009 Jun 23;106(25):10332-7.

45. Zhao C, Li M. c-Fos identification of neuroanatomical sites associated with haloperidol and clozapine disruption of maternal behavior in the rat. Neuroscience. 2010 Apr 14;166(4):1043-55.

46. van Velzen A1, Toth M. Role of maternal 5-HT(1A) receptor in programming offspring emotional and physical development. Genes Brain Behav. 2010 Nov;9(8):877-85.

47. Prinssen EP, Ballard TM, Kolb Y, Nicolas LB. The effects of serotonin reuptake inhibitors on locomotor activity in gerbils. Pharmacol Biochem Behav. 2006 Sep;85(1):44-9.

48. Heisler LK, Tecott LH. A paradoxical locomotor response in serotonin 5-HT(2C) receptor mutant mice. J Neurosci. 2000 Apr 15;20(8):RC71.

49. Arango V, Underwood MD, Mann JJ. Serotonin brain circuits involved in major depression and suicide. Prog Brain Res. 2002;136:443-53.

50. Gao J, Pan Z, Jiao Z, Li F, Zhao G, Wei Q, Pan F, Evangelou E. TPH2 gene polymorphisms and major depression--a meta-analysis. PLoS One. 2012;7(5):e36721. Deficient serotonin neurotransmission and depression-like serotonin biomarker alterations in tryptophan hydroxylase 2 (Tph2) loss-of-function mice. Mol Psychiatry. 2012 Jul;17(7):694-704.

51. Jacobsen JP, Siesser WB, Sachs BD, Peterson S, Cools MJ, Setola V, Folgering JH, Flik G, Caron MG.

52. Pum ME, Huston JP, Müller CP. The role of cortical serotonin in anxiety and

locomotor activity in Wistar rats. Behav Neurosci. 2009 Apr;123(2):449-54.

53. Holmes A, Lit Q, Murphy DL, Gold E, Crawley JN. Abnormal anxiety-related behavior in serotonin transporter null mutant mice: the influence of genetic background. Genes Brain Behav. 2003 Dec;2(6):365-80.

54. Porsolt RD, Anton G, Blavet N, Jalfre M. Behavioural despair in rats: a new model sensitive to antidepressant treatments. Eur J Pharmacol. 1978 Feb 15;47(4):379-91.

55. Abelaira HM, Réus GZ, Quevedo J. Animal models as tools to study the pathophysiology of depression. Rev Bras Psiquiatr. 2013;35 Suppl 2:S112-20.

56. Dumen CH. Models of depression. Vitam Horm. 2010;82:1-21.

57. McEwen BS. The neurobiology of stress: from serendipity to clinical relevance. Brain Res. 2000 Dec 15;886(1-2):172-189.

58. Haque Z, Akbar N, Yasmin F, Haleem MA, Haleem DJ. Inhibition of immobilization stress-induced anorexia, behavioral deficits, and plasma corticosterone secretion by injected leptin in rats. Stress. 2013 May;16(3):353-62.

59. Gocmez SS, Yazir Y, Sahin D, Karadenizli S, Utkan T. The effect of a selective neuronal nitric oxide synthase inhibitor 3-bromo 7-nitroindazole on spatial learning and memory in rats. Pharmacol Biochem Behav. 2015 Jan 28;131C:19-25.

60. Freund TF, Buzsáki G. Interneurons of the hippocampus. Hippocampus. 1996;6(4):347-470.

61. Magariños AM, Deslandes A, McEwen BS. Effects of antidepressants and

benzodiazepine treatments on the dendritic structure of CA3 pyramidal neurons after chronic stress. Eur J Pharmacol. 1999 Apr 29;371(2-3):113-22.

62. McEwen BS, Sapolsky RM. Stress and cognitive function. Curr Opin Neurobiol. 1995 Apr;5(2):205-16.

63. Polleux F, Ince-Dunn G, Ghosh A. Transcriptional regulation of vertebrate axon guidance and synapse formation. Nat Rev Neurosci. 2007 May;8(5):331-40.

64. Elchuri S, Oberley TD, Qi W, Eisenstein RS, Jackson Roberts L, Van Remmen H, Epstein CJ, Huang TT. CuZnSOD deficiency leads to persistent and widespread oxidative damage and hepatocarcinogenesis later in life. Oncogene. 2005 Jan 13;24(3):367-80.

65. Bhattacharya A, Ghosal S, Bhattacharya SK. Anti-oxidant effect of Withania somnifera glycowithanolides in chronic footshock stress-induced perturbations of oxidative free radical scavenging enzymes and lipid peroxidation in rat frontal cortex and striatum. J Ethnopharmacol. 2001 Jan;74(1):1-6.

66. Kim ST, Choi JH, Chang JW, Kim SW, Hwang O. Immobilization stress causes increases in tetrahydrobiopterin, dopamine, and neuromelanin and oxidative damage in the nigrostriatal system. J Neurochem. 2005 Oct;95(1):89-98.

67. McIntosh L.J, Sapolsky R.M. Glucocorticoids increase the accumulation of reactive oxygen species and enhance adriamycin-induced toxicity in neuronal culture. Exp. Neurol. 1996 Oct;141(2):201-206.

68. Ho E, Karimi Galougahi K, Liu CC, Bhindi R, Figtree GA.Biological markers of oxidative stress: Applications to cardiovascular research and practice. Redox Biol. 2013 Oct 8;1(1):483-91.

69. Wu LL, Chiou CC, Chang PY, Wu JT. Urinary 8-OHdG: a marker of oxidative stress to DNA and a risk factor for cancer, atherosclerosis and diabetics. Clin Chim Acta. 2004 Jan;339(1-2):1-9.

70. Fujita H, Sakamoto T, Komatsu K, Fujishima H, Morii T, Narita T, Takahashi T, Yamada Y. Reduction of circulating superoxide dismutase activity in type 2 diabetic patients with microalbuminuria and its modulation by telmisartan therapy. Hypertens Res. 2011 Dec;34(12):1302-8.

71. Watts NB. Clinical utility of biochemical markers of bone remodeling. Clin Chem. 1999 Aug;45(8 Pt 2):1359-68.

72. Togari A, Arai M, Kondo A. The role of the sympathetic nervous system in controlling bone metabolism. Expert Opin Ther Targets. 2005 Oct;9(5):931-40.

73. McEwen BS. Glucocorticoids, depression, and mood disorders: structural remodeling in the brain. Metabolism. 2005 May;54(5 Suppl 1):20-3.

74. Duman RS, Monteggia LM. A neurotrophic model for stress-related mood disorders. Biol Psychiatry. 2006 Jun 15;59(12):1116-27.

75. Sahin E, Gümüşlü S. Immobilization stress in rat tissues: Alterations in protein oxidation, lipid peroxidation and antioxidant defense system. Comp Biochem Physiol C Toxicol Pharmacol. 2007 Jan;144(4):342-7.

76. Selye H: Stress without distress. New York: Signet; 1974.

8. TABLE AND FIGURES

Table.1. List of vertebrate POU3F3 amino acids

POU3F3 amino acid sequences were acquired from the web database, Ensembl and NCBI. 28 POU3F3 transcripts were chosen and used for the multiple alignments. This table consists of the sequences in six mammals (orange), a bird (yellow), two reptiles (purple), two amphibians (green) and nine fishes (blue). Teleost POU3F3 were duplicated by the event of the whole genome duplication. The species names, accession gene names, accession numbers and amino acid length were described above.

Species	Accession name	Accession No.	Length
Homo sapiens	POU3F3	ENST00000361360	500aa
Mus musculus	Pou3f3	ENSMUST00000054883	497aa
Rattus norvegicus	Pou3f3	NP_620192.1	497aa
Heterocephalus glaber	Pou3f3	XP_004844534.1	491aa
Odobenus rosmarus divergens	POU3F3	XP_004416018.1	499aa
Monodelphis domestica	POU3F3	XP_007501474.1	515aa
Pseudopodoces humilis	POU3F3	XP_005516615.1	439aa
Anolis carolinensis	POU3F3	ENSACAT00000008913	454aa
Chrysemys picta bellii	POU3F3	XP_005307059.2	440aa
Xenopus tropicalis	*POU3f3-like*	XP_002941201	448aa
Ambystoma mexicanum	*POU domain transcription factor brn-1*	AAL27274	403aa
Latimeria chalumnae	POU3F3	ENSLACT00000017081	428aa
Danio rerio	pou1/zp23	ENSDART00000149202	425aa
	pou12/zp12	ENSDART00000133178	429aa
Gadus morhua	pou12	ENSGMOT00000017210	385aa
	pou23	ENSGMOT00000013837	391aa
Xiphophorus maculatus	brn1	ENSXMAT00000016283	388aa
	pou23	ENSXMAT00000011624	357aa
Poecilia formosa	brn1	ENSPFOT00000013732	435aa
	pou23	ENSPFOT00000015392	381aa
Gasterosteus aculeatus	pou12	ENSGACT00000018144	401aa
	pou23	ENSGACT00000003930	390aa
Oreochromis niloticus	brn1	ENSONIT00000016936	442aa
	pou23	ENSONIT00000025755	416aa
Tetraodon nigroviridis	brn1	ENSTNIT00000006199	397aa
	pou23	ENSTNIT00000002312	391aa
Takifugu rubripes	brn1	ENSTRUT00000026821	438aa
	Brn23	ENSTRUT00000026822	306aa

Fig.1 Comparative analysis of the alignment and phylogenic tree

A. Multiple alignment between 28 POU3F3 amino acid sequences. The six mammalian, an avian, two reptilian, two amphibian and seventeen fish POU3F3 amino acid sequences are displayed. The purple boxes indicated highly conserved POU-specific and POU-homeo domains. The conservation scores are represented as three characters (* > : > .) above each amino acid residue.

B. Neighbour-joining phylogenic tree based on 28 vertebrate POU3F3. Each species is indicated using color markers, mammal: red circle, bird: yellow inverted triangle, reptile: purple triangle, amphibian: green diamond and fish: blue square (filled and unfilled). Numbers at each node are the percentage of the 1000 bootstrap replicates.

C. Multiple alignment between 10 POU3F3 amino acid sequences in tetrapods. The black boxes indicated mammalian homopolymeric amino acid repeats. The purple boxes indicated POU-specific and POU-homeo domains. The conservation scores are represented as three characters (* > : > .) above each amino acid residue.

D. Neighbour-joining phylogenic tree based on 10 tetrapods POU3F3. Each species was indicated using color markers, mammal: red circle, bird: yellow inverted triangle, reptile: purple triangle, and amphibian: green diamond. Numbers at each node are the percentage of the 1000 bootstrap replicates.

E. Multiple alignment among POU class III genes, POU3F1, POU3F2, POU3F3 and POU3F4. POU3F1 have six (red), POU3F2 have three (blue) and POU3F3 have seven (black) HPAA repeats. In contrast, POU3F4 have no HPAA repeats. The purple boxes indicated POU-specific and POU-homeo domains.

A.

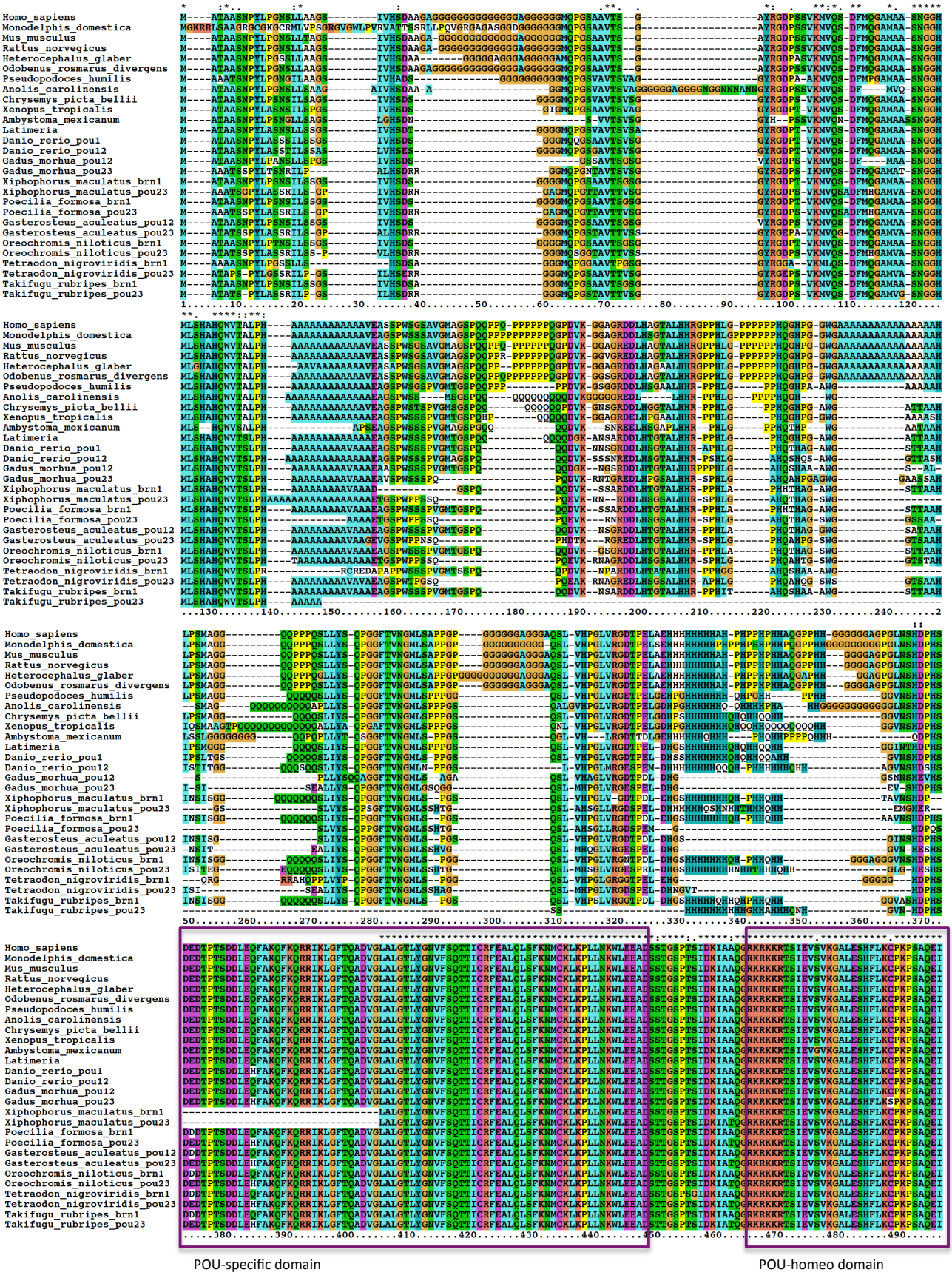
Homo_sapiens
Monodelphis_domestica
Mus_musculus
Rattus_norvegicus
Heterocephalus_glaber
Odobenus_rosmarus_divergens
Pseudopodoces_humilis
Anolis_carolinensis
Chrysemys_picta_bellii
Xenopus_tropicalis
Ambystoma_mexicanum
Latimeria
Danio_rerio_pou1
Danio_rerio_pou12
Gadus_morhua_pou12
Gadus_morhua_pou23
Xiphophorus_maculatus_brn1
Xiphophorus_maculatus_pou23
Poecilia_formosa_brn1
Poecilia_formosa_pou23
Gasterosteus_aculeatus_pou12
Gasterosteus_aculeatus_pou23
Oreochromis_niloticus_brn1
Oreochromis_niloticus_pou23
Tetraodon_nigroviridis_brn1
Tetraodon_nigroviridis_pou23
Takifugu_rubripes_brn1
Takifugu_rubripes_pou23
POU-specific domain
POU-homeo domain

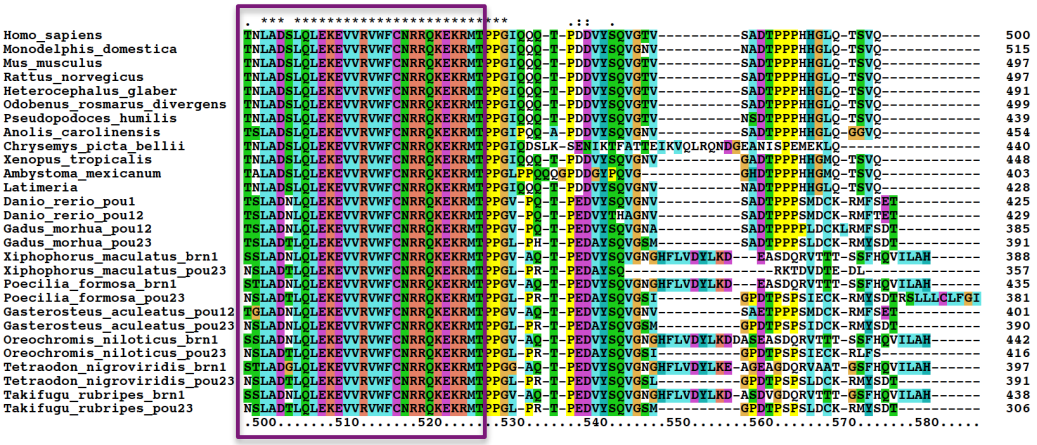
Homo_sapiens
Monodelphis_domestica
Mus_musculus
Rattus_norvegicus
Heterocephalus_glaber
Odobenus_rosmarus_divergens
Pseudopodoces_humilis
Anolis_carolinensis
Chrysemys_picta_bellii
Xenopus_tropicalis
Ambystoma_mexicanum
Latimeria
Danio_rerio_pou1
Danio_rerio_pou12
Gadus_morhua_pou12
Gadus_morhua_pou23
Xiphophorus_maculatus_brn1
Xiphophorus_maculatus_pou23
Poecilia_formosa_brn1
Poecilia_formosa_pou23
Gasterosteus_aculeatus_pou12
Gasterosteus_aculeatus_pou23
Oreochromis_niloticus_brn1
Oreochromis_niloticus_pou23
Tetraodon_nigroviridis_brn1
Tetraodon_nigroviridis_pou23
Takifugu_rubripes_brn1
Takifugu_rubripes_pou23
.500.....510.....520.....530.....540.....550.....560.....570.....580.....

B.

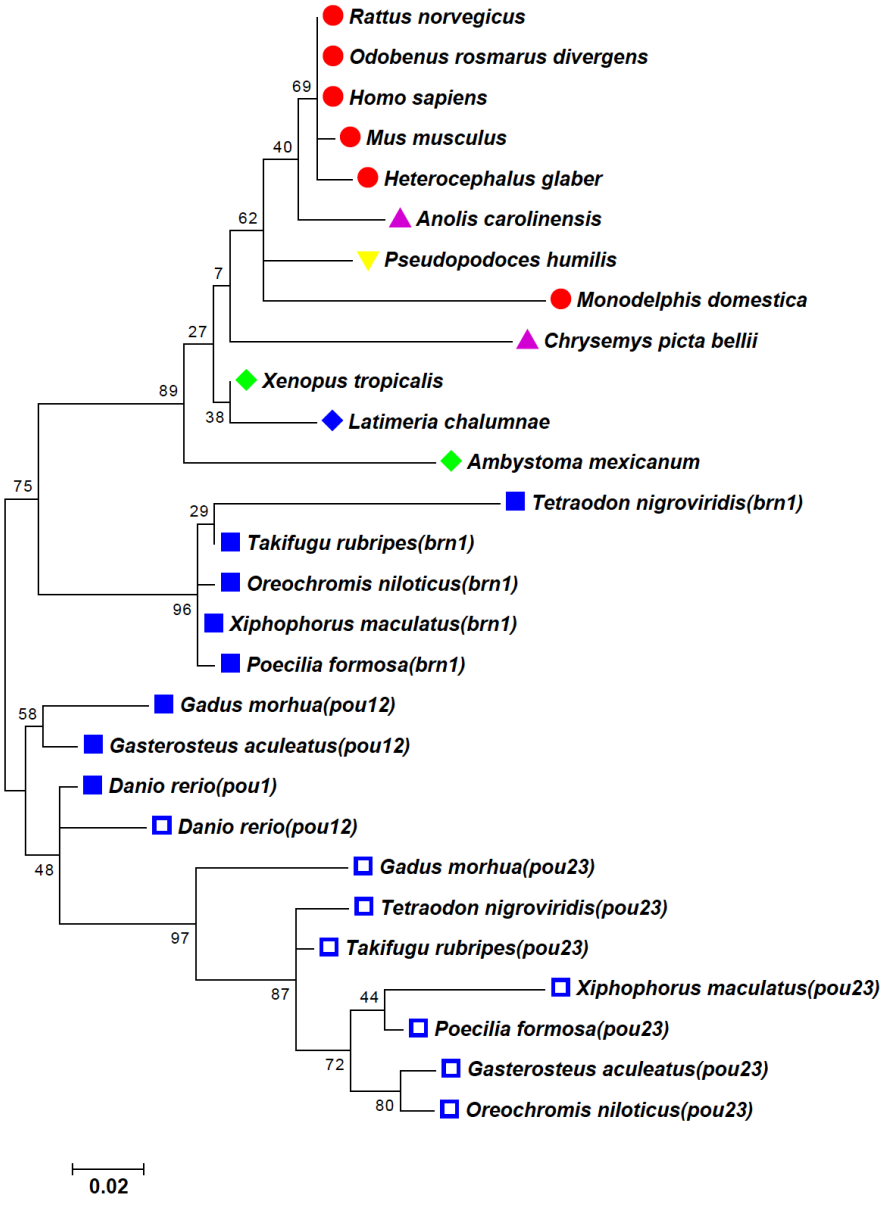
Rattus norvegicus
Odobenus rosmarus divergens
Homo sapiens
Mus musculus
Heterocephalus glaber
Anolis carolinensis
Pseudopodoces humilis
Monodelphis domestica
Chrysemys picta bellii
Xenopus tropicalis
Latimeria chalumnae
Ambystoma mexicanum
Tetraodon nigroviridis(brn1)
Takifugu rubripes(brn1)
Oreochromis niloticus(brn1)
Xiphophorus maculatus(brn1)
Poecilia formosa(brn1)
Gadus morhua(pou12)
Gasterosteus aculeatus(pou12)
Danio rerio(pou1)
Danio rerio(pou12)
Gadus morhua(pou23)
Tetraodon nigroviridis(pou23)
Takifugu rubripes(pou23)
Xiphophorus maculatus(pou23)
Poecilia formosa(pou23)
Gasterosteus aculeatus(pou23)
Oreochromis niloticus(pou23)
69
40
62
7
27
89
38
75
29
96
58
48
97
87
44
72
80
0.02

C.

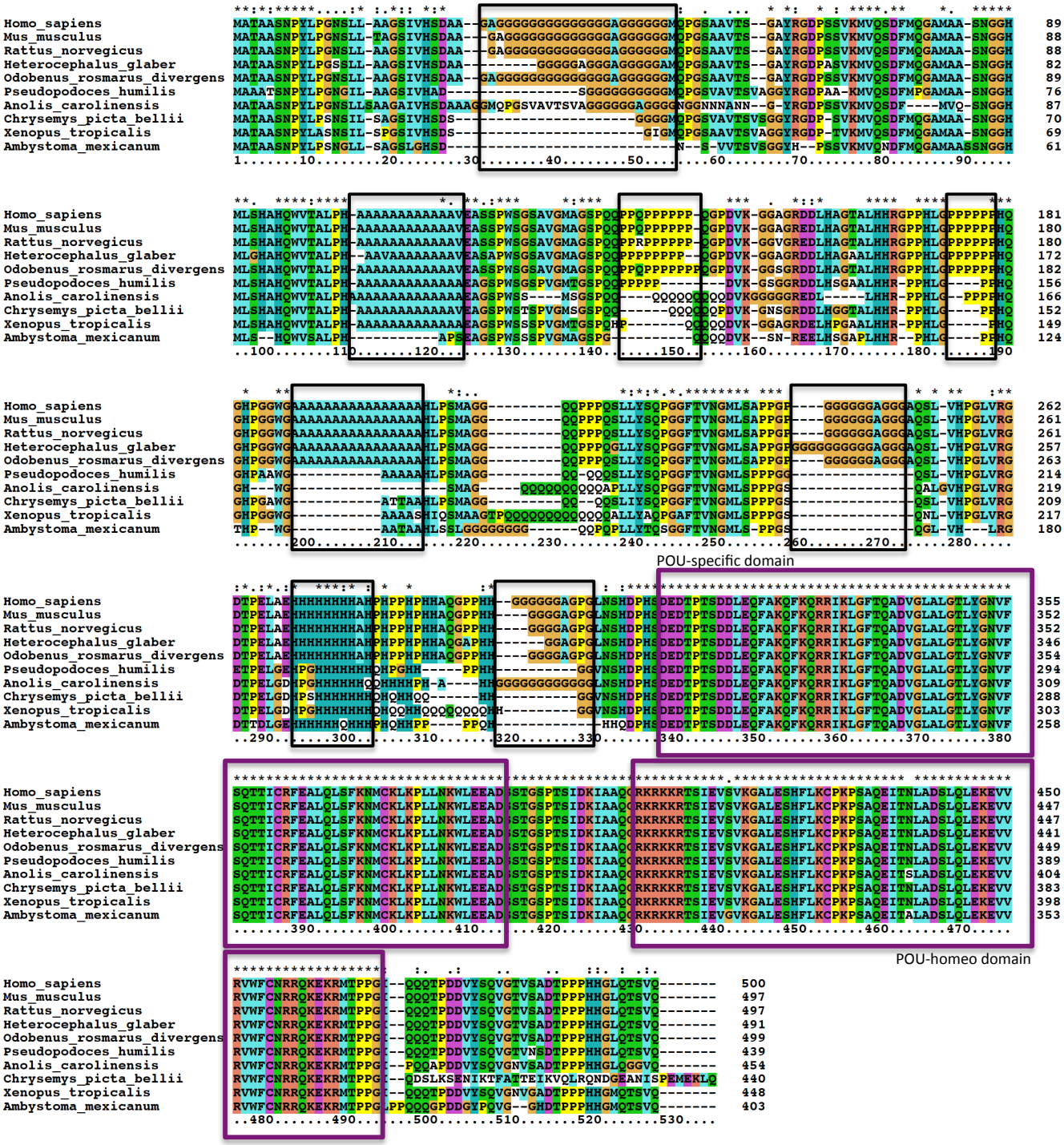
Homo_sapiens
Mus_musculus
Rattus_norvegicus
Heterocephalus_glaber
Odobenus_rosmarus_divergens
Pseudopodoces_humilis
Anolis_carolinensis
Chrysemys_picta_bellii
Xenopus_tropicalis
Ambystoma_mexicanum
POU-specific domain
POU-homeo domain

D.

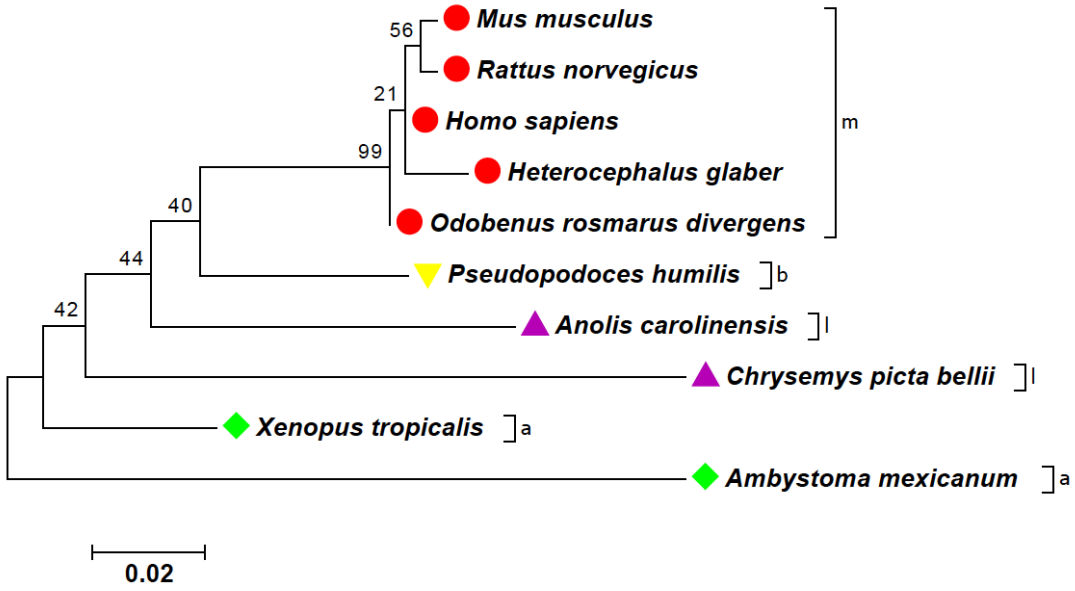
Mus musculus
Rattus norvegicus
Homo sapiens
Heterocephalus glaber
Odobenus rosmarus divergens
Pseudopodoces humilis
Anolis carolinensis
Chrysemys picta bellii
Xenopus tropicalis
Ambystoma mexicanum
56
21
99
40
44
42
m
b
l
l
a
a
0.02

E.

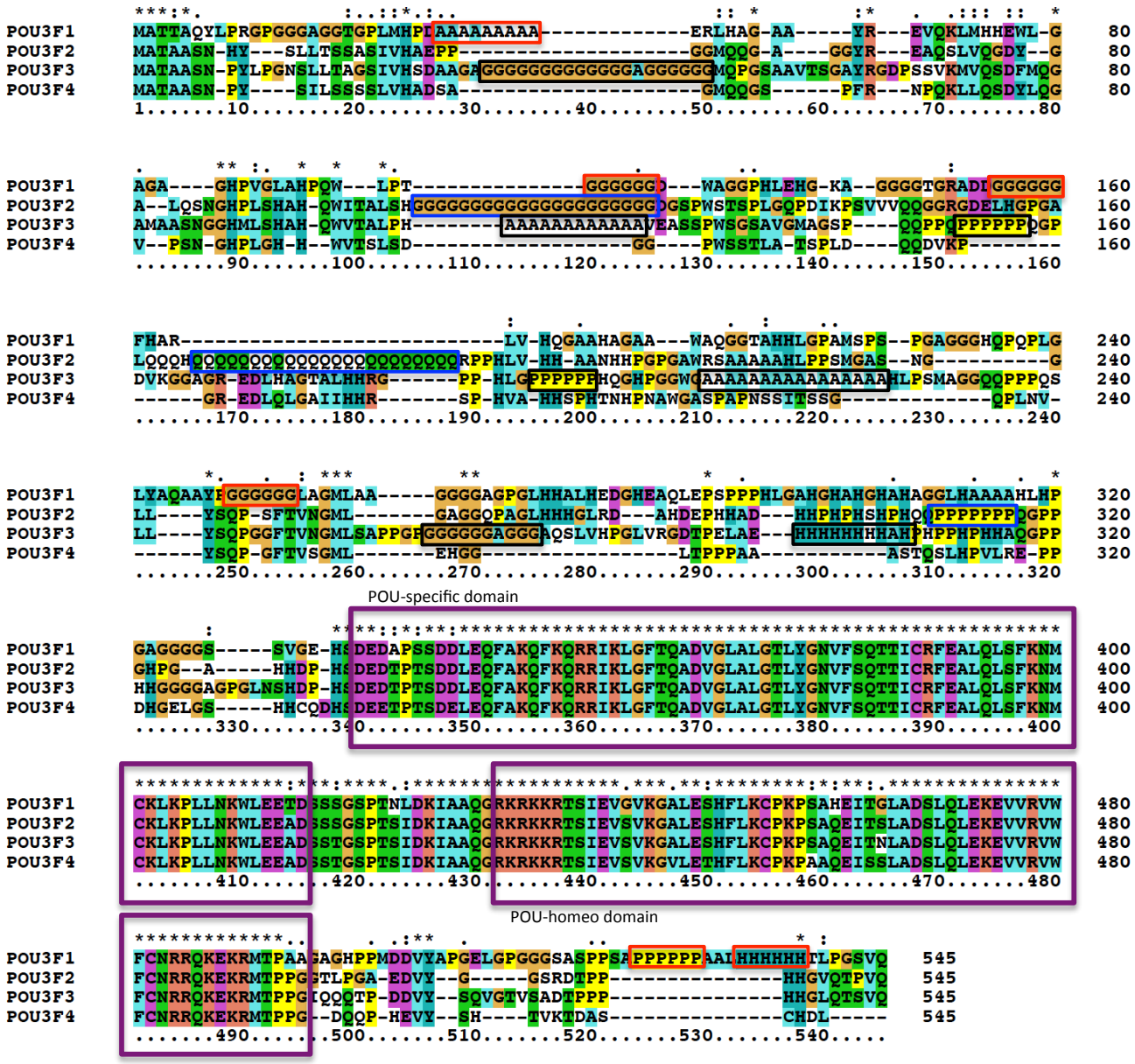

Fig.2 Generation of *xPou3f3* knock-in mice

A. Schematic drawing of *Pou3f3* genomic regions in *Mus musculus* and *Xenopus tropicalis*. Orange and light blue cylindrical boxes represent *Mus musculus Pou3f3* and *Xenopus tropicalis Pou3f3* respectively. Purple cylindrical boxes shows POU-specific and POU-homeo domains linked by 17 amino acids in the linker region. N-terminal regions contain variable homopolymeric amino acid repeats (red). In comparison of repetitive structures, the 8 homopolymeric amino acid repeats in *H. sapiens* (top), 7 in *M. musculus* (middle), and only 2 in *X. tropicalis* (bottom) exist in each POU3F3 orthologue.

B. Targeting vector (TV) construction and knock-in strategy. *xPou3f3* TV contains negative (diphtheria toxin A; *DT-A*) and positive (neomycin resistance gene; *Neo*^{r}) selection markers. Blue characters and bars indicate expected fragment size recognized by 5' or 3' probe in the digestion of each restriction enzyme (*Eco*81I and *Bam*HI).

C. 1st screening by Southern blot hybridization. Expected fragment sizes using 5'probe altered to 15,656 bp from 10,119 bp (*Eco*81I) (left). Expected fragment sizes using 3'probe altered to 5,844 bp from 10,858 bp (*Bam*HI) (right). Two ES clones (#14 and #25) were displayed double bands located in the positions of wild-type and targeted allele.

D. 2nd screening by Southern blot hybridization. Expected fragment sizes using 5'probe altered to 13,533 bp from 15,656 bp (*Eco*81I) (left). Expected fragment sizes using 3'probe altered to 3,915 bp from 5,844 bp (*Bam*HI) (right). #100 and #84 of pIC-Cre-electroporated ES clones derived from #14 and #25, respectively, were displayed double bands located in the positions of wild-type and *xPou3f3* knock-in allele.

A.

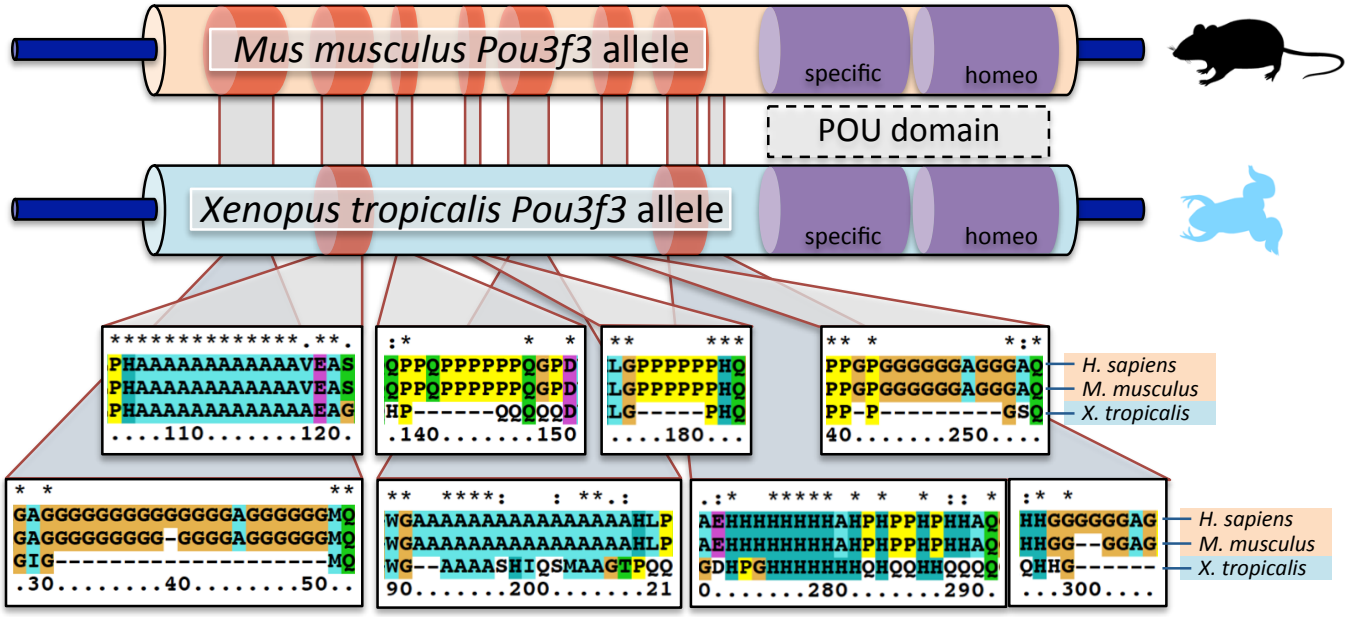
Mus musculus Pou3f3 allele
specific
homeo
POU domain
Xenopus tropicalis Pou3f3 allele
specific
homeo
H. sapiens
M. musculus
X. tropicalis
H. sapiens
M. musculus
X. tropicalis

B.

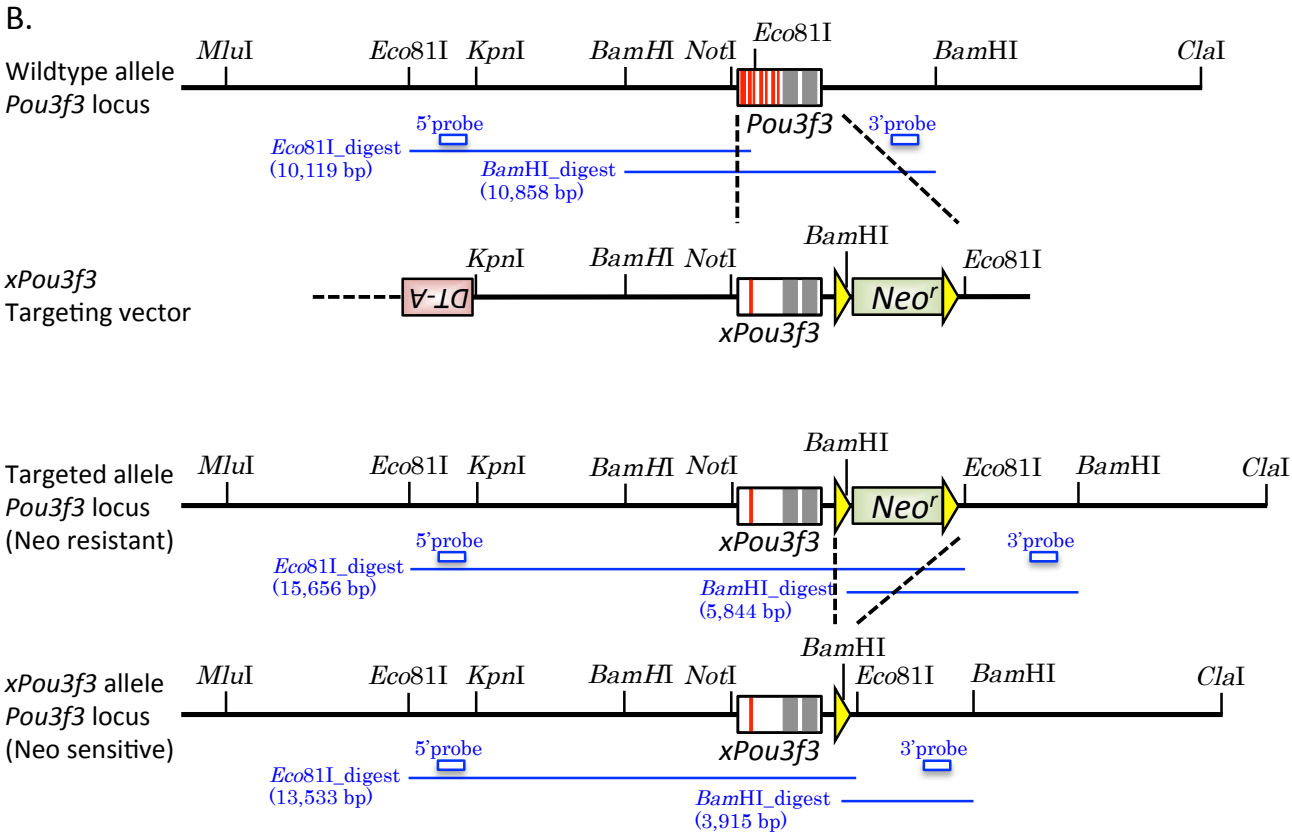
Wildtype allele
Pou3f3 locus
MluI
Eco81I
KpnI
BamHI
NotI
Eco81I
BamHI
ClaI
Pou3f3
5'probe
3'probe
Eco81I_digest
(10,119 bp)
BamHI_digest
(10,858 bp)
xPou3f3
Targeting vector
KpnI
BamHI
NotI
BamHI
Eco81I
DT-A
Neor
xPou3f3
Targeted allele
Pou3f3 locus
(Neo resistant)
MluI
Eco81I
KpnI
BamHI
NotI
BamHI
Eco81I
BamHI
ClaI
Neor
xPou3f3
5'probe
3'probe
Eco81I_digest
(15,656 bp)
BamHI_digest
(5,844 bp)
xPou3f3 allele
Pou3f3 locus
(Neo sensitive)
MluI
Eco81I
KpnI
BamHI
NotI
BamHI
Eco81I
BamHI
ClaI
xPou3f3
5'probe
3'probe
Eco81I_digest
(13,533 bp)
BamHI_digest
(3,915 bp)

C. 1st screening

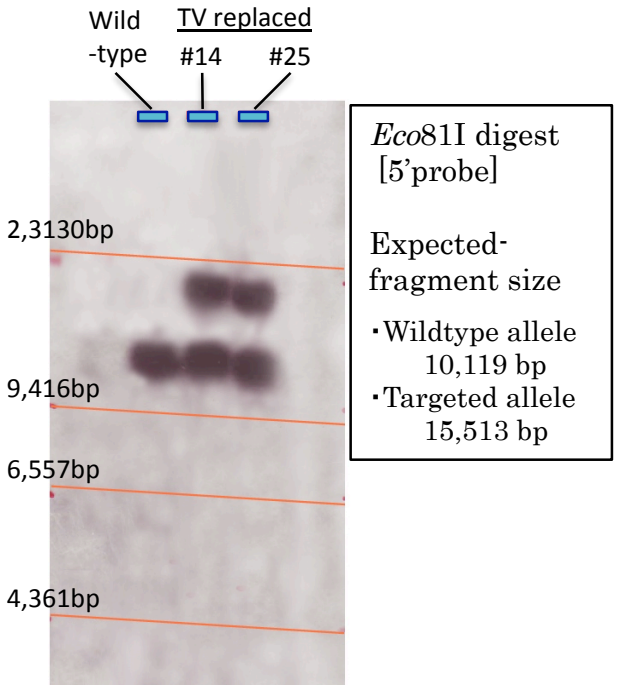

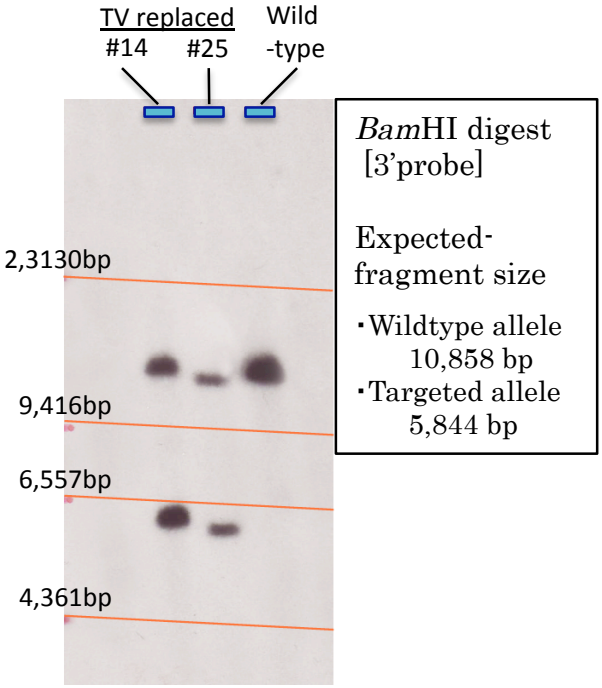

D. 2nd screening

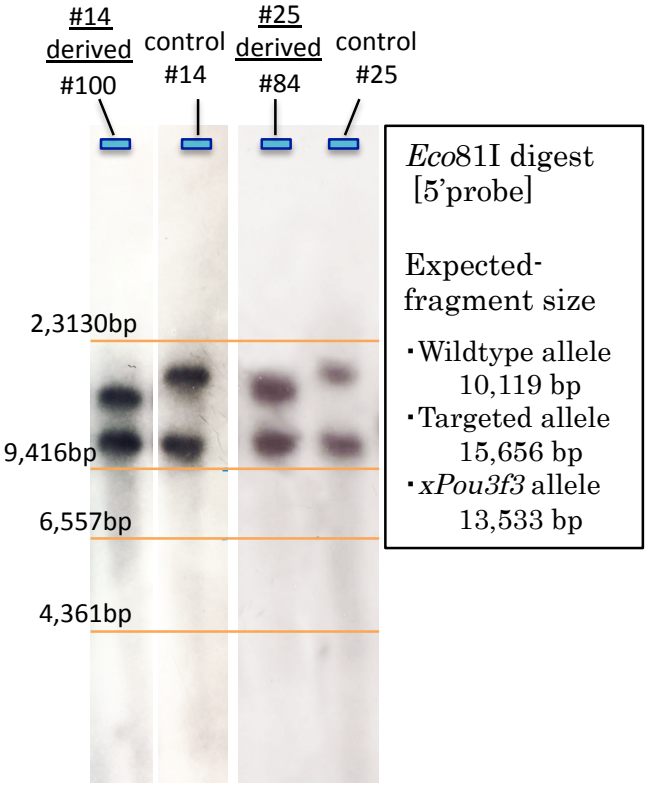

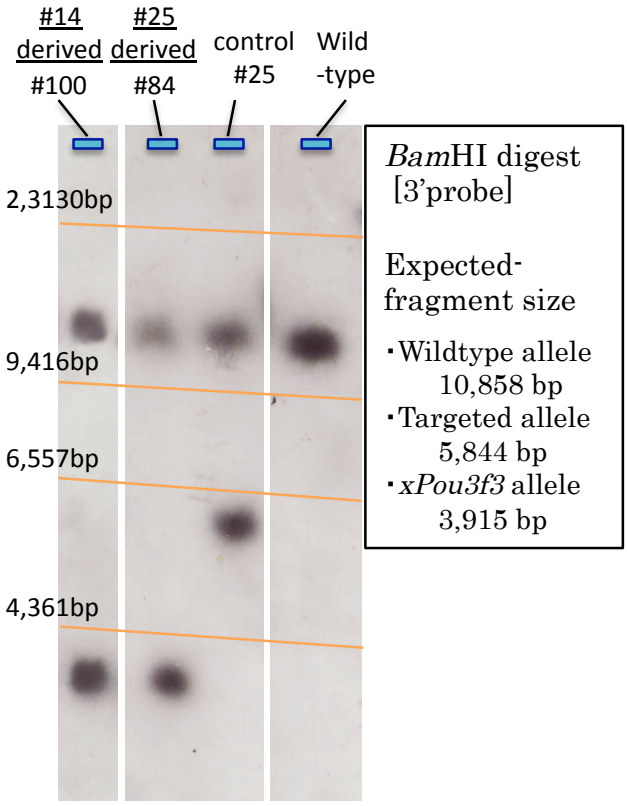

Fig.3. Morphological characters of *xPou3f3* knock-in mice

A. The comparison of body size at the age of 4 weeks age. *+/+* (left), *+/tro* (middle) and *tro/tro* (right) do not show obvious abnormalities.

B. Body weights. No significant differences in body weight between the three genotypes in 10 weeks of age.

C. Phenotype checking around facial area. At 10 weeks of age, no facial barbering, alopecia, eye abnormality and hydrocephalus were not observed.

D. Head skeleton in developmental day of E16.5 *+/+* and *tro/tro* mice stained with Alcian Blue (cartilage) and Alizarin Red (bone). Any retardation of ossification, bone loss and abnormal bone development were not observed. Figures show bone positional relationship about cranial bone (upper) and costal bone (lower). Each structure is shown with abbreviations: SQ, squamosal bone; LO, lamina obturans; PA, Parietal bone; FN, frontal bone; DE, dentary.

A.

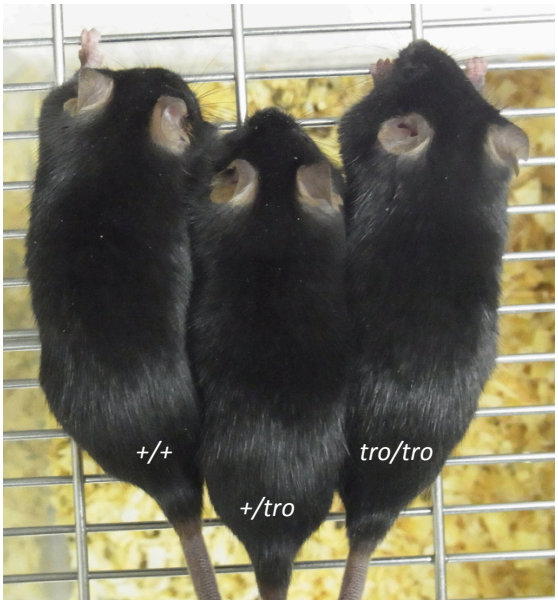
+/+
+/tro
tro/tro

B.

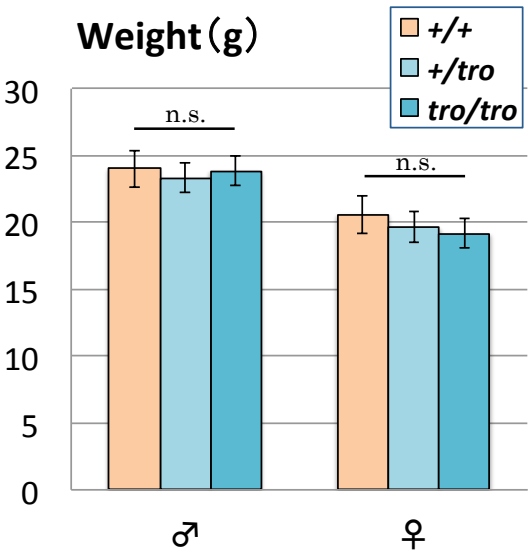
Weight (g)
+/+
+/tro
tro/tro
30
25
20
15
10
5
0
n.s.
n.s.
♂
♀

C.

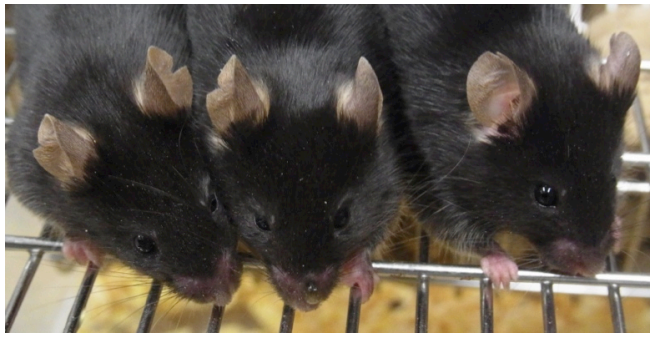

D.

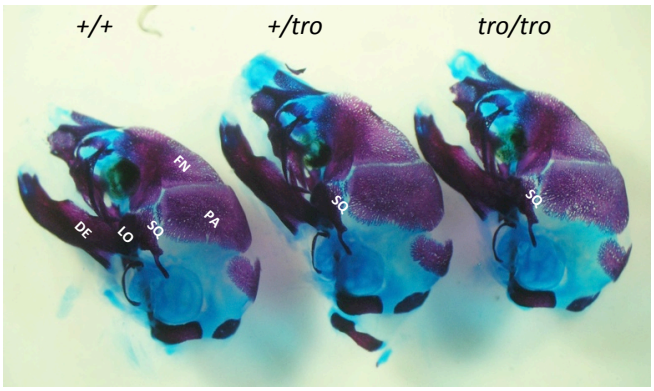
+/+
+/tro
tro/tro
FN
PA
SQ
DE
LO
SQ
SQ

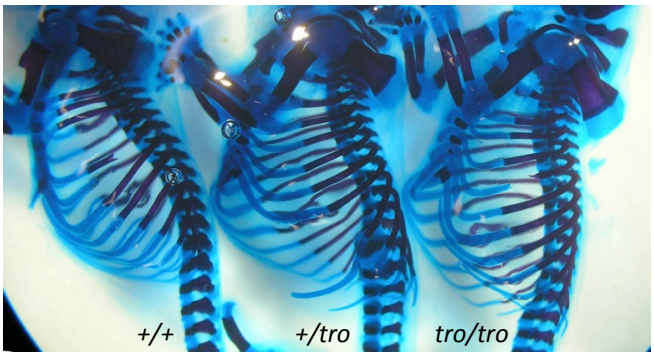
+/+
+/tro
tro/tro

Fig.4. The typical brain sectional analysis

A -C. HE staining of brain section in *+/+* (A), *+/tro* (B) and *tro/tro* (C). Remarkable brain atrophy (reported in *Pou3f2/Pou3f3* double knock-out mouse [37]) and ectopic layer formation (reported in *Pou3f3* knock-out mouse [38]) were not observed. Abbreviations: Cer, cerebellum; Cor, Cortex; Hip, Hippocampus; Ol, Olfactory bulb; Str, Neostriatum; Tha, Thalamus.

D -F. Confocal images of immuno-histochemical fluorescent staining using *Pou3f3* antibody in the neocortex (D), neostriatum (E), nucleus accumbens (F) and hypothalamus (G). The left figures showed immunohistochemical staining in *+/+* and the right figures showed that in *tro/tro* mice.

A.

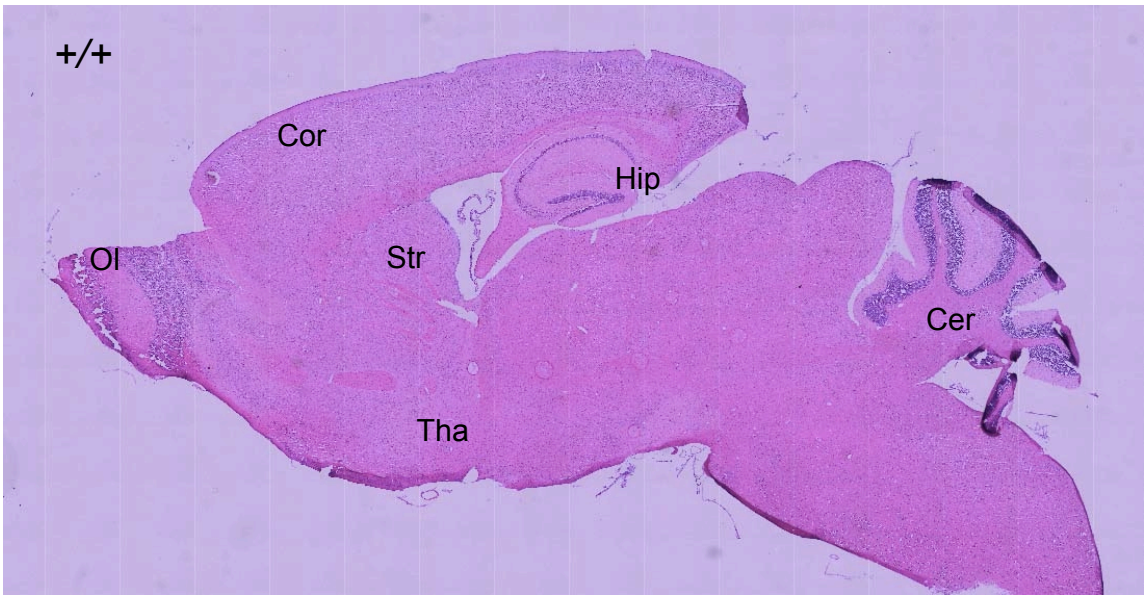

B.

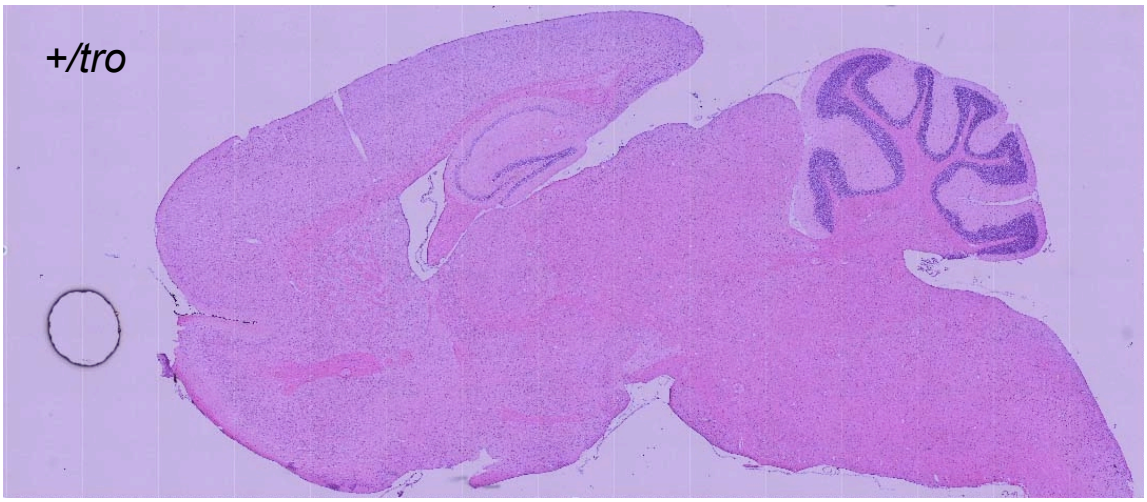

C.

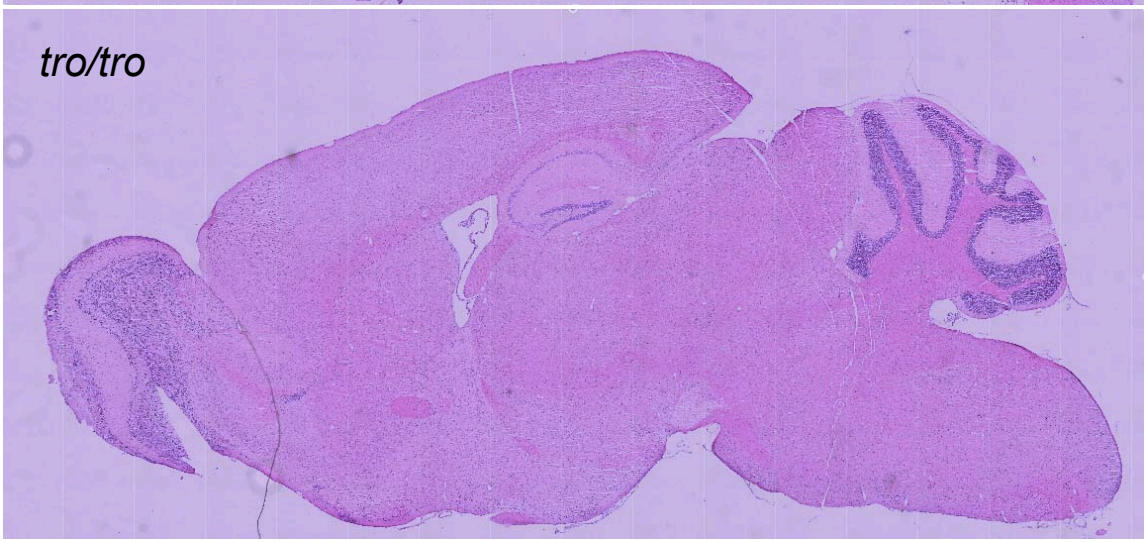

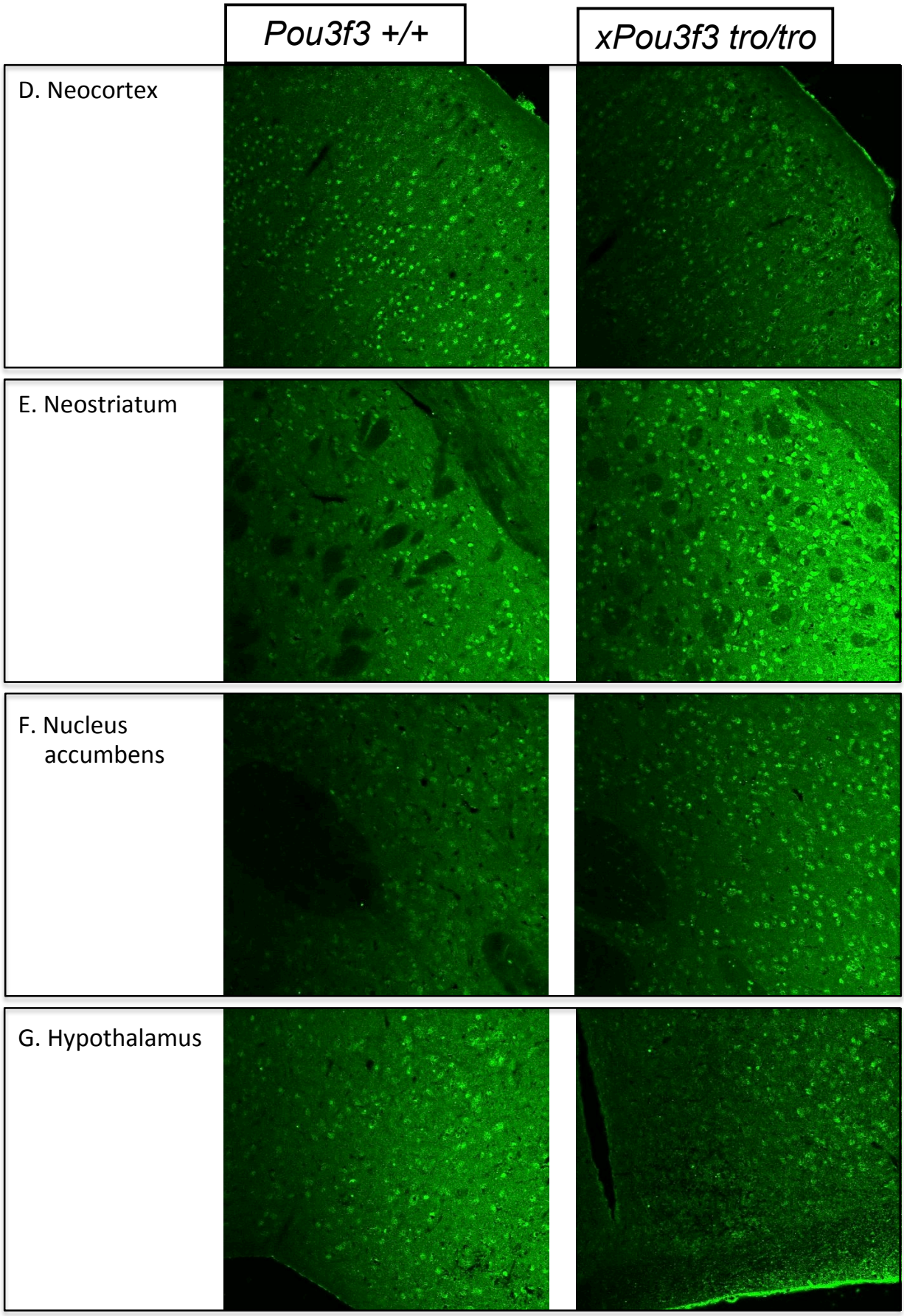
Pou3f3 +/+
xPou3f3 tro/tro
D. Neocortex
E. Neostriatum
F. Nucleus accumbens
G. Hypothalamus

Fig. 5. Sexual and maternal behaviors in *ΔGQP Pou3f2* and *xPou3f3* knock-in mice

A. Genotype ratio of pups from *+/Δ* parents. Sampling numbers of pups were 311 pups. Each color represents pups genotypes; *+/+* (orange), *+/Δ* (checker red), and *Δ/Δ* (red).

B. Genotype ratio of pups from *+/tro* parents. Sampling numbers of pups were 204 pups. Each color represents pups genotypes; *+/+* (orange), *+/tro* (checker blue), and *tro/tro* (blue).

C. The latency of delivery after mating in *ΔGQP Pou3f2* knock-in mice. Values shown on graphs represent the mean ± SEM. Sampling numbers were 30 pairs (*+/+* vs. *+/+,* orange) and 16 pairs (*Δ/Δ* vs. *Δ/Δ,* red). **P*<0.05 (Student's *t*-test)

D. The latency of delivery after mating in *xPou3f3* knock-in mice. Values shown on graphs represent the mean ± SEM. Sampling numbers were 10 pairs (*+/+* vs. *+/+,* orange) and 19 pairs (*tro/tro* vs. *tro/tro,* blue).

E. Pups viability in *ΔGQP Pou3f2* knock-in mice. 4 types of dams vs. sires combinations; *+/+* vs. *+/+*, *+/+* vs. *Δ/Δ, Δ/Δ* vs. *+/+* and *Δ/Δ* vs. *Δ/Δ.* The orange, checker red, and red bar represent *+/+*, *+/Δ*, and *Δ/Δ* genotypes in pups, respectively. ***P*<0.01 (Student's *t*-test)

F. Pups viability in *xPou3f3* knock-in mice. 2 types of dams vs. sires combinations; *+/+* vs. *+/+* and *tro/tro* vs. *tro/tro.* The genotypes of both parents and pups did not affect pups weaning ratio. The orange and blue bars represent *+/+* and *tro/tro* genotypes in pups, respectively.

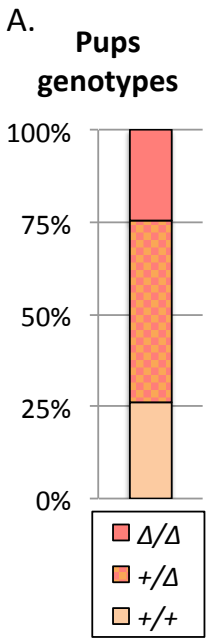
A.
Pups genotypes
100%
75%
50%
25%
0%
Δ/Δ
+/Δ
+/+

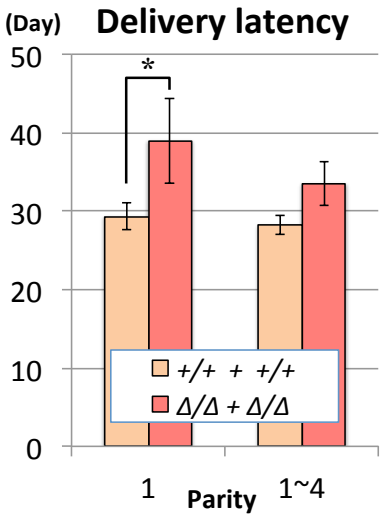
C.
(Day)
Delivery latency
50
40
30
20
10
0
*
+/+ + +/+
Δ/Δ + Δ/Δ
1
Parity
1~4

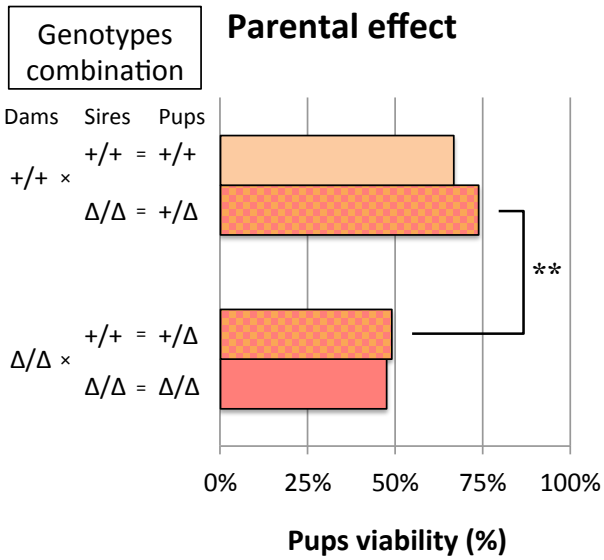
E.
Genotypes combination
Parental effect
Dams Sires Pups
+/+ × +/+ = +/+
Δ/Δ = +/Δ
Δ/Δ × +/+ = +/Δ
Δ/Δ = Δ/Δ
**
0%
25%
50%
75%
100%
Pups viability (%)

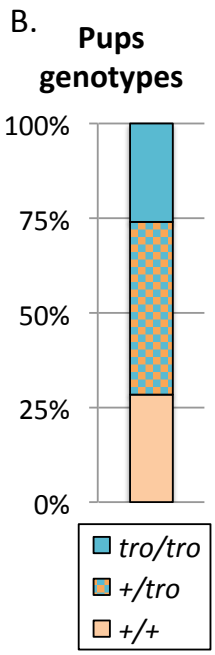
B.
Pups genotypes
100%
75%
50%
25%
0%
tro/tro
+/tro
+/+

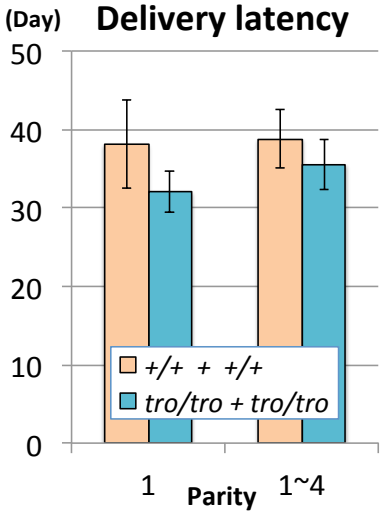
D.
(Day)
Delivery latency
50
40
30
20
10
0
+/+ + +/+
tro/tro + tro/tro
1
Parity
1~4

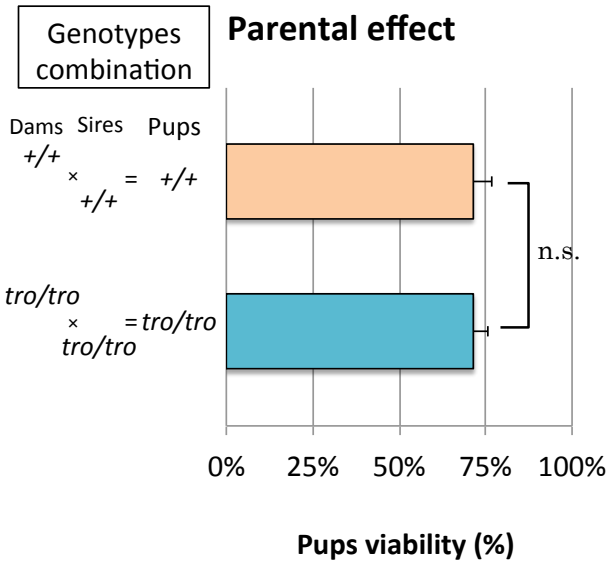
F.
Genotypes combination
Parental effect
Dams Sires Pups
+/+ × +/+ = +/+
tro/tro × tro/tro = tro/tro
n.s.
0%
25%
50%
75%
100%
Pups viability (%)

Fig. 6. Monoamine levels in non-mammalized *Pou3f2* and *xPou3f3* knock-in mice

(A -D) Quantitative immunohistochemistry for tyrosine hydroxylase (TH)

A. Sectional information of TH quantification. The coronal section located in 0.74 mm rostral from bregma was used. The measurement regions and abbreviations (Franklin and Paxinos 2008): STlat, lateral part of the neostriatum; STmed, medial part of the neostriatum; AcbS, shell of the nucleus accumbens; AcbC, core of the nucleus accumbens; Tu, olfactory tubercle; M1, primary motor cortex; S1, primary sensory cortex; DI, dysgranular insular cortex; Pir, piriform cortex; sepN, septal area.

B. Overview image of quantitative distribution containing the striatum. Each color shows the values of fluorescent intensities (color bar, below).

C. Quantitative analysis of the expression of TH in five positive and five control regions. Values shown on graph represent the mean ± SEM. **P*<0.05; ***P*<0.01.

D. The ventral striatum region was enlarged. TH expression in *Δ/Δ* was significantly reduced in comparison with *+/+* mice.

(E -H) Quantitative immunohistochemistry for tryptophan hydroxylase 2 (TPH2)

E. Sectional information of TPH2 quantification. The coronal section located in 4.60 mm caudal from bregma was used. The measurement regions and abbreviations (Franklin and Paxinos 2008): DRD, dorsal part of the dorsal raphe nucleus; DRV, ventral part of the dorsal raphe nucleus; DRL, lateral part of the dorsal raphe nucleus; MnR, median raphe nucleus; PMnR, paramedian raphe nucleus; ECIC, external cortex of the inferior colliculus; mRt, mesencephalic reticular formation; LL, lateral lemniscus; xscp, decussation of the superior cerebellar peduncle; RtTg, reticulotegmental

nucleus of the pons.

F. Overview image of quantitative distribution containing the raphe nucleus. Each color shows the values of fluorescent intensities (color bar, below).

G. Quantitative analysis of the expression of TPH2 in five positive and five control regions. Values shown on graph represent the mean ± SEM. *P<0.05; **P<0.01.

H. Region of the dorsal raphe nucleus was enlarged. TPH2 expression in *Δ/Δ* was significantly reduced in comparison with *+/+* mice.

(I -L) Comparative analysis between non-mammalized *Pou3f2* and *pou3f3* knock-in mice in the tyrosine hydroxylase (TH) and tryptophan hydroxylase 2 (TPH2)

The changes of brain monoamines in *xPou3f2* and *Pou3f2 ΔGQP* knock-in mice were calculated using the expression values measured by MapAnalyzer. The TH reduction rates were averaged in five regions (STlat, STmed, AcbS, AcbC and Tu) and the TPH2 reduction rates were averaged in five regions (DRD, DRV, DRL, MnR and PMnR) (I and J). Whereas, the changes of brain monoamines in *xPou3f3* knock-in mice were calculated using RNA-seq results. The reduction rates were defined as the ratio of the expression values in *tro/tro* mice to that in *+/+* mice (K and L).

I. The reduction rate of TH in *xPou3f2* knock-in mice (*tro/tro*, blue) and *Pou3f2 ΔGQP* knock-in mice (*Δ/Δ*, red).

J. The reduction rate of TH in *xPou3f3* knock-in mice (*tro/tro*).

K. The reduction rate of TPH2 in *xPou3f2* knock-in mice (*tro/tro*, blue) and *Pou3f2 ΔGQP* knock-in mice (*Δ/Δ*, blue).

L. The reduction rate of TPH2 in *xPou3f3* knock-in mice (*tro/tro*).

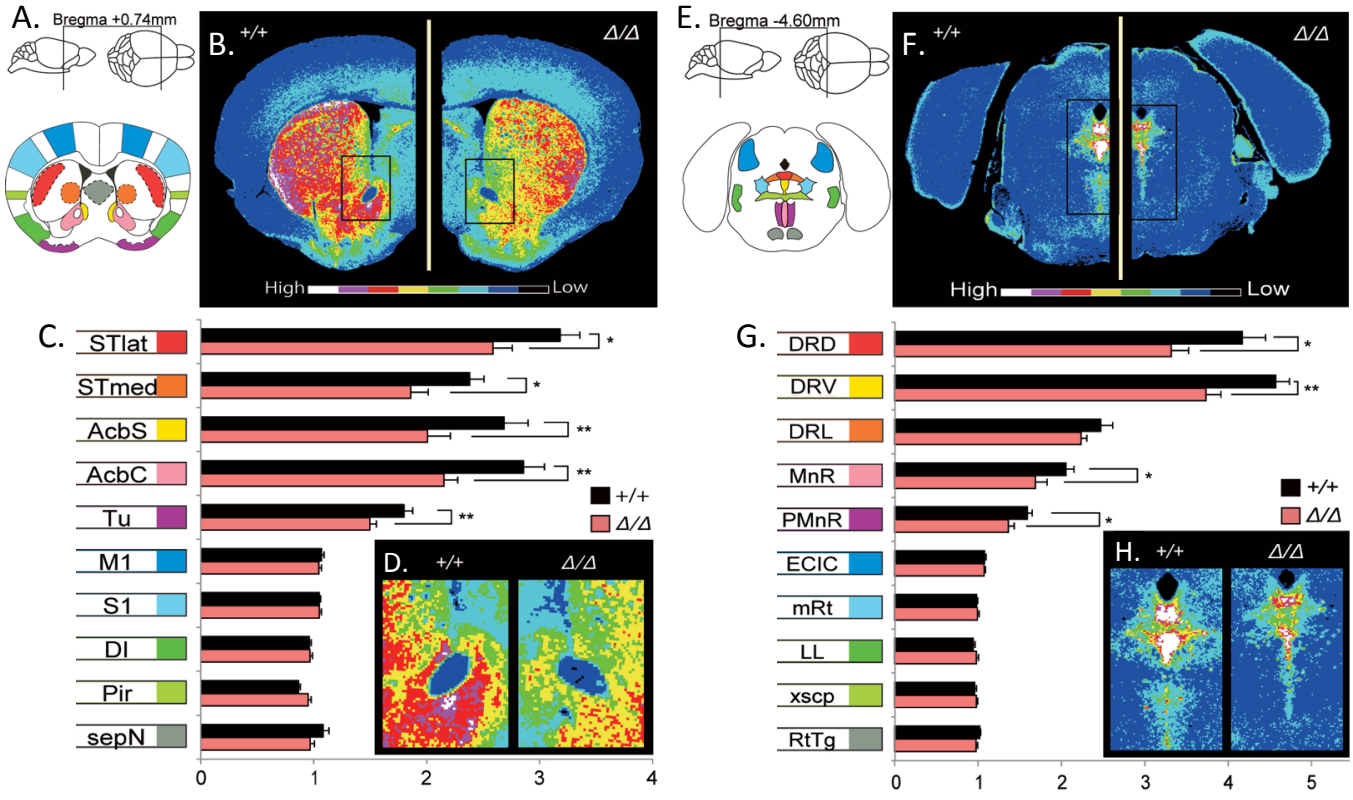
A.
Bregma +0.74mm
B.
+/+
Δ/Δ
High
Low
E.
Bregma -4.60mm
F.
+/+
Δ/Δ
High
Low
C.
STlat
STmed
AcbS
AcbC
Tu
M1
S1
DI
Pir
sepN
+/+
Δ/Δ
D.
+/+
Δ/Δ
0
1
2
3
4
G.
DRD
DRV
DRL
MnR
PMnR
ECIC
mRt
LL
xscp
RtTg
+/+
Δ/Δ
H.
+/+
Δ/Δ
0
1
2
3
4
5

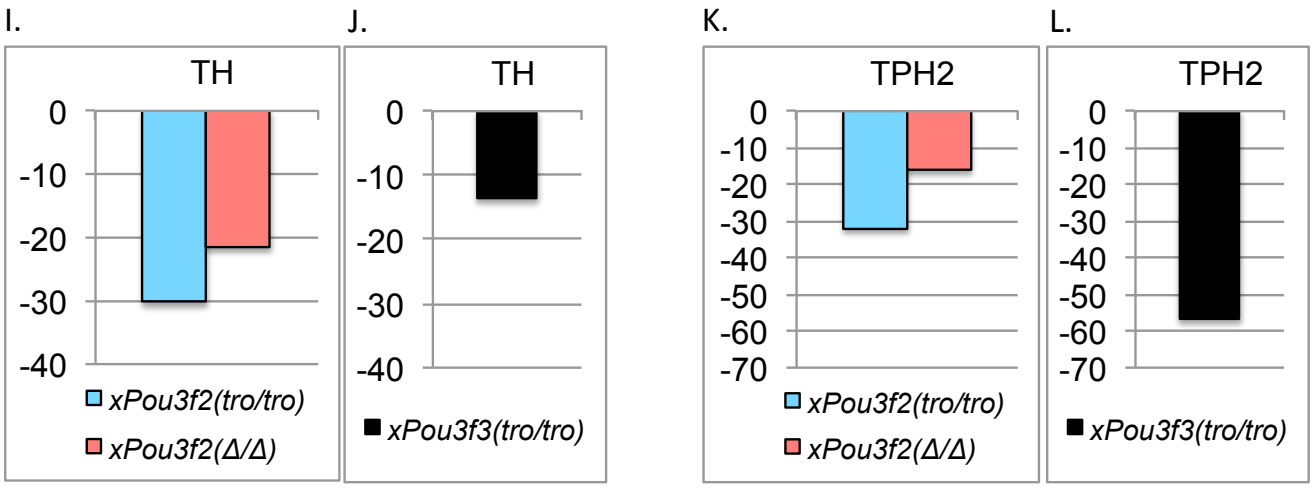
I.
TH
0
-10
-20
-30
-40
xPou3f2(tro/tro)
xPou3f2(Δ/Δ)
J.
TH
0
-10
-20
-30
-40
xPou3f3(tro/tro)
K.
TPH2
0
-10
-20
-30
-40
-50
-60
-70
xPou3f2(tro/tro)
xPou3f2(Δ/Δ)
L.
TPH2
0
-10
-20
-30
-40
-50
-60
-70
xPou3f3(tro/tro)

Fig. 7. Locomotor activity in male

A. Transition of locomotor activity over 5 continuous days (120 hours). The measurement session includes 6 light (L1-L6) and 5 dark (D1-D5) periods alternately.
B. The averaged locomotor activity among 6 light periods.
C. The averaged locomotor activity among 5 dark periods.
D. The total of novel seeking activity from start to 30 min.

Values shown on graphs represent the mean ± SEM. Sampling numbers were 23 of *+/+* males (orange) and 22 of *tro/tro* males (blue). The statistical significance are shown as $*P<0.05$.

xPou3f3 knock-in male mice showed elevated activities in dark periods significantly elevated to 1.16-fold. But novel seeking activities were not changed.

A.

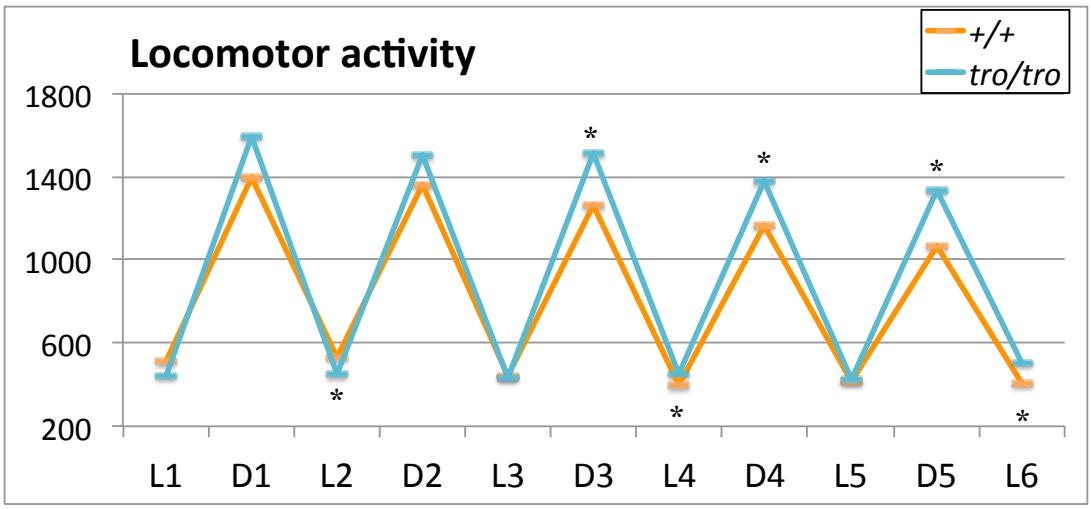
Locomotor activity
+/+
tro/tro
1800
1400
1000
600
200
L1
D1
L2
D2
L3
D3
L4
D4
L5
D5
L6
*

B.

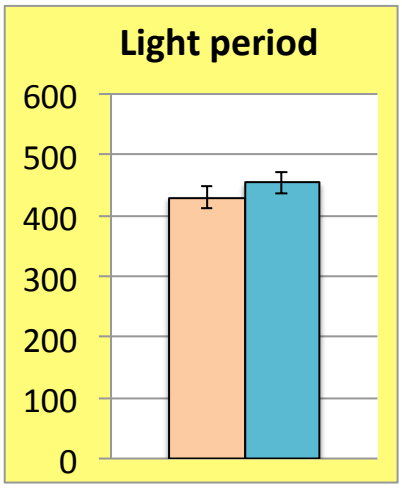
Light period
600
500
400
300
200
100
0

C.

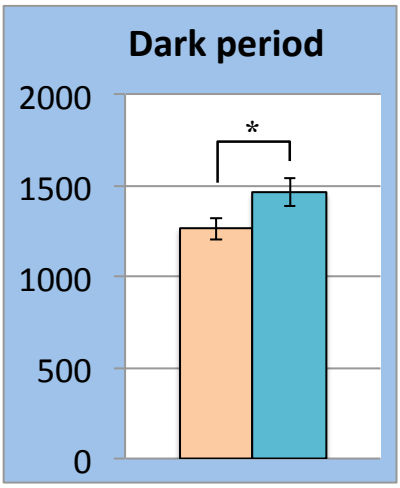
Dark period
2000
1500
1000
500
0
*

D.

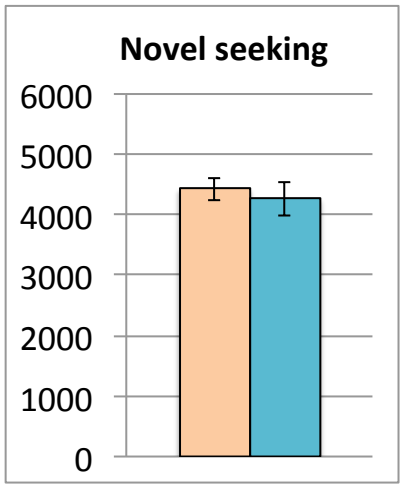
Novel seeking
6000
5000
4000
3000
2000
1000
0

Fig. 8. Prepulse inhibition test

A. Intensities of acoustic startle response. Apparatus presented 6 stepwise volumes, 60-120 dB, and recorded the power of press on acceleration sensor. The difference of the reactions against various pulse intensities were compared between genotypes

B. Inhibition rate of the startle response. Two-staged prepulses, 75 and 80 dB, were presented before main pulse, 110 and 120dB. Generally, the presentation of prepulse inhibits startle response by subsequent startle pulse. Values represent the mean ± SEM. Sampling numbers were 29 in *+/+* males (orange) and 30 *tro/tro* males (blue). Statistical significances were determined by Student *t*-test (**P*<0.05).

A.

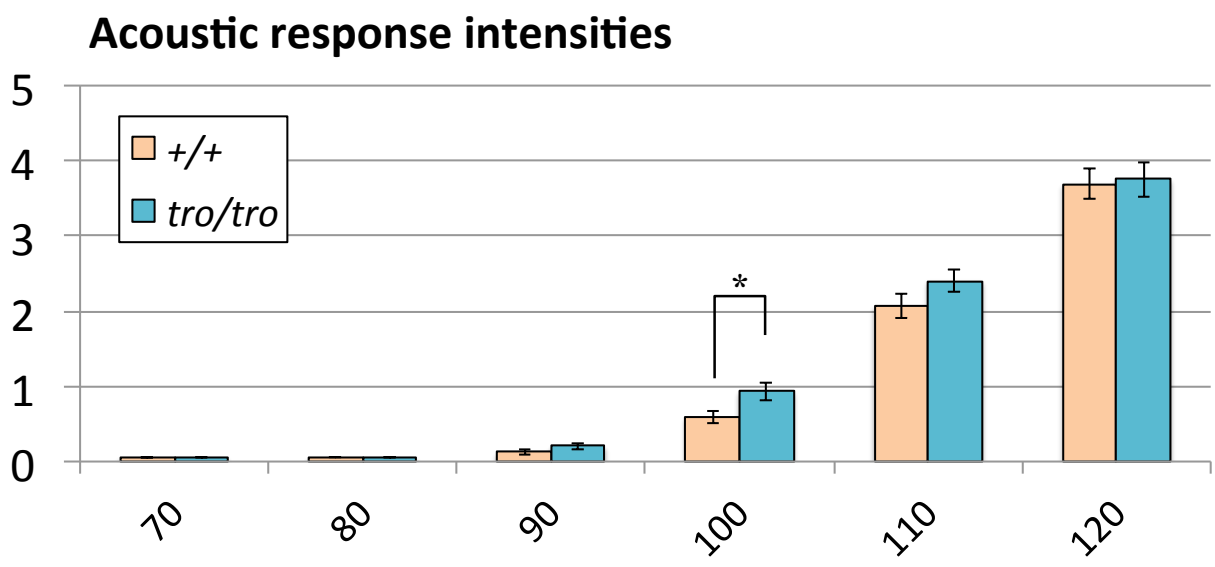
Acoustic response intensities
5
4
3
2
1
0
+/+
tro/tro
*
70
80
90
100
110
120

B.

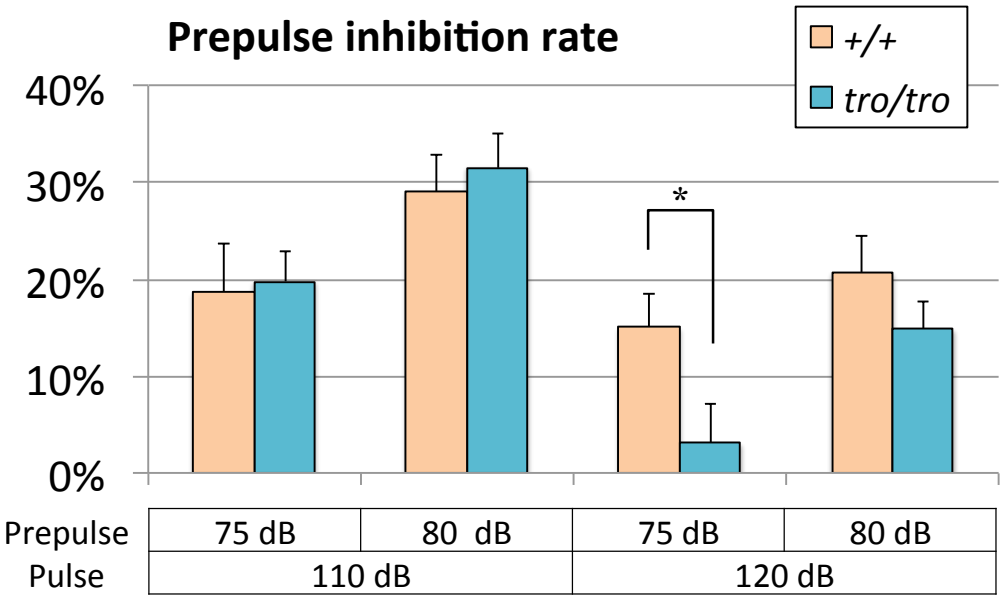
Prepulse inhibition rate
40%
30%
20%
10%
0%
+/+
tro/tro
*
Prepulse
75 dB
80 dB
75 dB
80 dB
Pulse
110 dB
120 dB

Fig. 9. Depressive-like behavior test

A -B. Forced swimming test. (A) Transitions of immobility over 10 min test time. (B) Average of immobility time in FST. Sampling numbers were 13 of *+/+* males (orange) and 20 of *tro/tro* males (blue). Values represent the mean ± SEM. Statistical significances were determined by Student *t*-test (**P*<0.05; ***P*<0.01; and ****P*<0.001)

C -D. Tail-suspension test. (C) Transitions of the duration time escaping motion over 10 min test time. (D) Average of immobility time in TST. Sampling numbers were 9 of *+/+* males (orange) and 9 of *tro/tro* males (blue). Values represent the mean ± SEM. Statistical significances were determined by Student *t*-test (**P*<0.05; ***P*<0.01; and ****P*<0.001)

A.

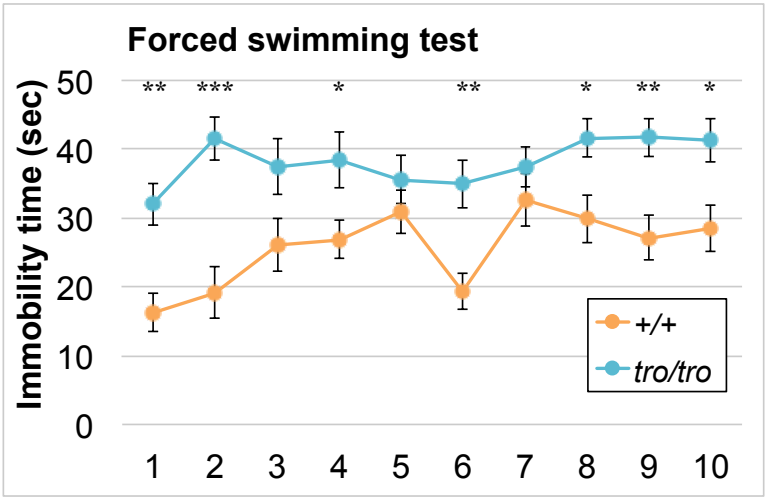
Forced swimming test
Immobility time (sec)
50
40
30
20
10
0
** *** * ** * ** *
1 2 3 4 5 6 7 8 9 10
+/+
tro/tro

B.

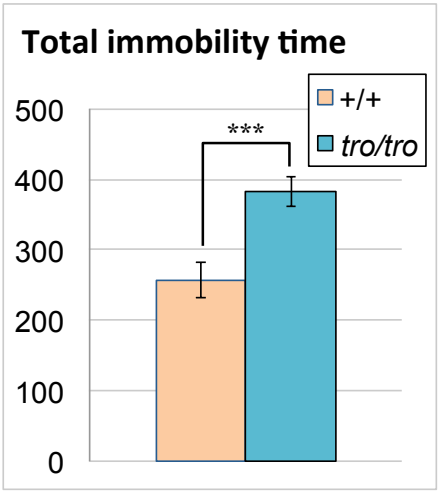
Total immobility time
500
400
300
200
100
0
***
+/+
tro/tro

C.

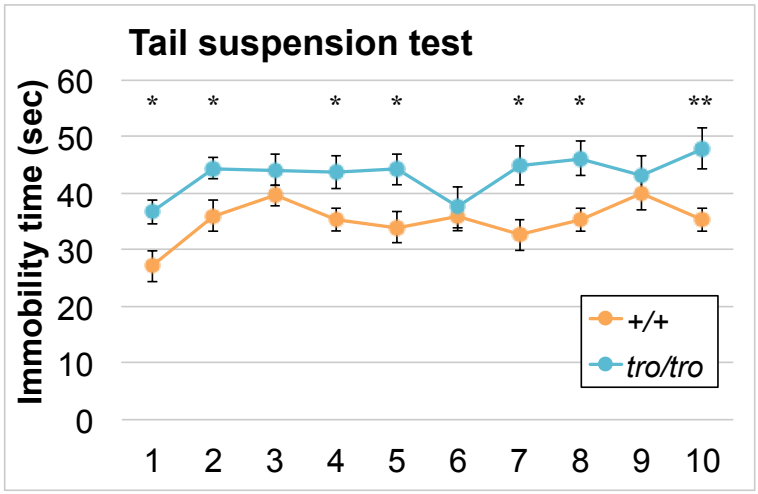
Tail suspension test
Immobility time (sec)
60
50
40
30
20
10
0
* * * * * * **
1 2 3 4 5 6 7 8 9 10
+/+
tro/tro

D.

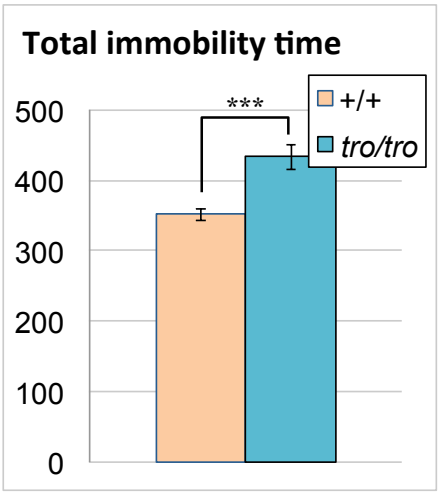
Total immobility time
500
400
300
200
100
0
***
+/+
tro/tro

Fig. 10. Chronic stress loading test

A. Modified unpredictable chronic stress (modified UCS) loading schedule. Stress-loading protocol was based on [30-33]. Various stressors were presented 6 continuous days pseudo-randomly. Mice were exposed to three long-period mild stressors (decline stress, wet bedding and shake stress) and four short-period strong stressors (auditory startle/restraint stress, heat stress, forced swimming stress and tail suspension stress). Stressful conditions in mice were quantified by the operation of light-dark transition test (Day 5). In the end of the schedule, mice were sacrificed and brain, blood, urine, and bones were isolated (Day 6).

B. Total visiting time in a dark box. Light-dark transition test was used for quantification of anxiety behaviors. The total visiting times in dark box were significantly elevated by modified UCS in both *+/+* mice (***P<0.001) and *tro/tro* mice (***P<0.001). There were no significant changes in total visiting time in dark box between stress-loaded *+/+* and *tro/tro* mice. The tested numbers were N=16 (*+/+*) and N=16 (*tro/tro*).

A.

Day1	Day2	Day3	Day4	Day5	Day6
PrePulse Inhibition test	Acoustic startle/ Restraint stress	Acoustic startle/ Restraint stress	Acoustic startle/ Restraint stress	Acoustic startle/ Restraint stress	Acoustic startle/ Restraint stress
	↓	↓	↓	↓	↓
	Shake stress	Decline stress	Shake stress	Decline stress	Shake stress
	↓	↓	↓	↓	↓
	Wed bedding stress	Heat stress	Forced swimming	Tail suspension	Acoustic startle/ Restraint stress
				↓	↓
				Light-dark Transiton test	Extract Samples

B.

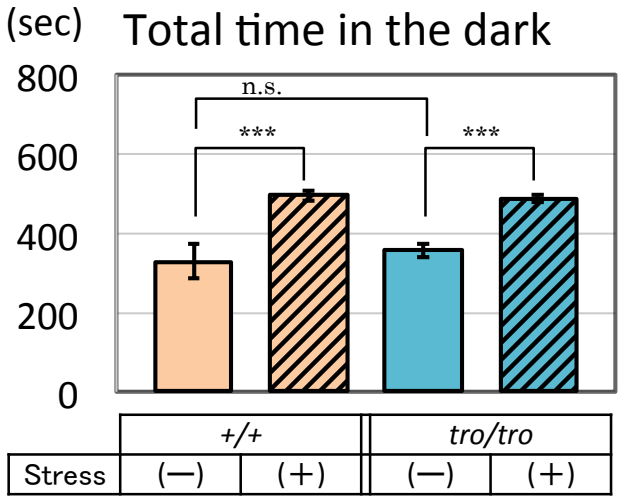

Fig. 11. Gene expression analysis

A. GO functional analysis for highly expressed genes in stress-loaded *tro/tro* mice. 71 functional GO terms were listed (P<0.001).

B. GO functional analysis for lowly expressed genes in stress-loaded *tro/tro* mice. 38 functional GO terms were listed (P<0.001).

C. The gene expression values of *Pomc*. POMC is a precursor polypeptide for ACTH, α-MSH and ß-endorphin, and ACTH has a crucial role in the HPA-axis. Each expression value was defined as total gene reads acquired by RNA-seq.

(D -I) Heat-map analysis are displayed using logarithmic (base 10) gene expression values and compared between *+/+* (stress- vs. stress+), *tro/tro* (stress- vs. stress+) (*P<0.05;, **P<0.01; ***P<0.001), and *+/+* (stress+) vs. *tro/tro* (stress+) (*WS vs. HS*, †P<0.05;, ††P<0.01; †††P<0.001).

D. Gene expression changes in glutamate receptor subunits. All AMPA, 2 of 5 kainate and 3 of 6 NMDA subunits were significantly reduced in *+/+* mice by stress-loading.

E. Gene expression changes in nitric oxide synthase. The neural types (*Nos1* and *Nos1ap*) were significantly reduced in *+/+* mice by stress.

F. Gene expression changes in $GABA_A$ receptor subunits. The 4 of 16 in *+/+* and 1 of 16 in *tro/tro* were significantly reduced by stress-loading.

G. Gene expression changes in opioid receptor subunits. In *+/+* mice, two opioid receptor subunits were significantly reduced.

H. Gene expression analysis of neurortrophic factor signaling. In Eph receptor family, Eph receptors A showed negative and Eph receptors B showed positive alteration in *+/+* by stress-loading.

I. Gene expression analysis in GO:0006979 (Response to oxidative stress).

21 genes in *+/+* and 4 genes in *tro/tro* were significantly changed.

J. 8-OHdG concentrations in urine. Values are represented as mean ± SEM. Sampling numbers were N=5 (*+/+* stress-), N=6 (*+/+* stress+), N=5 (*tro/tro* stress-) and N=6 (*tro/tro* stress+)

A. High expression in stress-loaded *tro/tro*

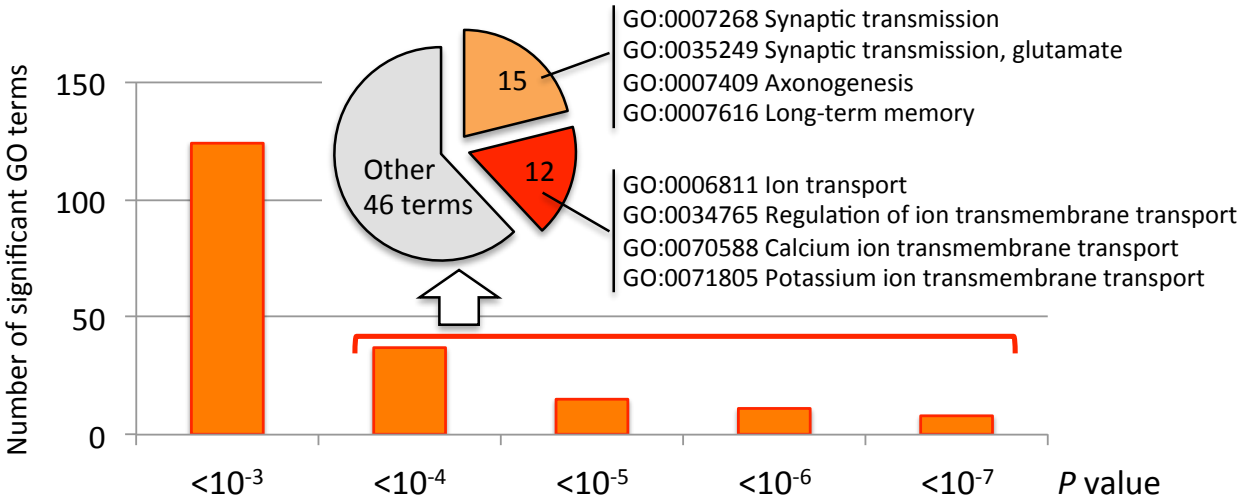

B. Low expression in stress-loaded *tro/tro*

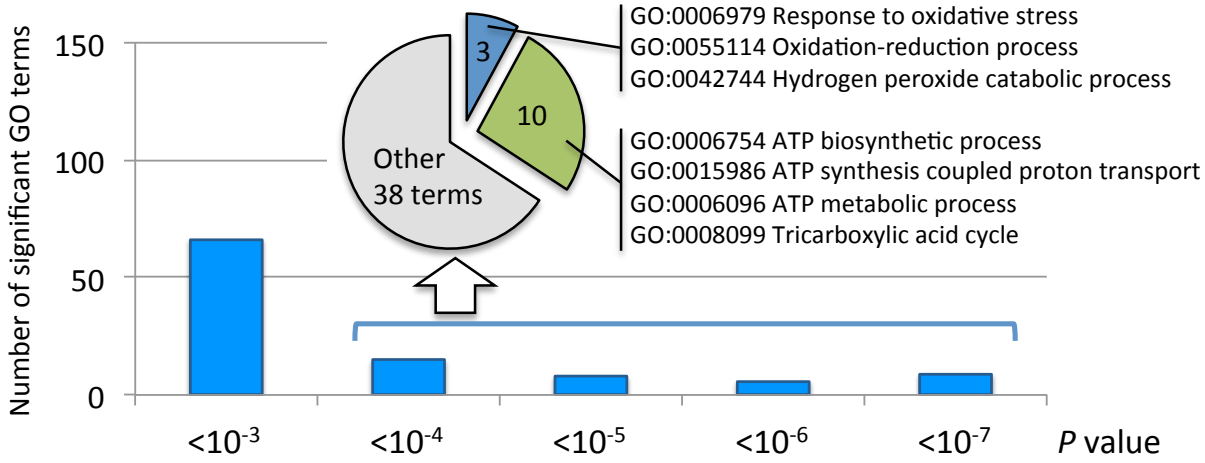

C. POMC

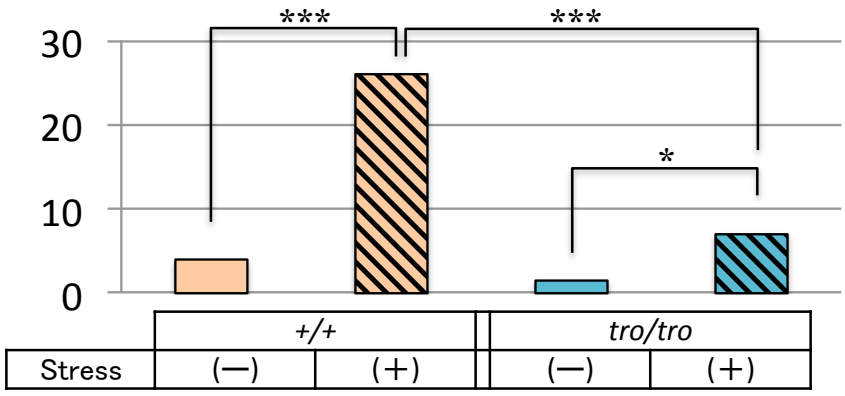

D. Glutamate receptor subunits

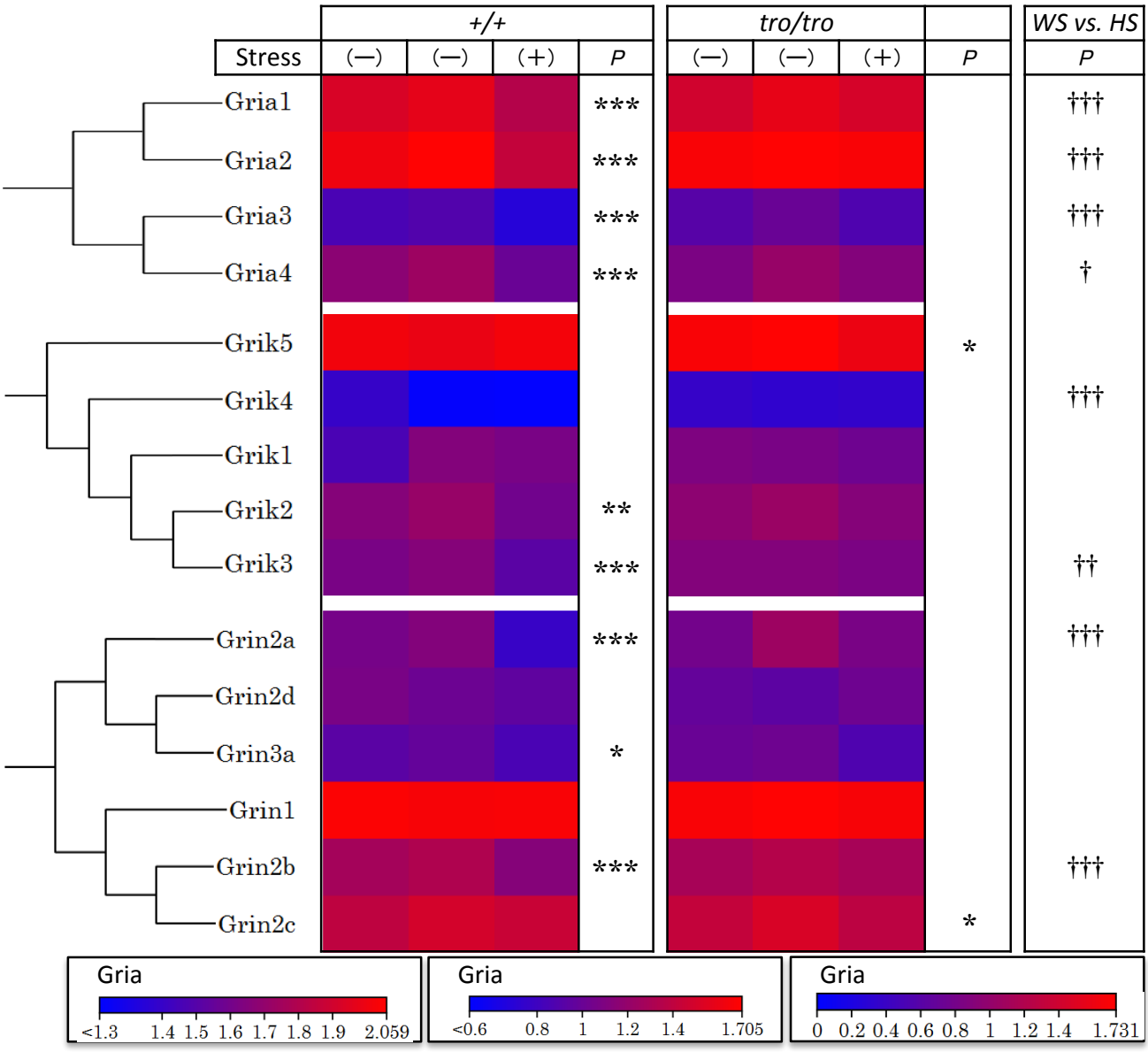

E. Nitric Oxide Synthase (NOS)

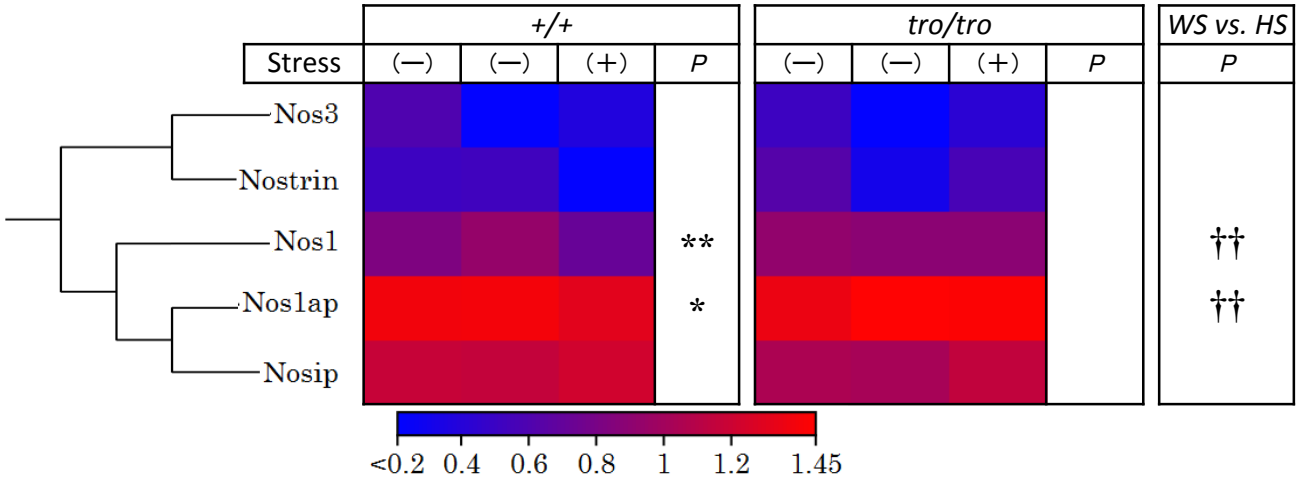

F. GABA receptor subunits

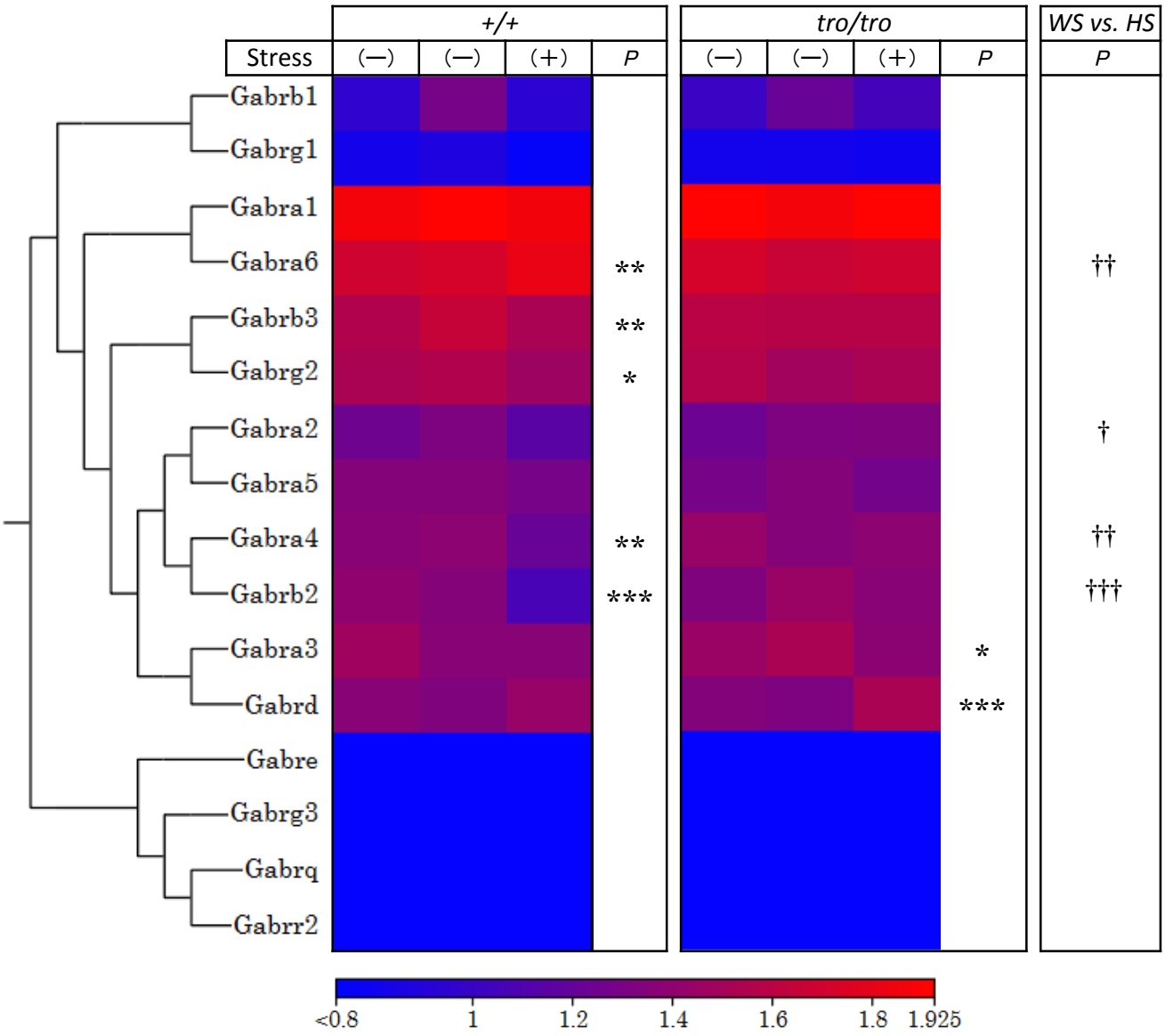

G. Opioid receptor subunits

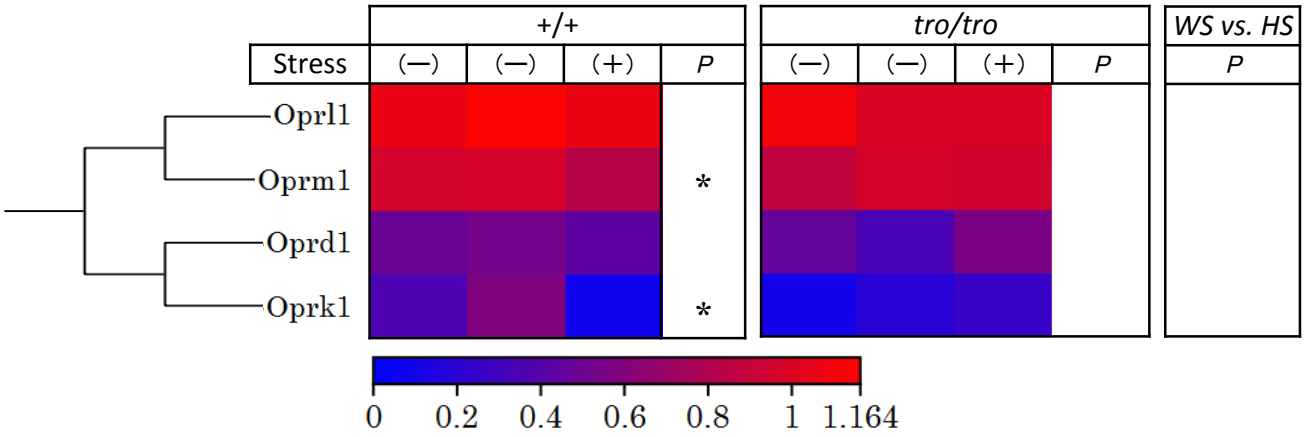

H. Ephrins

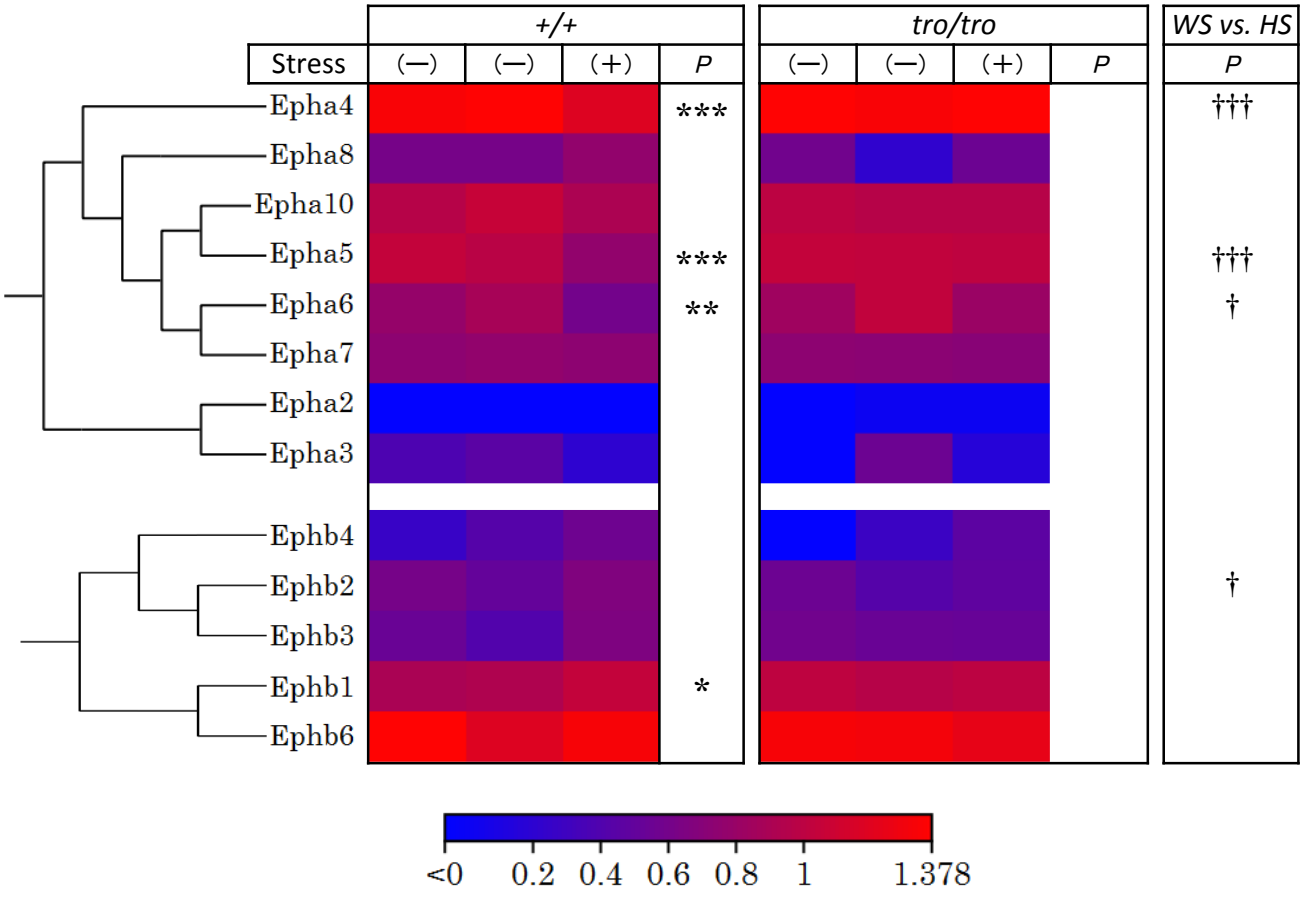
+/+
tro/tro
WS vs. HS
Stress
(—)
(—)
(+)
P
(—)
(—)
(+)
P
P
Epha4
Epha8
Epha10
Epha5
Epha6
Epha7
Epha2
Epha3
Ephb4
Ephb2
Ephb3
Ephb1
Ephb6
***
***
**
*
†††
†††
†
†
<0
0.2
0.4
0.6
0.8
1
1.378

I. Anti-oxidant genes

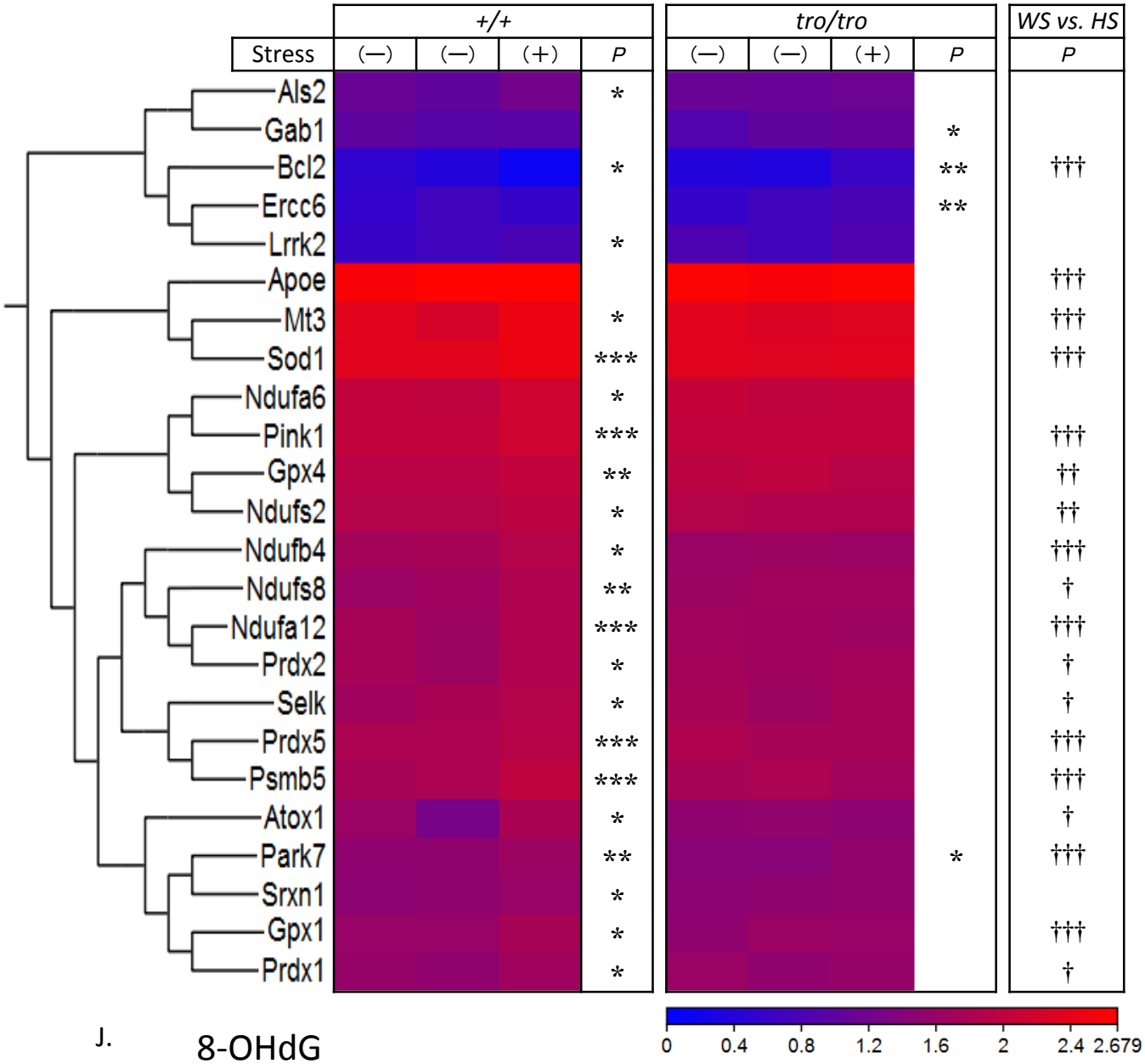

J.

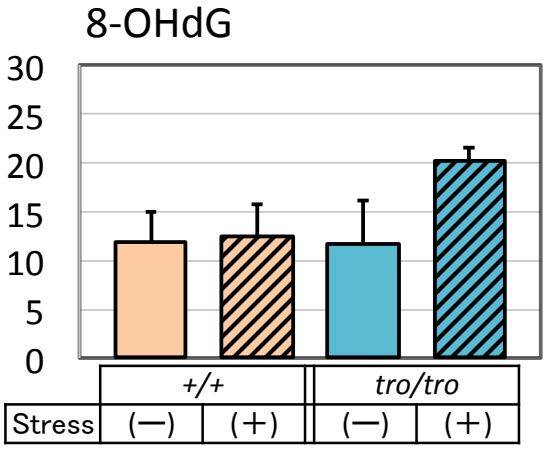

Fig. 12. Blood components and bone parameters

A. The decreased blood components in both genotypes. The concentrations of blood urea nitrogen (BUN, left) and calcium (Ca, right) in serum showed significant reduction by stress-loading.

B. The increased blood components specifically in *tro/tro* (stress+). Inorganic phosphate (IP) in serum was not changed in *+/+* (105.8%), but significantly increased in *tro/tro* (122.8%) by stress-loading.

C. The decreased blood components only in *+/+* (stress+). Alkaline phosphatase (ALP) in serum was not changed in *tro/tro* (92.0%, not significant), but significantly decreased to 81.3% in *+/+* by stress-loading.

D. The bone morphological measurements. The femur μCT images were located in the 1000 mm distance from the growth plate. The thickness of all sections were 500 mm. Bone parameters were reduced in bone volume / total volume (BV/TV, left below), bone surface (BS, middle below) and bone mineral contents (BMC, left below) in *+/+* mice by stress-loading in accordance with the changes in blood ALP concentrations.

All values of data showed mean ± SEM. The statistical significances were determined by Student *t*-test (**P*<0.05; ***P*<0.01; ****P*<0.001). The number of serum samples were N=43 (*+/+* (stress-)), N=22 (*+/+* (stress+)), N=48 (*tro/tro* (stress-)) and N=22 (*tro/tro* (stress+)). The number of bone samples were N=36 (*+/+* (stress-)), N=22 (*+/+* (stress+)), N=40 (*tro/tro* (stress-)) and N=22 (*tro/tro* (stress+))

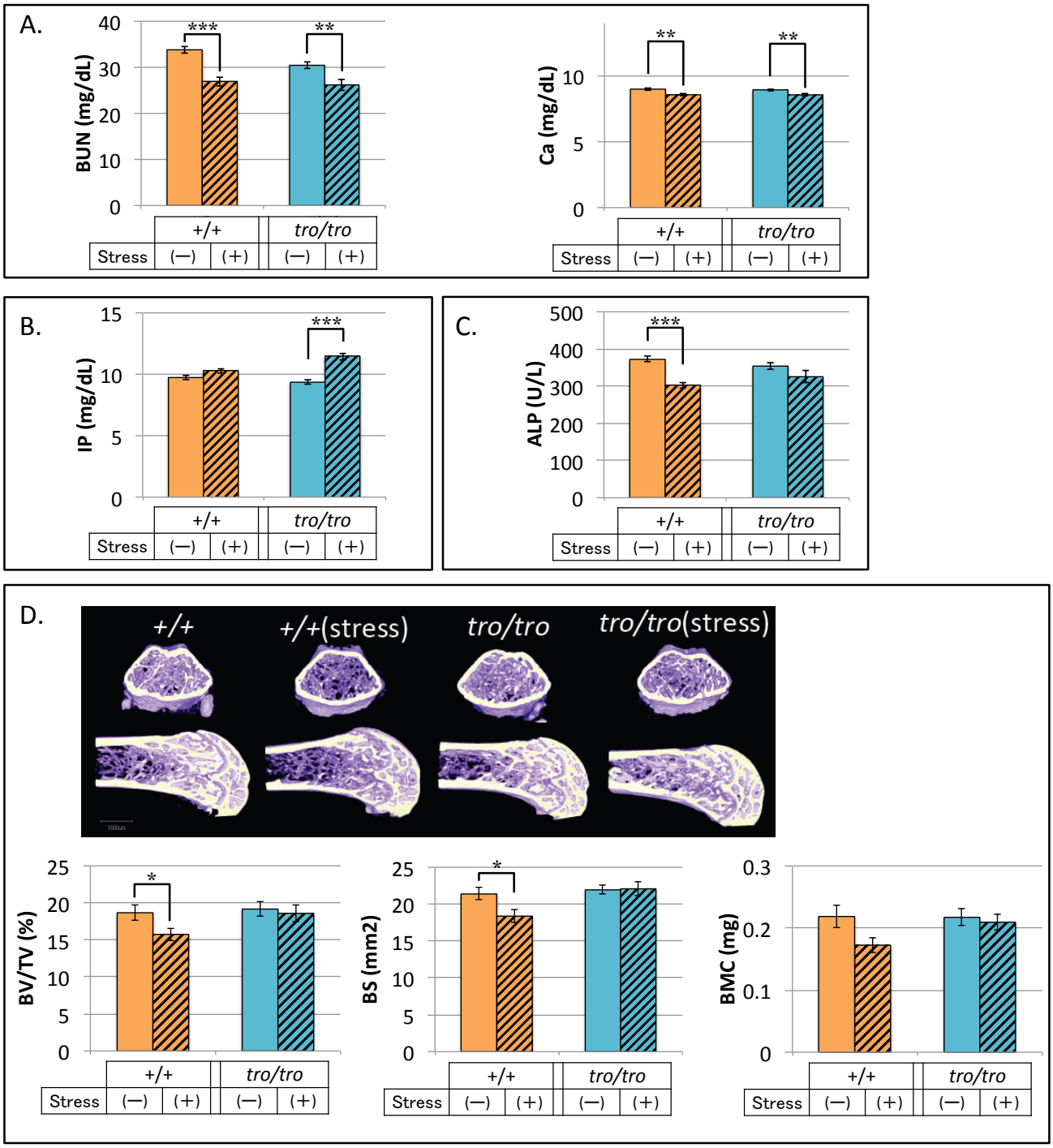
A.
BUN (mg/dL)
40
30
20
10
0
***
**
+/+
tro/tro
Stress
(−)
(+)
(−)
(+)
Ca (mg/dL)
10
5
0
**
**
B.
IP (mg/dL)
15
10
5
0
***
C.
ALP (U/L)
500
400
300
200
100
0
***
D.
+/+
+/+(stress)
tro/tro
tro/tro(stress)
BV/TV (%)
25
20
15
10
5
0
*
BS (mm2)
*
BMC (mg)
0.3
0.2
0.1
0

9. SUPPLEMENTARY TABLES AND FIGURES

Supplementary Table 1. Hypergenometric annotation test

A. The significant high expression in *tro/tro* stress against *+/+* stress as a reference. These GO terms were suppressed by stress-loaded in *+/+*. There were 71 GO terms with high significance (P<0.001). This list contains some remarkable altered contents of GO terms related to synaptic transmission (blue) and ion transport (green).

B. The significant low expression in *tro/tro* stress against *+/+* stress as a reference. These GO terms were accelerated by stress-loaded in *+/+*. There were 38 GO terms with high significance (P<0.001). This list contains some remarkable altered contents of GO terms related to oxidative stress response (red) and ATP biosynthesis process (orange).

A. *+/+*_stress expression < *tro/tro*_stress expression

Category	Description	Full set	In subset	Expected	Observed	p-value
7399	nervous system development	328	40	15	25	1.23E-08
16310	phosphorylation	680	64	31	33	2.45E-08
7268	synaptic transmission	133	23	6	17	2.86E-08
35235	ionotropic glutamate receptor signaling pathway	25	10	1	9	5.98E-08
35249	synaptic transmission, glutamatergic	38	12	2	10	6.19E-08
6811	ion transport	601	55	27	28	5.88E-07
45944	positive regulation of transcription from RNA polymerase II promoter	860	71	39	32	7.13E-07
7409	axonogenesis	93	17	4	13	8.06E-07
6810	transport	1798	124	81	43	1.24E-06
34765	regulation of ion transmembrane transport	176	24	8	16	1.39E-06
7616	long-term memory	27	9	1	8	1.7E-06
6355	regulation of transcription, DNA-dependent	1928	129	87	42	3.51E-06
1901660	calcium ion export	4	4	0	4	4.15E-06
70588	calcium ion transmembrane transport	116	18	5	13	4.54E-06
43524	negative regulation of neuron apoptotic process	141	20	6	14	5.62E-06
6351	transcription, DNA-dependent	1764	119	80	39	5.98E-06
71805	potassium ion transmembrane transport	121	18	5	13	8.33E-06
16568	chromatin modification	263	29	12	17	9.17E-06
10738	regulation of protein kinase A signaling cascade	8	5	0	5	9.33E-06
6816	calcium ion transport	135	19	6	13	1.07E-05
48167	regulation of synaptic plasticity	34	9	2	7	1.43E-05
35556	intracellular signal transduction	357	35	16	19	1.56E-05
48813	dendrite morphogenesis	35	9	2	7	1.85E-05
6874	cellular calcium ion homeostasis	84	14	4	10	2.24E-05
31175	neuron projection development	110	16	5	11	3.46E-05
6468	protein phosphorylation	581	48	26	22	4.47E-05
10842	retina layer formation	16	6	1	5	4.55E-05
19226	transmission of nerve impulse	16	6	1	5	4.55E-05
18105	peptidyl-serine phosphorylation	79	13	4	9	5.01E-05
7628	adult walking behavior	40	9	2	7	5.85E-05
48015	phosphatidylinositol-mediated signaling	24	7	1	6	6.64E-05
51924	regulation of calcium ion transport	33	8	1	7	8.56E-05
32317	regulation of Rap GTPase activity	3	3	0	3	9.21E-05
42391	regulation of membrane potential	84	13	4	9	9.65E-05
10976	positive regulation of neuron projection development	85	13	4	9	0.000109
51481	reduction of cytosolic calcium ion concentration	12	5	1	4	0.000113
48511	rhythmic process	86	13	4	9	0.000124
7156	homophilic cell adhesion	75	12	3	9	0.000128
7411	axon guidance	124	16	6	10	0.00015
7611	learning or memory	45	9	2	7	0.000155
6376	mRNA splice site selection	13	5	1	4	0.000177
21702	cerebellar Purkinje cell differentiation	13	5	1	4	0.000177
50885	neuromuscular process controlling balance	56	10	3	7	0.000182
30334	regulation of cell migration	57	10	3	7	0.000212
6813	potassium ion transport	128	16	6	10	0.000217
19233	sensory perception of pain	68	11	3	8	0.000219
7155	cell adhesion	490	40	22	18	0.000241
16567	protein ubiquitination	198	21	9	12	0.00026
10800	positive regulation of peptidyl-threonine phosphorylation	14	5	1	4	0.000266
9636	response to toxic substance	49	9	2	7	0.000305
50775	positive regulation of dendrite morphogenesis	22	6	1	5	0.000336
48675	axon extension	22	6	1	5	0.000336
1764	neuron migration	108	14	5	9	0.000362
7605	sensory perception of sound	121	15	5	10	0.00037
7216	G-protein coupled glutamate receptor signaling pathway	9	4	0	4	0.000435
1964	startle response	16	5	1	4	0.000537
7018	microtubule-based movement	64	10	3	7	0.000559
6887	exocytosis	88	12	4	8	0.000588
60291	long-term synaptic potentiation	34	7	2	5	0.000695
51493	regulation of cytoskeleton organization	10	4	0	4	0.0007
7019	microtubule depolymerization	10	4	0	4	0.0007
80182	histone H3-K4 trimethylation	10	4	0	4	0.0007
1900153	positive regulation of nuclear-transcribed mRNA catabolic process, deadenylation-dependent decay	10	4	0	4	0.0007
46579	positive regulation of Ras protein signal transduction	17	5	1	4	0.000733
34220	ion transmembrane transport	116	14	5	9	0.000752
7169	transmembrane receptor protein tyrosine kinase signaling pathway	67	10	3	7	0.00081
45893	positive regulation of transcription, DNA-dependent	522	40	24	16	0.000843
16082	synaptic vesicle priming	5	3	0	3	0.00086
45636	positive regulation of melanocyte differentiation	5	3	0	3	0.00086
10452	histone H3-K36 methylation	5	3	0	3	0.00086
22604	regulation of cell morphogenesis	18	5	1	4	0.000977

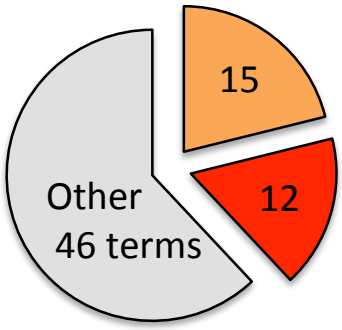

B. +/+_stress expression > *tro/tro*_stress expression

Category	Description	Full set	In subset	Expected	Observed	p-value
6412	translation	272	60	12	48	0
6810	transport	1798	134	78	56	3.16E-10
6979	response to oxidative stress	111	22	5	17	2E-09
51258	protein polymerization	27	11	1	10	6.68E-09
6754	ATP biosynthetic process	27	11	1	10	6.68E-09
15986	ATP synthesis coupled proton transport	15	8	1	7	5.99E-08
7017	microtubule-based process	34	11	1	10	1.11E-07
6096	glycolysis	35	11	2	9	1.55E-07
6184	GTP catabolic process	170	24	7	17	3.55E-07
46034	ATP metabolic process	27	9	1	8	1.22E-06
15992	proton transport	60	13	3	10	1.38E-06
55114	oxidation-reduction process	730	60	32	28	1.68E-06
6364	rRNA processing	104	17	5	12	2.34E-06
45892	negative regulation of transcription, DNA-dependent	438	41	19	22	3.49E-06
15991	ATP hydrolysis coupled proton transport	25	8	1	7	6.83E-06
6099	tricarboxylic acid cycle	27	8	1	7	1.3E-05
28	ribosomal small subunit assembly	9	5	0	5	1.66E-05
71353	cellular response to interleukin-4	21	7	1	6	1.93E-05
6200	ATP catabolic process	231	25	10	15	2.61E-05
48168	regulation of neuronal synaptic plasticity	22	7	1	6	2.73E-05
6734	NADH metabolic process	10	5	0	5	3.2E-05
6102	isocitrate metabolic process	6	4	0	4	4.93E-05
6457	protein folding	111	15	5	10	9.05E-05
6172	ADP biosynthetic process	7	4	0	4	0.000111
30163	protein catabolic process	36	8	2	6	0.000125
5975	carbohydrate metabolic process	184	20	8	12	0.000153
6413	translational initiation	58	10	3	7	0.000177
51453	regulation of intracellular pH	8	4	0	4	0.000214
462	maturation of SSU-rRNA from tricistronic rRNA transcript	4	3	0	3	0.000315
42744	hydrogen peroxide catabolic process	15	5	1	4	0.000318
44262	cellular carbohydrate metabolic process	9	4	0	4	0.000373
43524	negative regulation of neuron apoptotic process	141	16	6	10	0.000419
1902600	---	34	7	1	6	0.000546
31110	regulation of microtubule polymerization or depolymerization	10	4	0	4	0.0006
51603	proteolysis involved in cellular protein catabolic process	35	7	2	5	0.000657
50821	protein stabilization	82	11	4	7	0.000812
3016	respiratory system process	11	4	0	4	0.000911

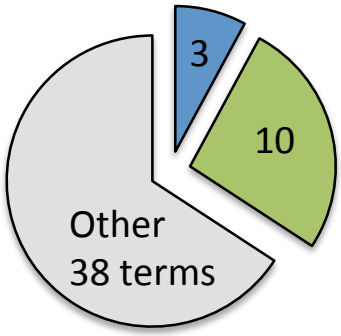

Supplementary Table 2. Gene Ontology

The comparison table of gene expression data among 4 groups (*+/+* (stress-), *+/+* (stress+), *tro/tro* (stress-) vs. *tro/tro* (stress+). Kal's Z test was performed between stress-loaded groups (*+/+* (stress+) vs. *tro/tro* (stress+)) and all genes were listed along with this statistical significance values. Red boxes represent the genes, whose expressions were changed significantly ($P<0.05$). Between each genotype, Barggerley's test was performed for the comparison of no-stress group (stress-) and stress-loaded group (stress+).

On the top, the results of HyperG annotation test are represented. 'Description' shows GO functional terms. 'Full set' means total number of the genes belonging to the term. 'In subset' means observed numbers of genes highly expressed (A, B) and lowly expressed (C, D) in *tro/tro* by stress-loading significantly ($P<0.01$).

A. 45 genes related to gutamatergic signaling pathway. Genes are belonging to GO:0035235 ionotropic glutamate receptor signaling pathway or GO:0035249 synaptic transmission, glutamatergic.
B. 23 genes related to GABA signaling pathway. Genes are belonging to GO:0007214 gamma-aminobutyric acid signaling pathway.
C. 113 genes related to oxidative stress response. Genes are belonging to GO:0006979 response to oxidative stress, GO:0032872 regulation of stress-activated MAPK cascade and GO:0043744 hydrogen peroxide catabolic process.
D. 69 genes related to ATP synthesis and metabolic process belonging to GO:0006754 ATP biosynthetic process, GO:0015986 ATP synthesis coupled proton transport, GO:0046034 ATP metabolic process and GO:0015991 ATP hydrolysis coupled proton transport.

A. Glutamatergic signaling pathway

Category	Description	Full set	In subset	Expected	Observed	*P*value
35235	ionotropic glutamate receptor signaling pathway	25	10	1	9	5.97E-08
35249	synaptic transmission, glutamatergic	38	12	2	10	6.19E-08

	Kal's Z test		Baggerley's test		*+/+*		Baggerley's test		*tro/tro*	
Feature ID	Fold change	*P*value	Fold change	*P*value	stress (−)	stress (+)	Fold change	*P*value	stress (−)	stress (+)
Gria2	1.477	1E-14	−1.477	7E-20	1005	609	−1.028	0.4714	1007.5	1062
Grin2b	1.6423	2E-10	−1.715	3E-17	471.5	246	−1.096	0.0979	482.5	477
Cacnb4	1.5202	2E-06	−1.691	3E-13	368.5	195	−1.093	0.3496	355	350
Shc3	5.2029	6E-06	−3.939	0.0003	31	7	1.4137	0.2153	29	43
Gria1	1.2976	1E-05	−1.387	5E-11	725.5	468	−1.03	0.5264	681.5	717
Camk2a	1.1407	3E-05	−1.069	0.4682	2122.5	1765	1.0262	0.3135	2138.5	2377
Gria3	1.366	6E-05	−1.351	6E-06	401.5	266	−1.107	0.0793	438.5	429
Grin2a	2.6468	0.0004	−2.825	1E-06	50.5	16	−1.246	0.1796	57.5	50
Napa	−1.346	0.0007	1.3384	0.0032	232	277	1.0035	0.9789	227	243
Cpeb4	1.416	0.0018	−1.38	0.0007	197.5	128	1.0594	0.5048	186.5	214
Grik3	1.4638	0.0034	−1.488	0.0003	153	92	−1.065	0.5166	156.5	159
Cacna1a	1.2638	0.0038	−1.277	0.0004	362.5	254	1.0012	0.9855	349.5	379
Grik4	2.1397	0.004	−1.737	0.1638	37.5	19	−1.004	0.983	44.5	48
Unc13a	1.1803	0.0147	−1.046	0.5227	434	371	1.0502	0.3773	454.5	517
Gria4	1.21	0.0156	−1.378	9E-07	420.5	273	−1.039	0.5408	374	390
Clstn3	−1.136	0.0248	1.1948	0.0054	569.5	608	1.0756	0.3572	546	632
Grik2	1.2433	0.0789	−1.375	0.0021	167.5	109	−1.147	0.143	169.5	160
Grm3	1.3763	0.0803	−1.286	0.1139	69	48	1.059	0.6889	68	78
Atp1a3	−1.038	0.1098	1.0359	0.5357	3659	3379	1.0216	0.5893	3482	3842
Als2	−1.181	0.1751	1.3204	0.0416	113	133	1.0645	0.6487	116	133
Grin2c	−1.172	0.1892	−1.04	0.7023	158	136	−1.257	0.0203	159	137
App	1.0403	0.1903	−1.029	0.4478	2289	1989	1.0579	0.478	2165.5	2443
Cdk5	−1.172	0.2021	1.2481	0.0528	115.5	129	1.1337	0.3202	106	130
Adora2a	1.3475	0.2712	−1.422	0.3319	35.5	22	1.2933	0.3509	25.5	35
Grik5	−1.106	0.2953	1.0779	0.4479	216	208	−1.215	0.0129	249	222
Grin2d	1.244	0.3398	−1.339	0.1707	48	32	1.2289	0.3347	35.5	47
P2rx1	######	0.3574	#DIV/0!	0.3173	0.5	0	#DIV/0!	0.3173	0	1
Cdk5r1	−1.081	0.3916	1.0618	0.4597	241	229	−1.016	0.8826	236	250
Grid2	1.1261	0.3997	−1.143	0.5249	111	88	−1.037	0.7497	112	117
Napb	1.0405	0.4901	1.0334	0.528	591.5	547	1.0516	0.3017	590	672
Ptk2b	1.0507	0.4937	−1.012	0.8782	391	345	−1.134	0.0294	448	428
Slc17a7	−1.035	0.4988	1.1526	0.3927	718	731	1.0082	0.9201	771.5	834
Adrb2	−1.771	0.5257	3.3523	0.2536	1	3	−1.521	0.6779	2.5	2
Cln3	−1.181	0.5646	1.4213	0.2509	19	24	1.4294	0.3031	16	24
Cnih3	1.1173	0.5661	−1.057	0.7485	55.5	47	−1.005	0.9771	57.5	62
Cnih2	−1.073	0.5803	1.1806	0.2232	113	119	1.1742	0.1601	103	131
Grin3a	1.1117	0.5804	−1.38	0.0386	74	48	−1.522	0.0022	88.5	63
Grik1	−1.107	0.6244	1.1744	0.5941	42	45	−1.151	0.4188	51	48
Grin1	−1.025	0.6714	1.0033	0.96	637	571	−1.066	0.1785	647.5	658
Unc13b	1.0679	0.6834	−1.038	0.7965	80	69	−1.225	0.1039	98.5	87
Grid1	−1.06	0.7252	1.073	0.6326	73	70	−1.083	0.6394	78.5	78
Grm8	1.089	0.7695	1.0282	0.9282	23	21	−1.304	0.2268	32.5	27
Grin3b	−1.181	0.8679	4.4698	0.2952	0.5	2	3.6929	0.3355	0.5	2
Cdh8	−1.012	0.9487	−1.197	0.3313	72.5	54	−1.47	0.0054	85.5	63
Plat	1.0026	0.9895	−1.078	0.74	59.5	49	−1.143	0.5927	63	58

B. Gamma-aminobutyric acid (GABA) signaling pathway

Category	Description	Full set	In subset	Expected	Observed	*P*value
7214	gamma-aminobutyric acid signaling pathway	23	5	1	4	0.00318

	Kal's Z test		Baggerley's test *+/+*				Baggerley's test *tro/tro*			
Feature ID	Fold change	*P*value	Fold change	*P*value	stress (−)	stress (+)	Fold change	*P*value	stress (−)	stress (+)
Cacnb4	1.5202	2E-06	-1.691	3E-13	368.5	195	-1.093	0.3496	355	350
Gabra4	1.5267	0.0021	-1.464	0.0012	132.5	81	-1.007	0.9645	138	146
Cacna1a	1.2638	0.0038	-1.277	0.0004	362.5	254	1.0012	0.9855	349.5	379
Gabra6	-1.336	0.0051	1.2901	0.0064	171.5	198	-1	0.9978	163.5	175
Plcl2	1.3794	0.0334	-1.076	0.6701	84.5	70	1.2456	0.0789	84.5	114
Gabra2	1.508	0.034	-1.364	0.0661	62.5	41	1.1423	0.3806	59	73
Gabrb3	1.1733	0.0568	-1.23	0.0038	335.5	244	-1.007	0.9288	314.5	338
Gabra1	1.1249	0.0597	-1.101	0.0811	551	448	1.0355	0.667	534	595
Atf4	-1.225	0.0666	1.2479	0.1623	150	166	1.2119	0.2084	124	160
Gabrg2	1.1661	0.092	-1.187	0.0299	274.5	207	-1.004	0.9785	269	285
Gabrq	-1.61	0.2259	-1.146	0.8204	18.5	15	-1.28	0.4753	13	11
Gabbr2	1.0894	0.2682	-1.118	0.0972	371	297	1.0149	0.8168	347.5	382
Gabre	2.1175	0.3587	-1.836	0.4881	4	2	1.5775	0.4814	3	5
Gabrg3	1.1999	0.4019	-1.243	0.2426	50	36	-1.168	0.3475	55	51
Gnai2	-1.079	0.4337	1.045	0.6084	216	202	1.028	0.8056	199.5	221
Plcl1	1.1173	0.5661	-1.152	0.6266	59.5	47	-1.066	0.6805	61	62
Gabra3	1.0568	0.6674	-1.164	0.4006	143	109	-1.242	0.0288	156	136
Gabrg1	1.1036	0.6699	-1.247	0.2548	46	33	-1.045	0.8121	41.5	43
Htr4	1.2705	0.7101	-1.437	0.4966	6.5	4	1.3656	0.6821	4.5	6
Gabrr2	-1.181	0.7243	1.9328	0.3031	5	9	1.2783	0.5841	6.5	9
Gabbr1	-1.017	0.7298	-1.006	0.8887	873.5	777	1.0051	0.9014	828.5	902
Bdnf	1.0712	0.7644	1.564	0.1043	24.5	34	1.1387	0.5982	35.5	43
Gabra5	-1.046	0.7976	-1.155	0.3226	80	62	-1.106	0.4816	71.5	70

C. Anti-oxidant genes _ oxidative stress response

Category	Description	Full set	In subset	Expected	Observed	*P*value
6979	response to oxidative stress	111	22	5	17	2.00E-09
55114	oxidation-reduction process	730	60	32	28	1.68E-06
42744	hydrogen peroxide catabolic process	15	5	1	4	0.0003

	Kal's Z test		Baggerley's test *+/+*				Baggerley's test *tro/tro*			
Feature ID	Fold change	*P*value	Fold change	*P*value	stress (−)	stress (+)	Fold change	*P*value	stress (−)	stress (+)
Pink1	−1.41	5E−07	1.2818	4E−05	408	468	−1.057	0.3689	382.5	392
Psmb5	−1.955	3E−05	1.6009	0.0009	70.5	101	−1.19	0.2479	67	61
Ndufb4	−1.848	5E−05	1.3952	0.0104	86.5	108	−1.005	0.9752	64	69
Prdx5	−1.499	8E−05	1.2982	0.0039	182.5	212	−1.137	0.4121	178.5	167
Cst3	−1.233	0.0001	1.1262	0.455	689	686	−1.155	0.0375	701.5	657
Bcl2	3.1762	0.0002	−2.113	0.0229	28.5	12	1.8185	0.0081	23	45
Apoe	−1.168	0.0002	1.1642	4E−05	1111.5	1158	1.0122	0.8686	1078.5	1171
Ndufa12	−1.659	0.0003	1.4401	0.0146	92	118	−1.1	0.5278	85.5	84
Prnp	−1.19	0.0005	1.0567	0.3042	841.5	795	−1.004	0.9365	731	789
Mt3	−1.44	0.0007	1.4668	0.0172	145.5	189	−1.075	0.6263	156	155
Sod1	−1.37	0.0009	1.3488	0.0005	198	239	1.0433	0.7193	183.5	206
Cygb	−1.634	0.0013	1.3066	0.0557	86.5	101	−1.135	0.3637	76.5	73
Ndufs2	−1.334	0.002	1.2049	0.0351	225.5	243	−1.082	0.4841	216	215
Gpx4	−1.336	0.0024	1.2646	0.0062	205	232	−1.136	0.1255	215	205
Atox1	−1.919	0.0106	2.0323	0.0452	22	39	−1.083	0.7464	24	24
Prdx2	−1.258	0.0123	1.3258	0.0289	208	245	1.0313	0.7985	208	230
Ercc6	1.6093	0.0139	−1.124	0.5215	49.5	40	1.5421	0.0084	45.5	76
Gpx7	−8.265	0.0181	1.9555	0.2435	4	7	−3.249	0.1757	3	1
Pxdn	1.4373	0.0187	−1.241	0.1169	91.5	66	1.2024	0.1391	86	112
Prdx1	−1.294	0.0195	1.3305	0.0146	144	171	−1.024	0.8898	151	156
Trp53	−1.795	0.0213	1.4952	0.0734	28.5	38	−1.278	0.2851	29.5	25
Park7	−1.317	0.0272	1.3914	0.0045	108.5	135	1.2768	0.0457	87.5	121
Selk	−1.344	0.0294	1.452	0.0035	88.5	115	1.095	0.6306	87	101
Gpx1	−1.45	0.0362	1.4485	0.0235	54	70	1.0319	0.8503	51	57
Mpo	######	0.0396	#DIV/0!	0.1573	1	0	1.9534	0.326	2	5
Ndufs8	−1.392	0.0454	1.509	0.0085	58.5	79	1.014	0.9271	61	67
Wrn	2.1175	0.0664	−2.685	0.0013	24	8	−1.273	0.3482	23.5	20
Rrm2b	1.4254	0.0708	−1.503	0.0127	69	41	−1.013	0.9335	64.5	69
Psip1	1.1456	0.0855	−1.236	0.0016	384	278	−1.046	0.6656	367	376
Ercc2	−1.458	0.0998	1.253	0.2614	37.5	42	−1.322	0.1517	41.5	34
Ndufa6	−1.259	0.1152	1.3766	0.0199	78	96	1.0146	0.9347	83	90
Gab1	1.3193	0.1177	−1.028	0.8878	60	52	1.3849	0.0339	54	81
Lias	−1.398	0.1264	−1.104	0.5692	55.5	45	−1.196	0.3469	42	38
Als2	−1.181	0.1751	1.3204	0.0416	113	133	1.0645	0.6487	116	133
Adrbk1	−1.128	0.1836	1.0626	0.5518	250	237	−1.048	0.6472	240.5	248
App	1.0403	0.1903	−1.029	0.4478	2289	1989	1.0579	0.478	2165.5	2443
Nfkb1	1.3346	0.1931	−1.003	0.9872	37	33	1.3153	0.1457	36.5	52
Tlr4	2.2586	0.2161	−1.093	0.9256	3.5	3	1.8465	0.2542	4	8
Hmox2	−1.238	0.2286	1.2342	0.4712	60	65	−1.043	0.8617	61.5	62
Car3	−3.542	0.2421	3.2109	0.2939	1	3	−1.438	0.8024	1.5	1
Stc2	−3.542	0.2421	−1.056	0.9403	3.5	3	−3.249	0.1757	3	1
Txnrd1	−1.181	0.2674	1.2649	0.1518	79	89	1.0815	0.5719	76	89
Lrrk2	1.1646	0.2763	1.4048	0.0186	70	88	1.1839	0.3485	96.5	121
Psen1	−1.181	0.2991	1.1045	0.5945	79.5	78	−1.194	0.1813	86	78
Rgs14	−1.233	0.3141	1.4051	0.0853	37.5	47	−1.216	0.2615	50.5	45
Mill2	1.9763	0.3142	−1.389	0.6987	4.5	3	−1.161	0.7393	7.5	7
Prdx3	−1.181	0.3359	−1.002	0.9905	75	67	−1.018	0.9088	63	67
Srxn1	−1.122	0.3429	1.3037	0.0204	114	133	1.1438	0.2203	113	140
Tor1a	1.2705	0.3432	−1.425	0.0905	41.5	26	1.3336	0.1877	27	39
Prdx6	−1.087	0.3464	1.2292	0.1194	223.5	244	1.0975	0.4105	225	265
Etfdh	1.2162	0.3473	−1.285	0.1561	56	39	1.3336	0.2549	40	56
Xpa	1.232	0.3554	1.0261	0.9076	36	33	1.7169	0.104	27.5	48
Epx	######	0.3574	1	1	0	0	1.8465	0.6869	0.5	1
Tat	######	0.3574	1	1	0	0	#DIV/0!	0.3173	0	1
Gclm	1.1293	0.3601	−1.154	0.6214	130	99	1.0591	0.8995	127	132

	Kal's Z test		Baggerley's test *+/+*				Baggerley's test *tro/tro*			
Feature ID	Fold change	*P*value	Fold change	*P*value	stress (−)	stress (+)	Fold change	*P*value	stress (−)	stress (+)
Cat	1.1784	0.3952	−1.4	0.2489	73	46	−1.017	0.9256	60.5	64
Mmp9	2.5409	0.4025	−4.573	0.0392	5	1	−1.028	0.9732	3	3
Rcan2	−1.067	0.4073	1.0825	0.2588	320	310	1.1072	0.1415	286	343
Abcc1	1.1957	0.4245	−1.033	0.8916	39.5	34	−1.061	0.738	47	48
Hmox1	1.5246	0.4463	1.1493	0.8449	5	5	1.426	0.4922	6	9
Sod2	1.0829	0.4534	1.0651	0.758	168	158	1.1734	0.2761	162	202
Abl1	1.1185	0.4555	−1.095	0.493	95.5	78	−1.046	0.7071	99.5	103
Pnkp	−1.23	0.4683	1.0968	0.7167	25.5	25	−1.05	0.8845	24	24
Ercc3	1.1858	0.4754	−1.31	0.2073	44	30	−1.044	0.8186	40.5	42
Ercc1	−1.181	0.506	1.194	0.4332	30	32	−1.269	0.2409	37.5	32
Dgkk	1.3175	0.5173	−1.561	0.2889	15.5	9	−1.104	0.7885	14.5	14
Mtf1	1.1434	0.5202	−1.219	0.4191	55	40	1.0288	0.868	48.5	54
Msrb2	1.2036	0.5354	−1.46	0.1188	31	19	−1.1	0.7817	28.5	27
Nqo1	−1.328	0.5578	1.658	0.3158	6	9	1.0107	0.9831	7.5	8
Gpx8	−1.417	0.5631	−1.112	0.8335	7.5	6	−1.053	0.953	5.5	5
Ppp1r15b	−1.09	0.5985	−1.017	0.9067	82	72	−1.202	0.303	87.5	78
Sirt1	1.1402	0.6121	−1.274	0.2657	37	26	−1.037	0.862	33.5	35
Msra	1.1145	0.6144	−1.293	0.1761	55	38	−1.211	0.2949	56	50
Idh1	−1.108	0.6161	1.0179	0.921	50.5	46	−1.189	0.3655	54	49
Msrb1	−1.181	0.6179	1.2996	0.399	15.5	18	1.1079	0.7349	15	18
Map2k1	−1.042	0.6198	1.1656	0.0685	260	271	1.0696	0.5483	268	307
Ppif	−1.119	0.6299	1.0335	0.8711	39	36	−1.011	0.9573	35.5	38
Mutyh	1.4116	0.6352	1.3122	0.7212	2.5	3	5.0297	0.1016	1	5
mt-Co1	1.0036	0.6622	−1.042	7E−09	31026	26634	−1.043	0.0689	30504	31559
Tpo	1.694	0.6633	−2.685	0.2562	3	1	−1.012	0.9894	2	2
Ptgs1	1.1858	0.6803	−1.564	0.1816	17.5	10	−1.238	0.491	16	14
Rcan1	1.0795	0.6825	1.098	0.6137	52	51	1.2123	0.2404	49.5	65
Jak2	−1.061	0.7168	−1.071	0.621	85	71	−1.24	0.0994	90.5	79
Aldh1a1	−1.048	0.7273	1.207	0.1661	95.5	103	−1.018	0.8778	109	116
G6pdx	1.0852	0.7288	−1.384	0.0916	49.5	32	−1.183	0.4268	45	41
Prkcd	−1.056	0.7315	−1.218	0.36	104.5	76	−1.016	0.9392	81.5	85
Neil1	−1.119	0.7333	1.268	0.4412	16	18	1.2505	0.554	14.5	19
Oxsr1	−1.065	0.7366	−1.109	0.586	68.5	55	−1.098	0.6926	63.5	61
Atrn	1.0298	0.743	−1.228	0.0059	311.5	227	−1.203	0.0087	306.5	276
Coq7	−1.09	0.7611	−1.119	0.6352	30	24	1.231	0.4253	19.5	26
Gpx3	1.0961	0.7762	−1.131	0.7744	21	17	1.0979	0.7321	18.5	22
Chrna4	1.0509	0.7861	−1.044	0.7893	63	54	−1.075	0.6252	66.5	67
Trpm2	−1.049	0.7926	1.4151	0.099	44.5	56	1.1154	0.7655	56	63
Ercc8	−1.102	0.7938	−1.014	0.9655	16	14	1.1587	0.6617	12	15
Epas1	1.0289	0.7968	−1.029	0.9038	174	149	1.0868	0.4548	154	181
Mmp2	−1.181	0.8141	−1.247	0.6917	5.5	4	−1.475	0.4797	5.5	4
Ptgs2	1.1011	0.8189	−1.253	0.5221	14	10	1.0437	0.9026	11.5	13
Msrb3	1.078	0.8521	−1.464	0.2313	18	11	−1.459	0.3576	19.5	14
Txnip	−1.042	0.8703	−1.3	0.3391	44	30	−1.019	0.9733	35.5	34
Ogg1	−1.063	0.8949	2.0309	0.1684	5	9	1.4204	0.4258	6.5	10
Gclc	−1.019	0.8991	1.0351	0.7904	95	88	−1.078	0.5322	101.5	102
Hnf1a	−1.181	0.9064	#DIV/0!	0.3173	0	1	1.8465	0.6869	0.5	1
Aifm1	1.0202	0.9218	−1.082	0.7092	53.5	44	1.0729	0.732	46	53
Camk2g	−1.005	0.9452	1.0171	0.8073	334	304	−1.059	0.3751	349	357
mt-Nd3	−1.001	0.982	−1.001	0.9755	1159	1036	1.0082	0.8182	1119	1222
Fgf8	1	1	1	1	0	0	1	1	0	0
Gpx2	1	1	1	1	0	0	1	1	0	0
Gpx5	1	1	1	1	0	0	1	1	0	0
Gpx6	1	1	#DIV/0!	0.1573	1	0	#DIV/0!	0.3173	0.5	0
Ucn	1	1	#DIV/0!	0.1573	1	0	#DIV/0!	0.1573	1	0
Upk3bl	1	1	1	1	0	0	#DIV/0!	0.3173	0.5	0

D. ATP synthesis and proton transport

Category	Description	Full set	In subset	Expected	Observed	*P*value
6754	ATP biosynthetic process	27	11	1	10	6.68E-09
15986	ATP synthesis coupled proton transport	15	8	1	7	5.99E-08
46034	ATP metabolic process	27	9	1	8	1.21E-06
15991	ATP hydrolysis coupled proton transport	25	8	1	7	6.83E-06

	Kal's Z test		Baggerley's test +/+				Baggerley's test tro/tro			
Feature ID	Fold change	*P*value	Fold change	*P*value	stress (−)	stress (+)	Fold change	*P*value	stress (−)	stress (+)
mt-Atp8	1.2275	2E-10	−1.575	0.0959	2826.5	1634	−1.231	3E-18	2691.5	2368
Aldoa	−1.223	1E-09	1.2616	0.004	1651.5	1853	1.0172	0.8285	1646.5	1789
Atp5a1	−1.249	1E-07	1.213	3E-05	1074	1165	1.0146	0.8222	1007.5	1101
Atp6v0c	−1.292	1E-07	1.2372	0.007	810.5	893	−1.067	0.3824	809.5	816
Pkm	−1.163	6E-06	1.243	0.0001	1595	1768	1.0644	0.3129	1570	1795
Atp5b	−1.164	3E-05	1.2327	0.0002	1372	1509	1.0561	0.3455	1345	1530
Atp5h	−1.495	3E-05	1.4483	0.0012	184.5	238	−1.18	0.113	205	188
Atp6ap1	−1.312	8E-05	1.2117	0.0091	405.5	439	−1.149	0.0201	419	395
Atp5g3	−1.322	0.0009	1.4495	3E-06	230.5	299	1.1154	0.1654	221	267
Atp6v1e1	−1.267	0.001	1.3004	7E-05	342	398	−1.055	0.6439	366.5	371
Atp5o	−1.233	0.0044	1.2039	0.005	349	376	−1.039	0.7449	350.5	360
Ak1	−1.411	0.0046	1.425	0.004	115.5	147	−1.209	0.2228	139	123
Atp5g1	−1.397	0.0047	1.1586	0.1478	149.5	155	−1.149	0.4348	142	131
Atp1a1	−1.13	0.0052	1.1385	0.0257	1005.5	1022	−1.025	0.7394	1019	1068
Atp5l	−1.34	0.0062	1.3556	0.002	152.5	185	−1.083	0.5551	164.5	163
Atp5d	−1.293	0.0085	1.4488	0.0565	171.5	219	1.2535	0.0987	149.5	200
Atp6v0b	−1.291	0.0102	1.5337	9E-06	153	210	1.0103	0.914	175.5	192
Atp6v1a	1.1562	0.0142	−1.181	0.0012	650.5	493	−1.014	0.8295	630.5	673
Atp7a	3.3879	0.0203	−2.554	0.0691	11.5	4	1.0845	0.8334	14	16
Chchd10	−1.426	0.0206	1.1884	0.1926	87.5	93	−1.308	0.0385	93	77
Atp5j2	−1.348	0.0243	1.219	0.1066	111	121	1.0059	0.9752	99.5	106
Slc25a13	−3.542	0.0428	1.0958	0.8546	9	9	−3.791	0.0057	10.5	3
Surf1	−1.421	0.0451	1.3768	0.0951	58	71	−1.019	0.9256	56	59

	Kal's Z test		Baggerley's test +/+				Baggerley's test tro/tro			
Feature ID	Fold change	*P*value	Fold change	*P*value	stress (−)	stress (+)	Fold change	*P*value	stress (−)	stress (+)
Ampd3	1.694	0.0577	−1.55	0.0907	33	19	−1.126	0.5407	39.5	38
mt-Atp6	−1.027	0.0583	−1.069	6E-08	10886	9116	−1.124	1E-23	10869	10476
Ak4	−1.309	0.0747	1.1317	0.4808	91.5	92	−1.097	0.5659	84.5	83
Atp1a3	−1.038	0.1098	1.0359	0.5357	3659	3379	1.0216	0.5893	3482	3842
Slc25a25	−1.234	0.1128	1.431	0.0483	91.5	116	1.1614	0.3331	89	111
Atp5f1	−1.134	0.1224	1.1714	0.0328	280.5	294	1.0589	0.5871	269	306
Atp5c1	−1.134	0.1397	1.0774	0.322	279	269	−1.037	0.6228	268	280
Tgfb1	−2.361	0.148	2.031	0.2456	4.5	8	−1.354	0.5908	5	4
Atp6v1f	−1.273	0.1634	1.2165	0.2063	63.5	69	−1.125	0.4289	66.5	64
Atp6v0d1	−1.128	0.1671	1.0689	0.5019	269.5	257	1.0202	0.8623	246	269
Bad	1.4711	0.1774	1.2132	0.5126	17.5	19	1.3821	0.256	22.5	33
Atp5k	−1.203	0.1776	1.1608	0.2234	103	107	1.103	0.7001	92	105
Atp4a	######	0.1931	#DIV/0!	0.0365	2	0	1.5801	0.6989	1	2
Atp5j	−1.149	0.2313	1.0663	0.5282	153	146	1.0373	0.7208	133.5	150
Atp6v0a4	−3.542	0.2421	#DIV/0!	0.0833	0	3	−3.041	0.3746	2.5	1
Atp6v0e2	−1.081	0.2923	1.0757	0.2698	361.5	348	1.0486	0.6204	337	380
Tatdn2	−1.204	0.3496	1.2389	0.2378	46	51	1.1259	0.5159	41	50
Guk1	−1.181	0.379	−1.02	0.9002	64	56	−1.122	0.4721	58	56
Tatdn3	−1.181	0.4153	−1.035	0.8423	55.5	48	−1.348	0.2644	61.5	48
Ak3	1.0813	0.4223	−1.147	0.1009	241	188	−1.063	0.4617	235.5	240
Atp6v0a1	1.0438	0.4261	−1.011	0.8791	707.5	624	1.0027	0.9736	714.5	769
Adcyap1	−1.219	0.4317	1.2547	0.3242	28.5	32	1.3544	0.3592	22	31
Atp6v1c1	−1.068	0.4488	−1.016	0.8496	289.5	255	−1.083	0.2679	282	282
Atp5e	−1.123	0.4628	1.6549	0.0075	53	78	1.4284	0.0207	53	82
Atp6v0e	−1.128	0.5714	1.3164	0.1733	36.5	43	1.0011	0.9953	41.5	45
Atp1a2	1.0206	0.5773	1.0475	0.5631	1465	1366	1.0475	0.3831	1455.5	1646
Tatdn1	−1.09	0.5985	−1.198	0.1764	96.5	72	−1.023	0.9076	75	78
Ctns	−1.123	0.6036	1.3669	0.1458	32	39	1.1857	0.4309	32	41
Atp6v0a2	1.0913	0.6363	−1.101	0.5495	64	52	1.0256	0.883	60.5	67
Atp6v1h	1.0479	0.664	−1.033	0.8083	181	156	1.0638	0.4977	167.5	193
Atp6v1b2	1.0215	0.6647	1.0595	0.2837	799	757	1.1231	0.0065	750.5	913
Ak2	−1.09	0.7096	1.3055	0.283	31	36	1.3285	0.263	27.5	39
Atp5s	1.1048	0.7191	1.1423	0.6126	22.5	23	1.1096	0.6576	25	30
Ldhd	−1.099	0.7234	1.0586	0.8093	28.5	27	1.6384	0.0692	16.5	29
Gbas	−1.045	0.738	1.0271	0.819	117.5	108	−1.05	0.7293	119	122
Entpd5	1.048	0.789	−1.058	0.7565	70	59	1.1049	0.5065	61	73
Atp6v1c2	−1.181	0.8679	−3.187	0.046	7	2	−3.169	0.0648	6	2
Ndufs1	−1.014	0.8826	1.0708	0.5026	216.5	207	1.1278	0.32	199.5	241
Ak5	−1.008	0.948	1.0529	0.6678	142.5	134	−1.048	0.646	152	157
Atp12a	1	1	1	1	0	0	#DIV/0!	0.3173	0.5	0
Atp1a4	1	1	#DIV/0!	0.3173	0.5	0	1	1	0	0
Atp6v0d2	1	1	1	1	0	0	1	1	0	0
Atp6v1e2	1	1	1	1	0	0	1	1	0	0
Atp6v1g3	1	1	1	1	0	0	1	1	0	0
Ldhc	1	1	1	1	0	0	#DIV/0!	0.3173	0.5	0
Pklr	1	1	1	1	0	0	1	1	0	0

Supplementary Fig. 1. Multiple alignment of POU3F3

The multiple alignment of POU3F3 amino acid sequences between 3 species (*Homo sapiens, Mus musculus* and *Xenopus tropicalis*). The black boxes indicate the positions of mammalian homopolymeric amino acid repeats. The purple boxes indicate POU-specific and POU-homeo domains.

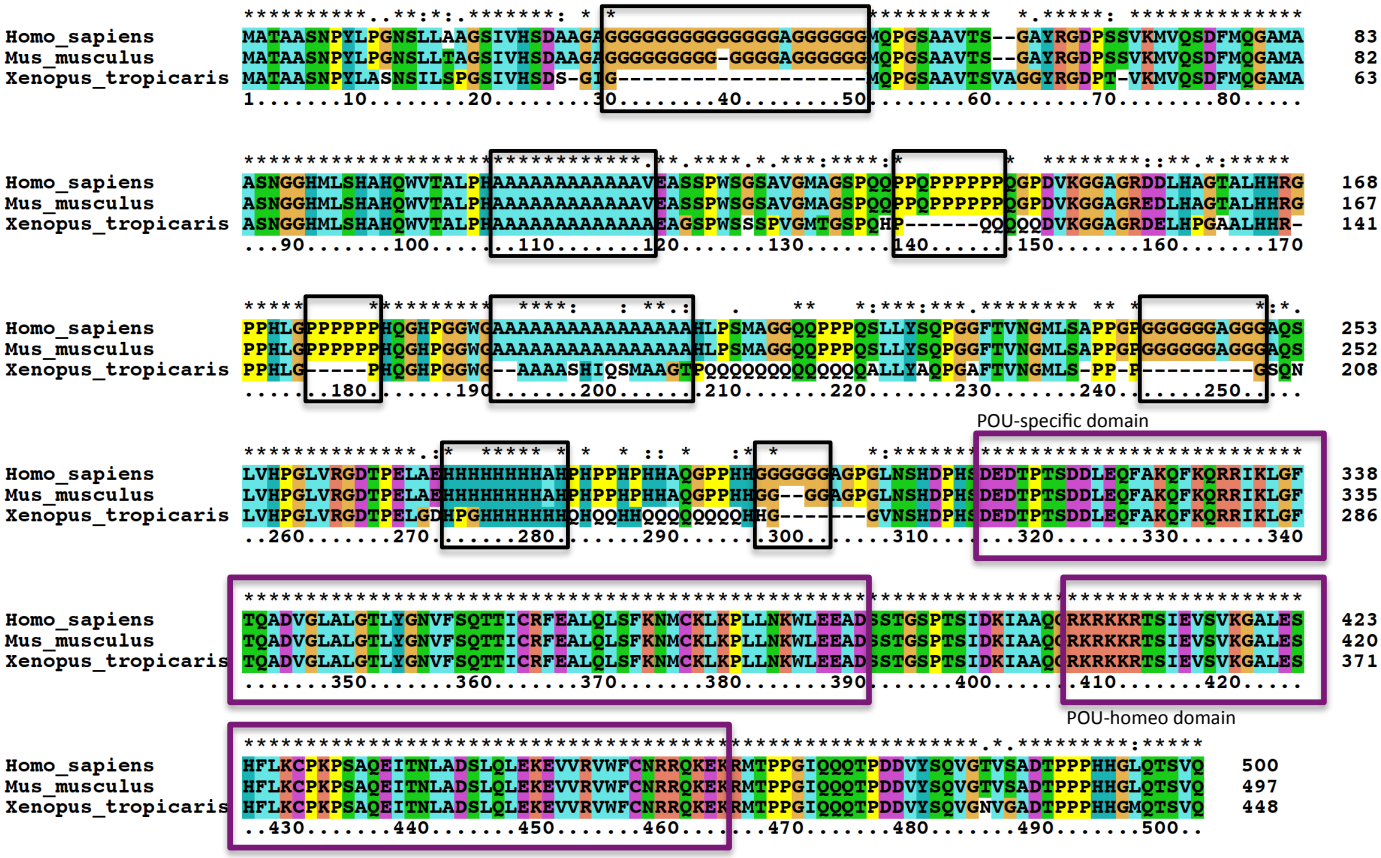
POU-specific domain
POU-homeo domain

Supplementary Fig. 2. Locomotor activity in female

A. Transition of locomotor activity over 5 continuous days (120 hours). The measurement session includes 6 light (L1-L6) and 5 dark (D1-D5) periods alternately.
B. The averaged locomotor activity among 6 light periods.
C. The averaged locomotor activity among 5 dark periods.
D. The total of novel seeking activity from start to 30 min.

Values shown on graphs represent the mean ± SEM of 14 of *+/+* females (orange) and 11 of *tro/tro* females (blue). Statistical significance are shown as **P*<0.05 and ***P*<0.01.

xPou3f3 knock-in female mice showed more apparent elevation of locomotor activities. The activities in both light and dark periods were significantly elevated to 1.28-fold in light and 1.30-fold in dark period. But novel seeking activities were not changed in the same way of male individuals.

A.

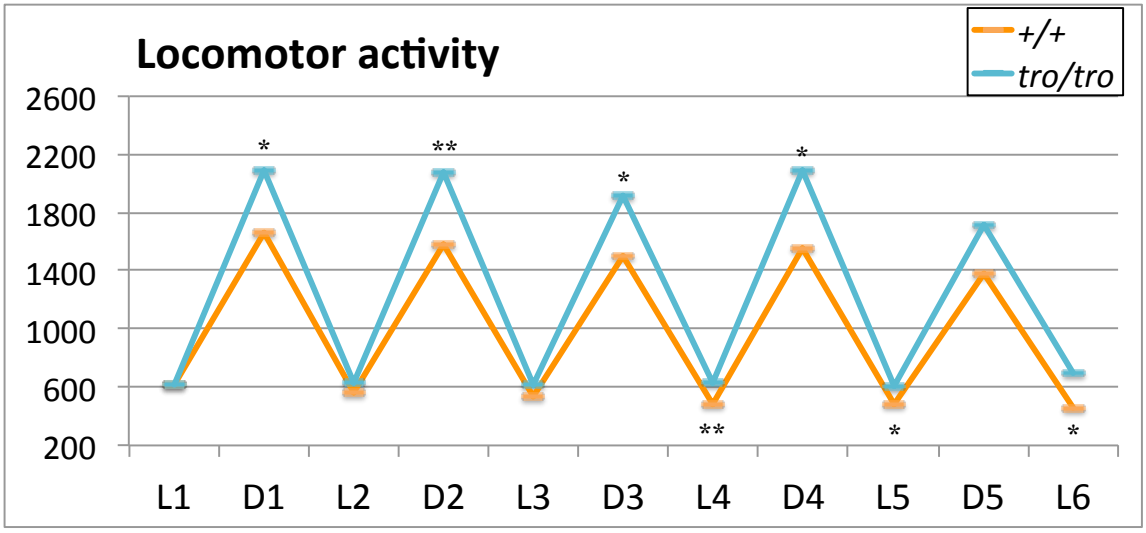
Locomotor activity
+/+
tro/tro
2600
2200
1800
1400
1000
600
200
L1
D1
L2
D2
L3
D3
L4
D4
L5
D5
L6

B.

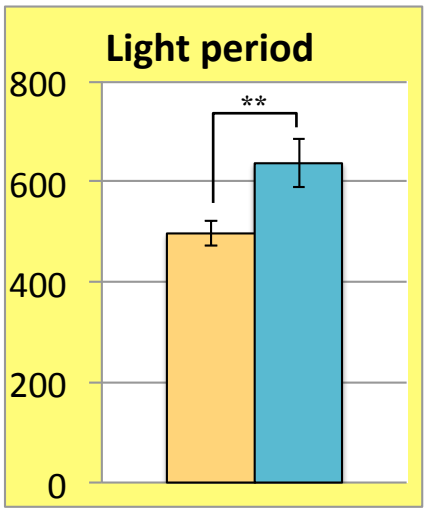
Light period
800
600
400
200
0

C.

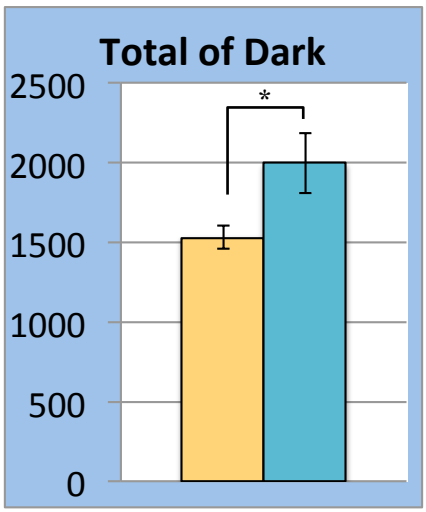
Total of Dark
2500
2000
1500
1000
500
0

D.

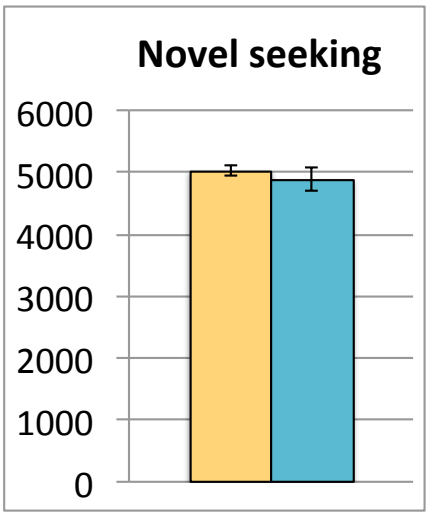
Novel seeking
6000
5000
4000
3000
2000
1000
0

Supplementary Fig 3. Volcano plot (*+/+* (stress+) vs. *tro/tro* (stress+))

In statistics, a volcano plot analysis based on Log_2 fold-changes (proportions) and Log_{10} *P*-values. Blue circle indicators show the magnitude and significance of one or more genes expression changes between stress-loaded *+/+* and *tro/tro*. The x-axis shows Log_2 fold change (proportions) and y-axis shows Log_{10} *P* value calculated by Kal's Z test.

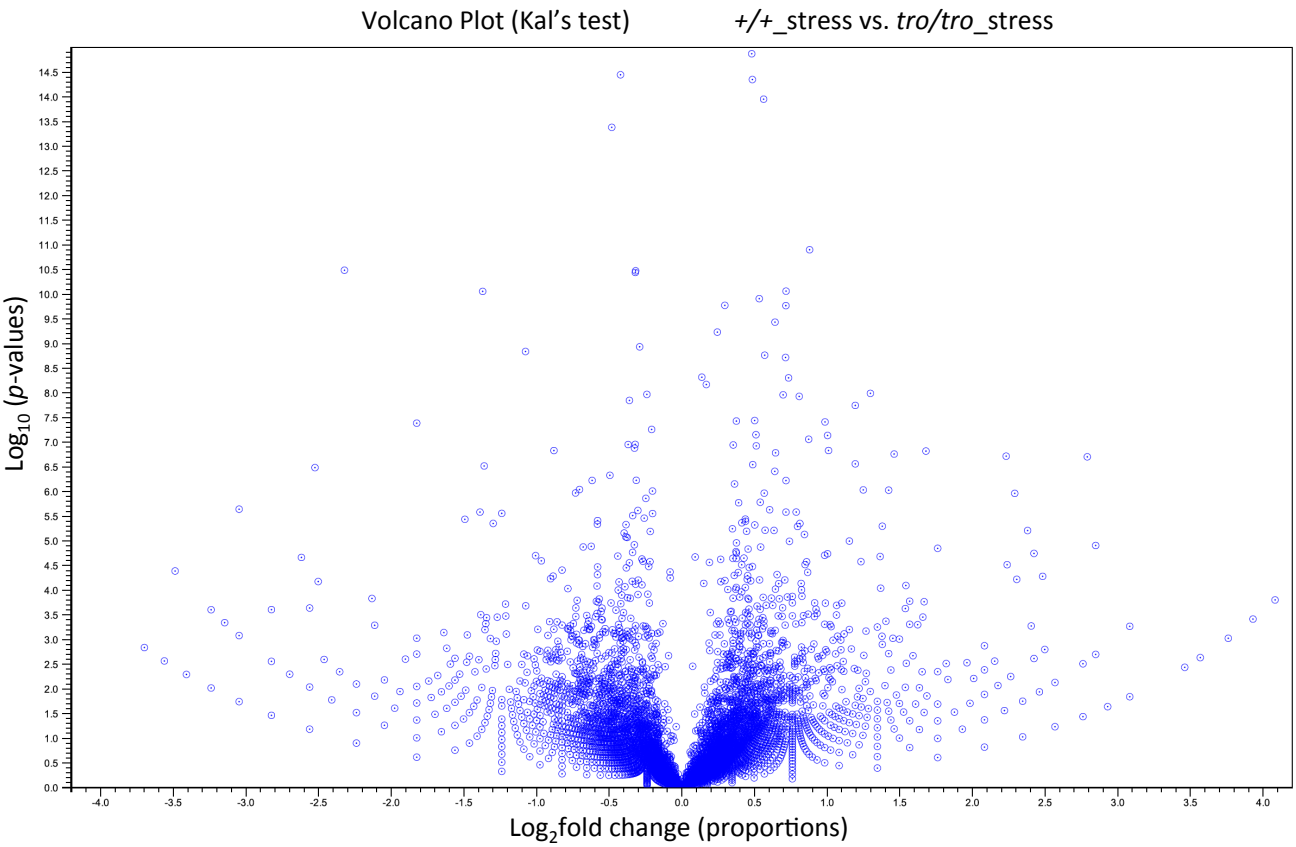
Volcano Plot (Kal's test)
+/+_stress vs. tro/tro_stress
Log10 (p-values)
Log2fold change (proportions)

Supplementary Fig. 4. Stress-related expression analysis

A. Heat-map images display the gene expression belonging to the category of GO:0006979 response to oxidative stress. 111 genes were listed and analyzed their expression changes.

B. Heat-map images display the genes expression belonging to the category of GO:0006754 ATP biosynthetic process, GO:0015986 ATP synthesis coupled proton transport, GO:0046034 ATP metabolic process, and GO:0015991 ATP hydrolysis coupled proton transport. The increasing tendency of these terms only in +/+ were indicated in Supplementary Table 1B and 2D.

C. All significantly changed genes with significant *P*-values in Kal's Z-test ($P<0.05$) in Supplementary Fig. 4B were picked up and shown as heat-map images.

Heat-map analyses are displayed using logarithmic (base 10) gene expression values. The statistical significances are indicated as $*P<0.05$, $**P<0.01$ and $***P<0.001$ in comparison between same genotypes (*+/+* or *tro/tro*) and †$P<0.05$, ††$P<0.01$ and †††$P<0.001$ in comparison between stress-loaded individuals.

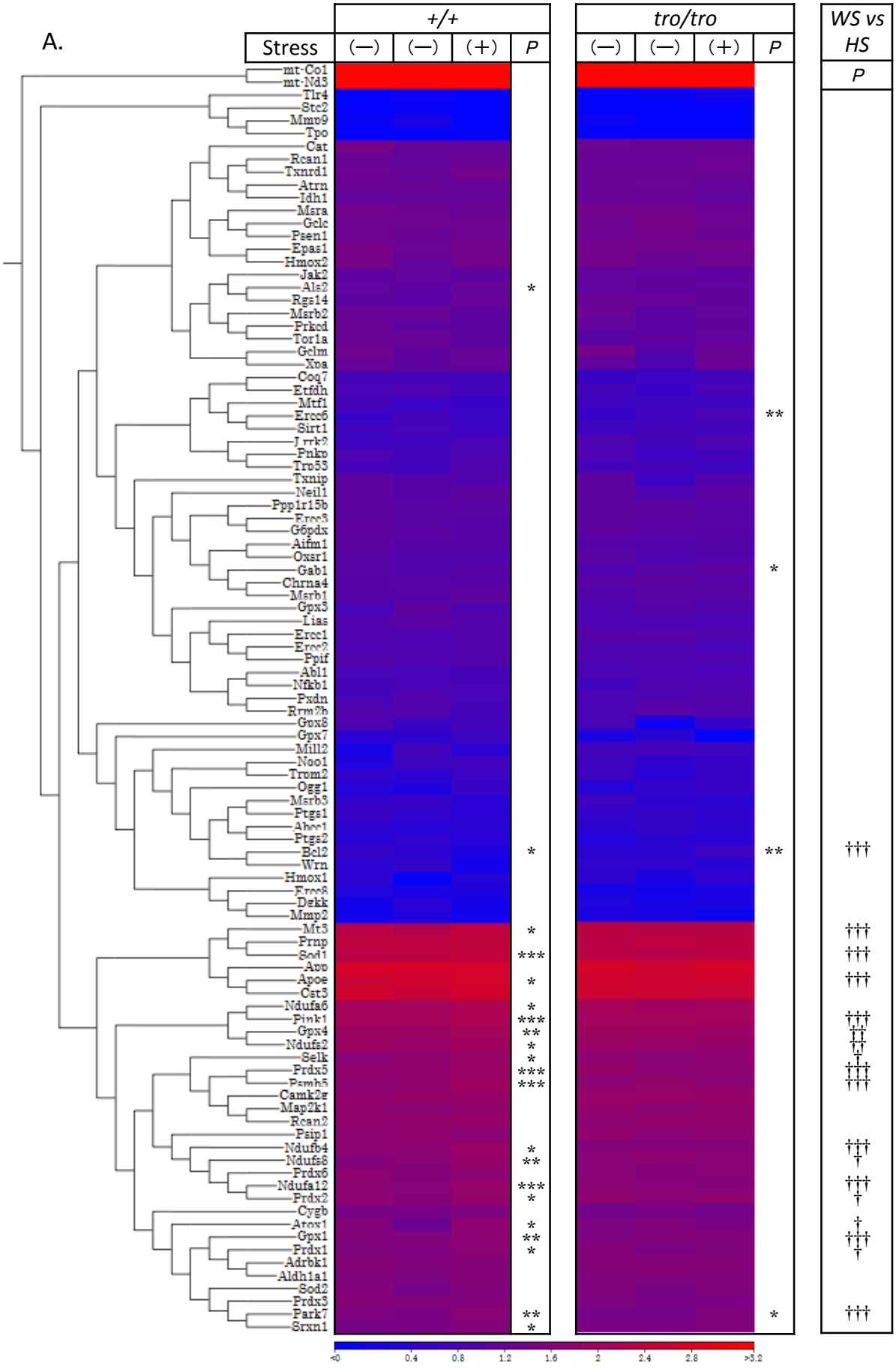
A.
Stress
+/+
tro/tro
WS vs HS
(—)
(—)
(+)
P
mt-Co1
mt-Nd3
Tlr4
Stc2
Mmp9
Tpo
Cat
Rcan1
Txnrd1
Atrn
Idh1
Msra
Gclc
Psen1
Epas1
Hmox2
Jak2
Als2
Rgs14
Msrb2
Prkcd
Tor1a
Gclm
Xpa
Coq7
Etfdh
Mtf1
Ercc6
Sirt1
Lrrk2
Pnkp
Trp53
Txnip
Neil1
Ppp1r15b
Ercc3
G6pdx
Aifm1
Oxsr1
Gab1
Chrna4
Msrb1
Gpx3
Lias
Ercc1
Ercc2
Ppif
Abl1
Nfkb1
Pxdn
Rrm2b
Gpx8
Gpx7
Mill2
Noo1
Trom2
Ogg1
Msrb3
Ptgs1
Ahcy1
Ptgs2
Bcl2
Wrn
Hmox1
Ercc8
Dkk
Mmp2
Mt3
Prnp
Sod1
App
Apoe
Cst3
Ndufa6
Pink1
Gpx4
Ndufs2
Selk
Prdx5
Psmb5
Camk2g
Map2k1
Rcan2
Psip1
Ndufb4
Ndufs8
Prdx6
Ndufa12
Prdx2
Cygb
Atox1
Gpx1
Prdx1
Adrbk1
Aldh1a1
Sod2
Prdx3
Park7
Srxn1
<0
0.4
0.8
1.2
1.6
2
2.4
2.8
>3.2

B.

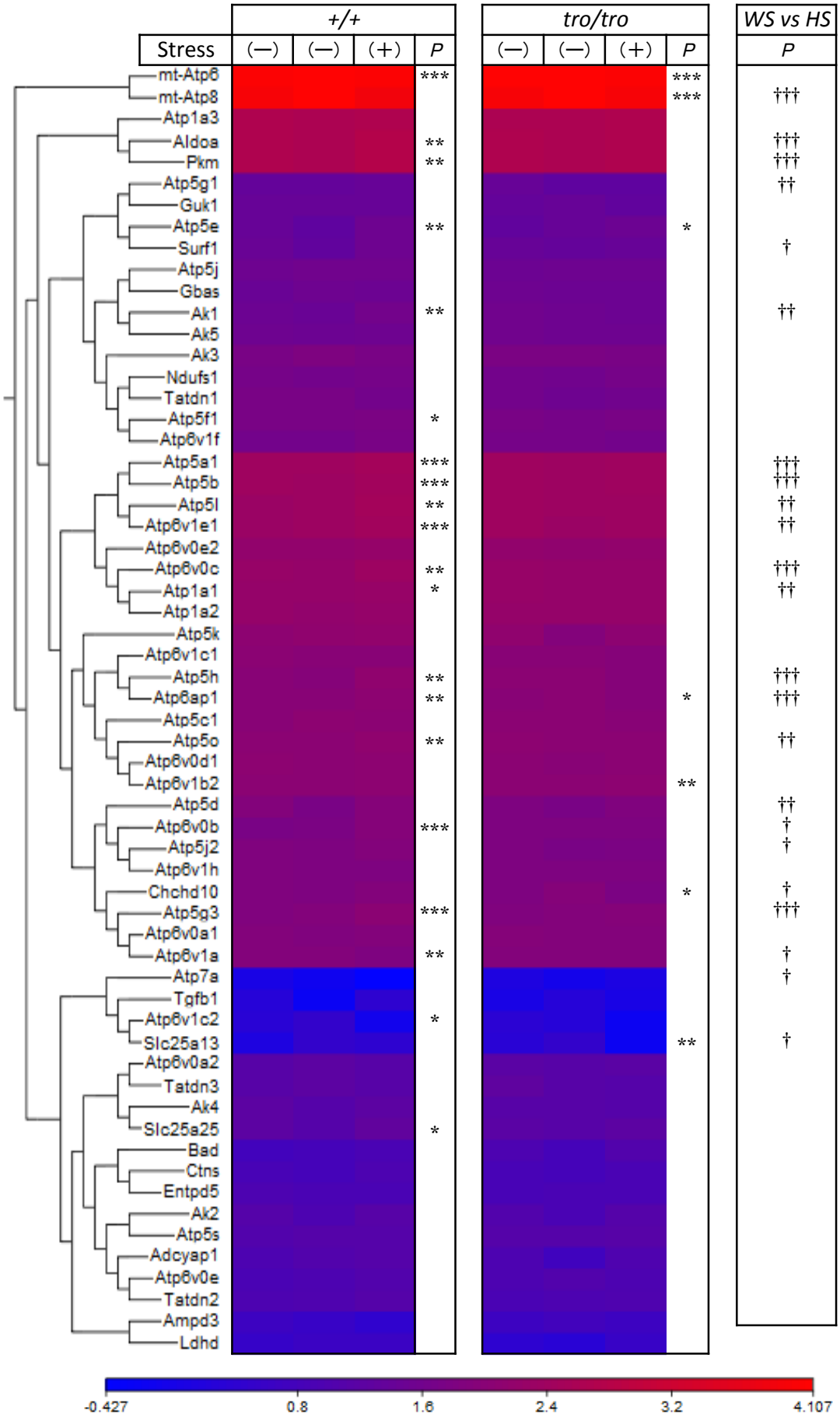
+/+
tro/tro
WS vs HS
Stress
(—)
(—)
(+)
P
mt-Atp6
mt-Atp8
Atp1a3
Aldoa
Pkm
Atp5g1
Guk1
Atp5e
Surf1
Atp5j
Gbas
Ak1
Ak5
Ak3
Ndufs1
Tatdn1
Atp5f1
Atp6v1f
Atp5a1
Atp5b
Atp5l
Atp6v1e1
Atp6v0e2
Atp6v0c
Atp1a1
Atp1a2
Atp5k
Atp6v1c1
Atp5h
Atp6ap1
Atp5c1
Atp5o
Atp6v0d1
Atp6v1b2
Atp5d
Atp6v0b
Atp5j2
Atp6v1h
Chchd10
Atp5g3
Atp6v0a1
Atp6v1a
Atp7a
Tgfb1
Atp6v1c2
Slc25a13
Atp6v0a2
Tatdn3
Ak4
Slc25a25
Bad
Ctns
Entpd5
Ak2
Atp5s
Adcyap1
Atp6v0e
Tatdn2
Ampd3
Ldhd
-0.427
0.8
1.6
2.4
3.2
4.107

C.

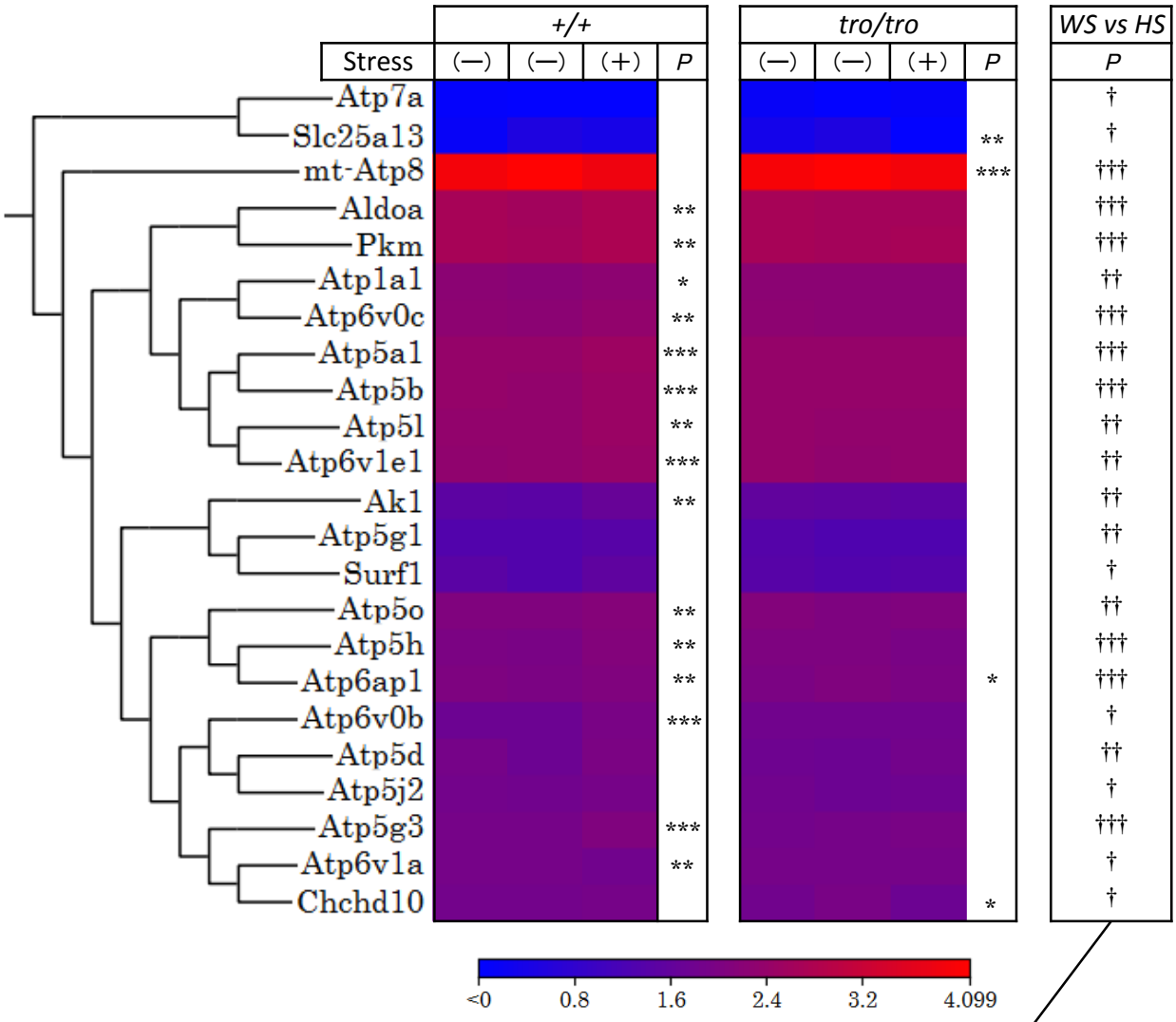

Significantly high expression only in *+/+*_stress
(*+/+* (stress+) vs. *tro/tro* (stress+))
(Kal's test $P<0.05$)